MOLECULAR STUDIES ON CALCIUM OXALATE KIDNEY STONES: A

WINDOW INTO THE PATHOGENESIS OF NEPHROLITHIASIS

Victor Hugo Canela

Submitted to the faculty of the University Graduate School
in partial fulfillment of the requirements
for the degree
Doctor of Philosophy
in the Department of Anatomy and Cell Biology,
Indiana University

May 2022

Accepted by the Graduate Faculty of Indiana University, in partial fulfillment of the requirements for the degree of Doctor of Philosophy.

Doctoral Committee

<div style="text-align:right">

_____

James C. Williams, Ph.D., Chair

_____

Tarek M. Ashkar, M.D.

</div>

November 22, 2021

<div style="text-align:right">

_____

Janice S. Blum, Ph.D.

_____

Uma Sankar, Ph.D.

</div>

DEDICATION

This dissertation is dedicated to all those (past, present and future) who have suffered due to nephrolithiasis and its complications. I hope this work one day contributes, even in the slightest of ways, to future preventable and efficacious treatments of kidney stone disease.

This dissertation is also dedicated to those who have donated their bodies to science. You have granted me the great honor to learn, teach and perform anatomical research and have led to critical discoveries presented in this dissertation. In toto, studies and results from anatomical research can potentially increase mankind's overall knowledge that can one day improve patient care. I sincerely thank the donors and their families for trusting us with such invaluable gift. These donors and their families deserve our highest gratitude.

ACKNOWLEDGEMENT

I would like to give a special thank you to Dr. Randy R. Brutkiewicz for believing in me when we first met and for that brief but critical discussion about scientific research on that sunny afternoon in California. He helped me achieve the goals I always had but was never able to articulate or coherently express at the time being. I thank him dearly for trusting me and for continuing to mentor me all these years.

I thank my committee members, Drs. Janice Blum, Uma Sankar, and Tarek Ashkar for proving excellent advice and mentorship throughout my doctoral studies; I thank them for their scientific expertise, guidance, and enthusiastic encouragement throughout the years. Additionally, I would like to thank them for providing moral and emotional support when I most needed it.

Thank you to the Indiana University School of Medicine, Indiana BioMedical Gateway program, the Department of Anatomy, Cell Biology & Physiology, the Department of Urology, and the division of Nephrology for granting me the intellectual space to cultivate my clinical and scientific curiosities and where to complete this work.

Victor Hugo Canela

MOLECULAR STUDIES ON CALCIUM OXALATE KIDNEY STONES: A

WINDOWN INTO THE PATHOGENESIS OF NEPHROLITHIASIS

Nephrolithiasis will affect one-in-eleven people, and more than half of those

individuals will have stone recurrence within a decade of their first episode. Despite

decades of biomedical research on nephrolithiasis and extraordinary advances in

molecular and cell biology, the precise mechanisms of kidney stone formation are not

fully understood. Currently, there are limited treatments or preventative measures for

nephrolithiasis. Therefore, it is crucial to scrutinize kidney stones from a molecular and

cell biology perspective to better understand its pathogenesis and pathophysiology; and

to, hereafter, contribute to effective therapeutic targets and preventative strategies.

Kidney stones are composed of an admixture of crystal aggregated material and

an organic matrix. 80% of all kidney stones are composed of calcium oxalate (CaOx) and

half of all CaOx patients grow their stones on to Randall's plaques (RP). RP are

interstitial calcium phosphate mineral deposits in the renal papilla. Thus, we developed

and optimized methodologies to directly interrogate CaOx stones.

CaOx stones were demineralized, sectioned, and imaged by microscopy, utilizing

micro CT for precise orientation. Laser microdissection (LMD) of specific regions of

stone matrix analyzed by proteomics revealed various proteins involved in inflammation

and the immune response. Analyses on jackstone calculi, having arm protrusions that

extend out from the body of the stone, revealed that they are a rare subtype of CaOx stone

formation. Micro CT analyses on 98 jackstones showed a radiolucent, organic-rich core

in the arm protrusions. Fluorescence imaging on RP stones showed consistent differences

in autofluorescence patterns between RP and CaOx overgrowth regions. Moreover, cell nuclei were discovered with preserved morphology in RP regions, along with variable expressions of vimentin and CD45. In comparing spatial transcriptomic expression of reference and CaOx kidney papillae, CaOx patients differentially expressed genes associated with pathways of immune cell activation, reactive oxygen damage and injury, extracellular remodeling, and ossification.

Our findings provide novel methodologies to better understand the role of molecules and cells in CaOx stone matrix. Several of the proteins and cells identified in these studies may serve as potential biomarkers, and future therapeutic targets in preventing kidney stone disease.

<div align="right">James C. Williams, Ph.D., Chair</div>

TABLE OF CONTENTS

LIST OF TABLES

LIST OF FIGURES

LIST OF ABBREVIATIONS

7-AAD	7-aminoactinomycin D
α-SMA	alpha smooth muscle actin
ABCC6	ATP binding cassette subfamily C member 6
APOD	apolipoprotein D
ATF3	activating transcription factor 3
ATP	adenosine triphosphate
BCE	before the common (or current) era
BMP	bone morphogenetic protein
BMP2	bone morphogenetic protein 2
BMP7	bone morphogenetic protein 7
BMPR2	bone morphogenetic protein receptor 2
CaOx	calcium oxalate
CaP	calcium phosphate
CCL2	c-c motif chemokine ligand 2
CD15	3-fucosyl-N-acetyl-lactosamine, cluster of differentiation 15
CD33	cluster of differentiation 33, sialic acid binding Ig-like lectin 3
CD44	cluster of differentiation 44
CD45	cluster of differentiation 45
CD68	cluster of differentiation 68
cDNA	complementary DNA

CHIT1	chitinase 1
COD	calcium oxalate dihydrate
COM	calcium oxalate monohydrate
CT	computer tomography
DAB	3,3'-diaminobenzidine tetrahydrochloride hydrate
DAPI	4',6-diamindino-2-phenylindole
DEG	differentially expressed genes
DNA	deoxyribonucleic acid
EDTA	ethylenediaminetetraacetic acid
ELISA	enzyme-linked immunosorbent assay
EMT	epithelial-to-mesenchymal transition
ER-TR7	ER-thymic reticulum antibody 7, fibroblast antibody marker
FT-IR	Fourier-transform infrared
FOS	Fos proto-oncogene, AP-1 Transcription Factor Subunit
GPX3	glutathione peroxidase 3
GO	gene ontology
H&E	hematoxylin and eosin
HIF3A	hypoxia inducible factor 3 alpha subunit alpha

HRP	horseradish peroxidase
IgG	immunoglobulin G
IGHA1	immunoglobulin heavy constant alpha 1
IGKC	immunoglobulin kappa constant
IHC	immunohistochemistry
IL11	interleukin 11
IR	infrared spectroscopy
IRB	Institutional Review Board
IU	Indiana University
JUN	Jun proto-oncogene, AP-1 Transcription Factor Subunit
KO	knockout
LCN2	lipocalin-2, neutrophil gelatinase-associated lipocalin
LFQ	label-free quantification value
LMD	laser micro-dissection
LYZ	Lysosozyme
MARCO	macrophage receptor with collagenous structure
MGP	matrix gla protein
MHC I	major histocompatibility complex class I

MHC II	major histocompatibility complex class II
MMP7	matrix metalloproteinase 7
MMP9	matrix metalloproteinase 9
MPO	myeloperoxidase
mRNA	messenger ribonucleic acid
MSC	mesenchymal stem cell
NH_4Cl	ammonium chloride
OCT	optimal cutting temperature
OPG	osteopotegerin
OPN	osteopontin
OSX	osterix, Sp7 transcription factor
p-c-JUN	phosphorylated c-JUN
PFA	paraformaldehyde
pH	potential of Hydrogen
PTGS1	prostaglandin-endoperoxide synthase 1
RANK	receptor activator of NF- κB
RNA	ribonucleic acid
ROBO	robo roundabout receptor family member

ROS   reactive oxygen species

RP   Randall's plaque

RUNX1   runt-related transcription factor 1

RUNX2   runt-related transcription factor 2

S100A8   Calgranulin A, urinary stone protein band A

S100A9   Calgranulin B, leukocyte L1 complex heavy chain

SEM   scanning electron microscopy

SHG   second harmonic generation

SLIT   slit guidance ligand family member

SOD2   superoxide dismutase 2

Sp7   transcription factor Sp7, osterix

SPP1   secreted phosphoprotein 1, osteopontin

SRAF   Super-Resolution Auto-Fluorescence

THP   Tamm-Horsfall Protein, uromodulin

TNF   tumor necrosis factor

TNFRSF11A TNF receptor superfamily member 11A, RANK

TNFRSF11B TNF receptor superfamily member 11B, osteopotegerin

UMOD   uromodulin

VIM   vimentin

Chapter 1: Introduction

<u>1.1 Overture: Nephrolithiasis—A Current Forecast on Kidney Stone Disease</u>

Nephrolithiasis or kidney stone disease is one of the oldest diseases known to man (Modlin, 1980). People in ancient Mesopotamia and Egypt described urinary stones and included treatment options in their medical texts as early as 3200 and 1200 BCE (Shah, 2002). Today, kidney stone disease is a major clinical issue affecting approximately 12% of the world population (Sorokin, 2017). In the United States, prevalence of kidney stone disease appears to be rising but the reason for this trend is not fully understood (Lieske, 2015). Furthermore, one-in-eleven people will have a kidney stone event in their lifetime, and more than half of those individuals will have stone recurrence within a decade of their first episode (Scales, 2016). Stone disease affects both men and women, being only modestly more common in men (Coe, 2005) (Lieske, 2015). Despite decades of biomedical research on nephrolithiasis and extraordinary advances in molecular and cell biology, the precise mechanisms of kidney stone formation are not fully understood (Evan, 2014). As a result, there are limited treatments or preventative measures for kidney stone disease (Sakhaee, 2011) (Khan, 2021).

Kidney stones are mineral crystallizations precipitated out of solution from supersaturated urine (Coe, 2005). Current literature on nephrolithiasis suggests that at least 80% of all kidney stones are composed of calcium oxalate (CaOx) (Worcester 2010) (Lieske, 2014) (Bird & Khan, 2017). Uroliths are clinically observed free in the urinary bladder (Douenias, 1991) (Childs, 2013), either unattached in the renal calyces and pelvis, obstructing the ureter, and/or anchored to the renal papillae in the kidneys (Cifuentes, 1987) (Khan, 2016). Moreover, kidney stone disease has been associated with

an increased risk of end-stage renal failure, chronic kidney disease and metabolic syndrome (Hung CT, 2020) (Johri, 2010). Given these ongoing clinical trends, stone disease prevalence will likely persist and continue to rise due to our limited knowledge on the mechanistic underpinnings contributing to stone formation. Therefore, a better understanding of the mechanisms involved in stone growth and formation is needed to generate significant advances in overall treatment strategies and prevention of nephrolithiasis.

This introductory chapter aims to cover selected topics on the fundamentals of CaOx kidney stone disease. To achieve this, a foundation on what is currently understood about CaOx stone matrix and formation will be provided. Following the brief section on CaOx stone matrix, an overview on the fundamentals of renal papillary biology will ensue to give way to the topic of ectopic biomineralization in the papilla. Establishing the basics of CaOx stone matrix and mineralization in the papilla will provide a solid foundation to begin appreciating the complexity of the human kidney stone disease and begin to focus on the development of stones anchored to Randall's plaque. The remainder of the chapter will briefly discuss Randall's plaque in idiopathic stone formers along with contemporary theories aiming to explain its pathogenesis. Finally, a short note on an animal model of Randall's plaque will be provided as an overture to appreciate the different research projects conducted in this thesis. Each research project has been organized into individual chapters containing their own brief introductory section, materials and methods, as well as results and discussions pertinent to each study. This format should allow one to follow each subsequent chapter, irrespective of order, and to

grasp the fundamental concepts aimed in each research study on CaOx kidney stone disease.

1.2 CaOx Stone Formation: The role of CaOx Stone Matrix

It has been estimated that approximately half of all CaOx stone formers are idiopathic patients. Of these, most CaOx patients form their stones attached to calcium phosphate (CaP) subepithelial plaque or Randall's plaques (Randall, 1937). Of note, a subset of CaOx stones may develop without an anchoring mechanism or attachment (e.g., Randall's plaques or plugs) as intralobular deposits in the terminal collecting ducts or papillary ducts of the kidney (Khan 2021).

Kidney stones are composed of an admixture of crystal aggregated material and organic matrix (**Figure 1.1**) (Khan, 2021). The majority of the crystal component from a stone is typically used to categorize the stone type (e.g., a stone composed of 74% uric acid and 26% CaOx will be categorized as a uric acid stone). Boyce et al. suggested that, on average, kidney stones contained only about 1.5%-3% protein, by weight (Boyce, 1956). Studies by Khan et al. have shown that crystals within a stone are surrounded by the organic matrix (Khan, 1984). However, the role of the organic matrix in stone formation remains elusive.

The kidney stone matrix has been shown to be protein enriched (Canales, 2008) (Okumura, 2013) (Witzmann, 2016). It is hypothesized that the stone matrix proteins function as the cementum that holds and aggregates stone crystals together. Stone matrix proteins have been theorized to function as either renal stone promoters or stone inhibitors (Fleisch, 1978). Further, several studies have shown that matrix proteins are

associated with the immune system and the inflammatory response (Merchant, 2008) (Boonla, 2014) (Witzmann, 2016) (Wesson, 2017).

Okumura and colleagues published work on the proteomic profiles of 9 CaOx kidney stones (Okumura, 2013). Their studies reported a total of 92 proteins from the analyzed CaOx stones. The proteins reported included prothrombin, Tamm Horsfall protein (THP), calgranulins A and B, and myeloperoxidase. The authors classified the protein components from the stones into three major groups that would help describe their origin and/or function. These classifications were listed as Kidney Proteins, Blood Proteins and Leuc[k]ocyte-related proteins. The proteins under "Leukocyte-related proteins" are commonly expressed in macrophages and neutrophils and suggest a strong immune and/or inflammatory role associated to the development of kidney stones. These proteins included neutrophil defensin 3, fetuin A, lactotransferrin, azurocidin, myeloperoxidase, cathepsin G and the calgranulins A and B.

Witzmann et al. used label-free quantitative mass spectrometry to extract proteins from pulverized human CaOx stones (Witzmann, 2016). Their studies identified a total of 1,059 unique proteins in two human CaOx kidney stones (revealing a more complex matrix proteome than previously described). Witzmann and colleagues highlight proteins related to calcium binding and mineralization as well as potential modulators of crystal formation: Annexins A1, A2, calmodulin, calsequestin-2, osteopontin, Protein S100-A8 (Calgranulin-A), and Protein S100-A9 (Calgranulin-B), THP, prothrombin, CD44, and various types of collagens. Their gene enrichment analyses showed pathways significantly associated with the complement system, production of nitric oxide and reactive oxygen species in macrophages. Further, they reported Functional Annotation

clusters of the CaOx matrix proteins relating to the inflammatory response and immune system responses, as well as extracellular glycoprotein signaling, wound healing and cytoskeletal structural molecule activity.

The proteomic studies briefly described here support the hypothesis that inflammation and immune processes, and extracellular modifications may play an important role in the development and progression of stone disease. More recently, a systematic bioinformatics research reviewed data on proteomic analysis in the stone matrix and concluded similar conclusions presented above. The stone matrix proteins revealed common inflammation-related proteins (including those involved in the immune system) (Yang, 2021). Although we are learning more about the proteins present in CaOx stone matrix, we have yet to fully describe the precise mechanisms of how exactly they contribute to crystal retention and aggregation. Although it is likely that most proteins found in the matrix are adsorbed on to the stone by chance, certain questions remain unanswered. Are these proteins somehow affecting crystal formation directly and then becoming part of the stone mass? Are we detecting inflammatory and immune proteins as a response to the presence of stones? Are there specific cells of the kidney secreting or producing these proteins, and as a result, inadvertently propagating stone formation?

1.3 The Kidney Papilla and CaOx Stone Formation

As mentioned above, some idiopathic CaOx stones appear to develop on to the renal papillary calcifications known as Randall's plaque (RP) (**Figure 1.2**) (**Figure1.3**) (Williams, 2006) (Letavernier, 2016). It is not known what mechanisms contribute to the genesis of plaque development or how the renal papillary interstitium becomes mineralized. Evan et al. suggests that the origin of RP occurs at the basement membranes

of the limbs (loops) of Henle and then spread into the surrounding interstitial space eventually migrating to the papillary tip (**Figure1.4**) (Evan, 2007). But the specific molecular and cellular determinants driving these events remain largely unknown. To begin exploring what cells and molecules may contribute to the development of plaques, it would be important to describe what is known about the anatomy of the renal papilla.

There is very limited knowledge about the anatomy of human renal papilla. It is known that the papilla is at the tip of the inner medulla (and grossly, at the tip of the renal pyramid) where we find connective tissue interstitium, terminal collecting ducts and some vasa recta. Given the anatomical position of the papilla, it assumed that it is the site of a unique physiological microenvironment within the kidney (it is both hyperosmotic and hypoxic). However, the complete cellular and molecular make-up in this region has been seldom studied.

Of the few studies focusing on the structural organization of the mammalian kidney, researchers have highlighted two major cell types in the interstitium of the inner medulla of model organisms. Interstitial cells, type I, or stromal fibroblasts (fibroblast-like) were described by Professors Kevin V. Lemely and Wilhelm Kriz in the medullary interstitial compartment (Lemley and Kriz, 1991). Ultrastructure observations of this region show an intimate association between these cells and tubules and vessels, including an increase in cytoskeletal elements (Kriz and Kaissling, 2000). Additionally, the presence of lipid granules in fibroblasts have been noted in specific cell environments (lipid-laden cells). It is believed that some of these cells retain the capacity to transform myofibroblasts under conditions of interstitial inflammation in vitro via alpha smooth muscle actin and desmin upregulation (Grupp, 1997). The second type is the bone

marrow-derived interstitial dendric cell. The dendritic cells are major histocompatibility complex (MHC) class II positive (MHC-II+) which may module immune cell activity. However, the presence and function of these cells in healthy and diseased human inner medullary kidneys is still unclear.

Vanslambrouck et al. described the current literature as being relatively silent on processes of renal papillary elongation and maturation during kidney development (Vanslambrouck, 2011). Thus, it is not surprising that we currently know very little about the specific cells residing in the healthy or diseased kidney papilla. Vanslambrouck and colleagues report implications of the kidney papilla as being the site of a potential stem cell niche. The hypoxic microenvironment mirrors the niche microenvironment harboring stem cells in bone marrow and brain where hypoxic environments likely play a role in the maintenance and in the protection against DNA damage (Morrison, 2000). Oliver et al. in vitro studies on renal papillary cells show that they form spheres co-expressing mesenchymal and epithelial markers mirroring those of neural stem cells (Oliver 2009). Additionally, Oliver and colleagues suspect that some of the renal papillary cells may play a role in the homeostasis of the papilla and including renal repair due to in response to injury. Their experimental observations, however, are limited to the migration of the papillary cells to the cortex in response to injury. Contrary to these observations, Song et al. sought to identify a kidney papillary stem cell population using telomerase. Their reports identified epithelial-like cells expressing telomerase activity, with label retaining media (stem cell marker) but could not report proliferating or migratory cell activity during tubular repair (Song, 2011). As is apparent, there is currently debate about the

specific cell population housed within the inner medullary interstitium and throughout the renal papillae in humans.

<u>1.4 Mineralization in the Renal Papilla</u>

Researchers have previously reported models that compare the initial stages of bony ossification and interstitial crystal deposition in the kidney papilla. One intriguing hypothesis suggests that interstitial cells (mesenchymal stem cells?) of the renal medulla transdifferentiate into a bone-like phenotype (osteoblast-like cells), thus initiating a direct cell mediated process of mineralization (Vermooten, 1942). Another view closely related to this one, suggests that increased calcium and phosphate levels in the papillary interstitium lead to the deposition of apatite crystals on to a sea of collagen matrix in the papilla. Perhaps in unison, these events contribute to the initial mineralization of the kidney papilla.

The multipotential mesenchymal stem cell (MSC) plays an important role in the production of osteoprogenitor cells and other specialized cells (e.g. fibroblasts, chondroblasts) (Denu, 2016) (Chen, 2016). Are resident fibroblasts in the renal papilla transdifferentiating into osteoblast-like cells? Or, alternatively, does the renal papillary mineralization closely mirror vascular calcification? In an experimental rat model of hyperoxaluria and renal intratubular CaOx crystal deposition, researchers identified the following upregulated genes in the kidneys: RUNX1 and 2, Osterix (Sp7), BMP2, MPB7, BMPR2, collagen, osteopontin, osteopotegrin (TNFRSF11B) vimentin, and MGP (Khan, 2014) (Joshi, 2015). These genes point to a possible bone-like phenotype; furthermore, these genes have also been shown to be active in vascular calcification (Khan, 2021).

Indeed, cells such as pericytes, myofibroblasts and smooth muscle cells have also been shown to contribute to vascular mineralization and thus may be of interest in the initiation of renal papillary mineralization (Giachelli, 2004) (Giachelli, 2005) (Khan, 2021). Are the pericytes (α-SMA+ and VIM+), surrounding the loops of Henle or the vasa recta, contributing to the mineralization of the papillary interstitium? Given the hypoxic and hyperosmolar microenvironment of the papillary tip, is this region more prone to vascular injury in the vasa recta? Can this damage promote similar events to blood vessel calcification in atherosclerosis? Studies have shown a strong association between cardiovascular diseases and nephrolithiasis (Khan, 2012). In both diseases, the role of inflammation and reactive oxygen species may be critical. Additionally, macrophage activity has been identified in the progression of vascular calcification. One function of macrophages may be the modulation of pro-inflammatory phenotypes or the formation of crystal deposits as a result of phagocytosis (Khan, 2021). As discussed above, immune cell activity, including macrophage activity, have been proposed in CaOx stone matrix. Are resident or migratory immune cells responding to injury and ROS, in the renal papilla and thus, activating mineralization pathways?

It is still unclear what specific factors are at play during the formation of Randall's plaque in patients. The involvement of ossification and extracellular remodeling, immune cell activity and inflammation in the pathogenesis of RP patients continues to be investigated. In the advent of newer technologies and innovative methodologies, answers to these questions may shed more light about the potential role of fibroblasts, osteoblast-like cells, macrophages, or pericytes in the development of RP and stone formation.

1.5 Randall's Plaque and CaOx Stones

For CaOx stone formation to occur onto RP, damage, or injury to the papillary urothelium, may have to first ensue (we have yet to determine what activities may lead to the disruption of this region in the kidney) (Evan, 2007). The biological apatite of RP is interstitial and in close association to the macromolecules of the papillary connective tissue (fibroblasts, collagen) (Khan, 2012). The papillary epithelium naturally separates the plaque from the calyceal urine. Perhaps by way of the osteogenic changes, inflammation, and immune cell activity or processes similar to those of vascular calcification (Taylor, 2015), the papillary epithelium is breached. Thus, exposure of plaque to urine macromolecules attracts apatite and over time, accumulates CaOx crystals deposition along with the matrix protein constituents discussed above. This gives way to the formation and growth of CaOx stones on to RP (**Figure 1.3**) (**Figure 1.4**).

The region between RP and CaOx overgrowth is of great interest in the study of CaOx stone formation. Evan and Sethmann studied this interface region independently (Evan, 2007) (Sethmann, 2017). Their findings have pointed to an admixture of apatite and CaOx at, perhaps, the earliest stages of CaOx stone formation. However, very little is still known about what specific activities may be at play during the initial events of stone formation. Studies outlined in Chapters 4 and 5 aim to elucidate new light in this understudied area.

The utilization of micro computed tomography (micro CT) has been extremely useful in the classification and direct study of CaOx stones growing on RP (**Figure 1.3**) (Williams, 2018). Zarse et al. first demonstrated the capabilities of nondestructive analysis of urinary stones by micro CT and extend it as an imaging diagnostic of stone

mineral composition (Zarse, 2004). When analyzed by micro CT, RP stones often show multiple lumens representing calcified tubules or vessels in the apatite region. One can readily discriminate the CaOx mineral from the apatite with micro CT. This technology coupled with other methodologies, lends itself for novel investigation of the plaque and stone interface.

Winfree et al. more recently attempted to investigate the interface between RP and the CaOx overgrowth (Winfree 2020). Their multimodal imaging techniques revealed unique, label-free signatures in RP. The group utilized micro CT imaging to guide careful polishing of RP stones to expose the region between RP and CaOx overgrowth. Winfree et al. hypothesized that RP organic molecules are unique to RP and can be differentiated from the CaOx overgrowth by native fluoresnce. Their imaging data detected a unique blue native fluoresnce signature in RP that helped discriminate it from the CaOx overgrowth (**Figure 1.5**). Furthermore, they confirmed these findings in papillary tissue from patients with kidney stone disease. Of note, Chapters 2-4 in this body of work will demonstrate how we applied both micro CT and the aforementioned native fluoresnce modalities to further investigate CaOx stone growth and RP development.

1.6 Randall's Plaque and CaOx Stones: Animal Models

Researchers currently lack reliable animal models that closely resemble human RP and CaOx stone formation. A recent Abcc6-/- knockout mouse was recently proposed to model RP development in humans (Letavenier, 2018) (Letavenier, 2019). The ATP binding cassette subfamily C member 6 (ABCC6) gene in humans is mainly expressed in the liver and in the kidney. The protein product of the ABCC6 gene, multidrug

resistance-associated protein 6, enables the production of sources of pyrophosphate, which may be an important inhibitor of active mineralization (Letavenier, 2018) (Letavenier, 2019). Abcc6-/- KO mice exhibit nephrocalcinosis in older mice and CaP deposition adjacent to the loops of Henle and vasa recta (a striking similarity to the plaque structures observed in RP). Interestingly, the investigators detected the mineral modulators osteopontin and fetuin A in the renal mineral deposits of KO mice; these same modulators have also been detected in stone matrix and RP. These findings, along with BMP signaling and collagen mineralization in Abcc6-/- KO models further indicate osteogenic and extracellular processes associated with RP (Blazquez-Medela, 2015) (Yao,2016) (Khan, 2021).

1.7 A Commentary on the Genetics of Nephrolithiasis

To recapitulate, nephrolithiasis is an extremely complex disorder, and one theory (genetic or otherwise) will not suffice to fully explain its true etiology. Kidney stone disease is likely caused by the interaction of multiple genetic and environmental factors that we continue to actively investigate (Vezzoli, 2019) (Howles, 2019) (Howles, 2020). The prevalence of monogenic nephrolithiasis in stone clinics has been reported to be about 15% (Howles, 2020). However, for those stone former patients without a monogenic cause, the heritability rate is greater than 45%. Contemporary studies, including genome-wide association studies, have indicated several genes and molecular pathways that may contribute to the risk of kidney stone formation (e.g. Vitamin D metabolism pathways and calcium sensing receptor signaling) (Howles, 2019). Thus, there is an urgent need for a better understanding of the monogenic and polygenetic factors contributing to the risk of nephrolithiasis. Advances in this area will also aid in

the proper subcategorization of stone disease patients for optimal stone prevention management and treatment.
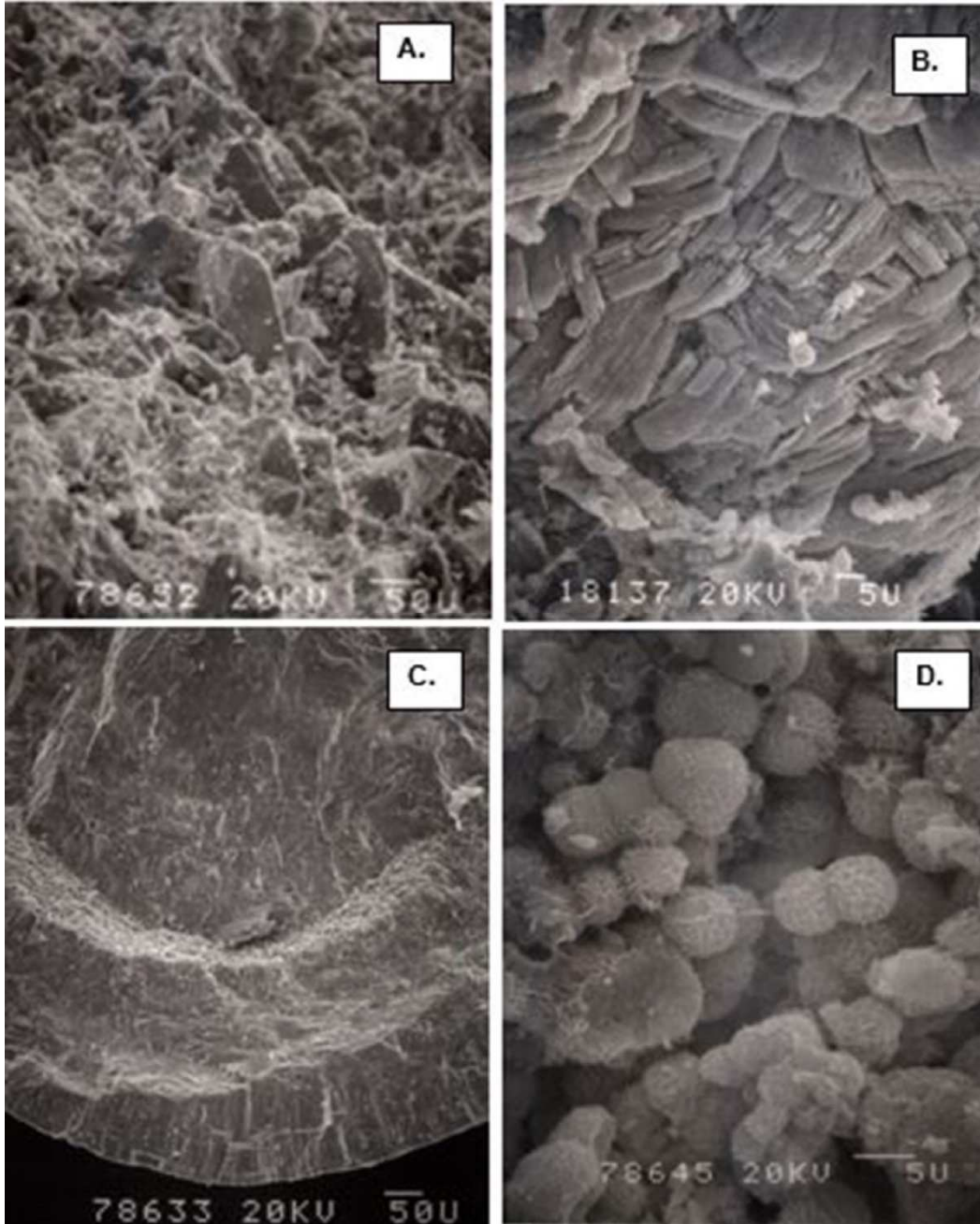
Figure 1.1: Scanning electron microscopy (SEM) of human calcium oxalate (CaOx) Kidney Stones

A. SEM image showing the ultrastructure of the surface of a CaOx dihydrate stone. **B.** Stone surface by SEM showing CaOx monohydrate crystals. **C.** Concentric laminations of COM crystals. **D.** Spherical calcium phosphate crystals (Khan, 2021).
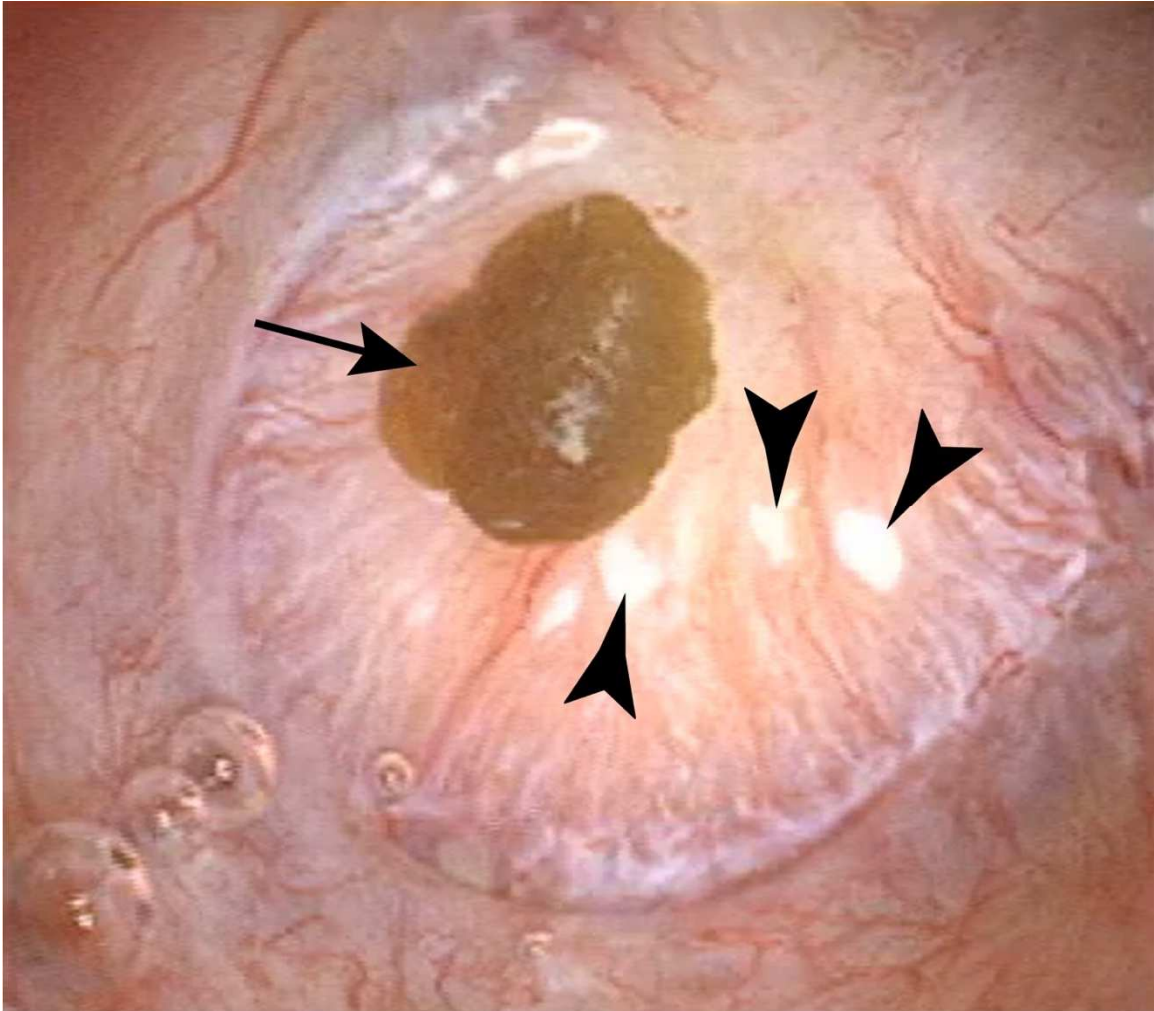
Figure 1.2: Example of a Calcium Oxalate (CaOx) growing on to interstitial Randall's Plaque (RP)

Endoscopic view of an attached CaOx stone on the renal papilla (arrow). Shown in this image are examples of RP lesions on the renal papilla of this stone patient (arrowheads).
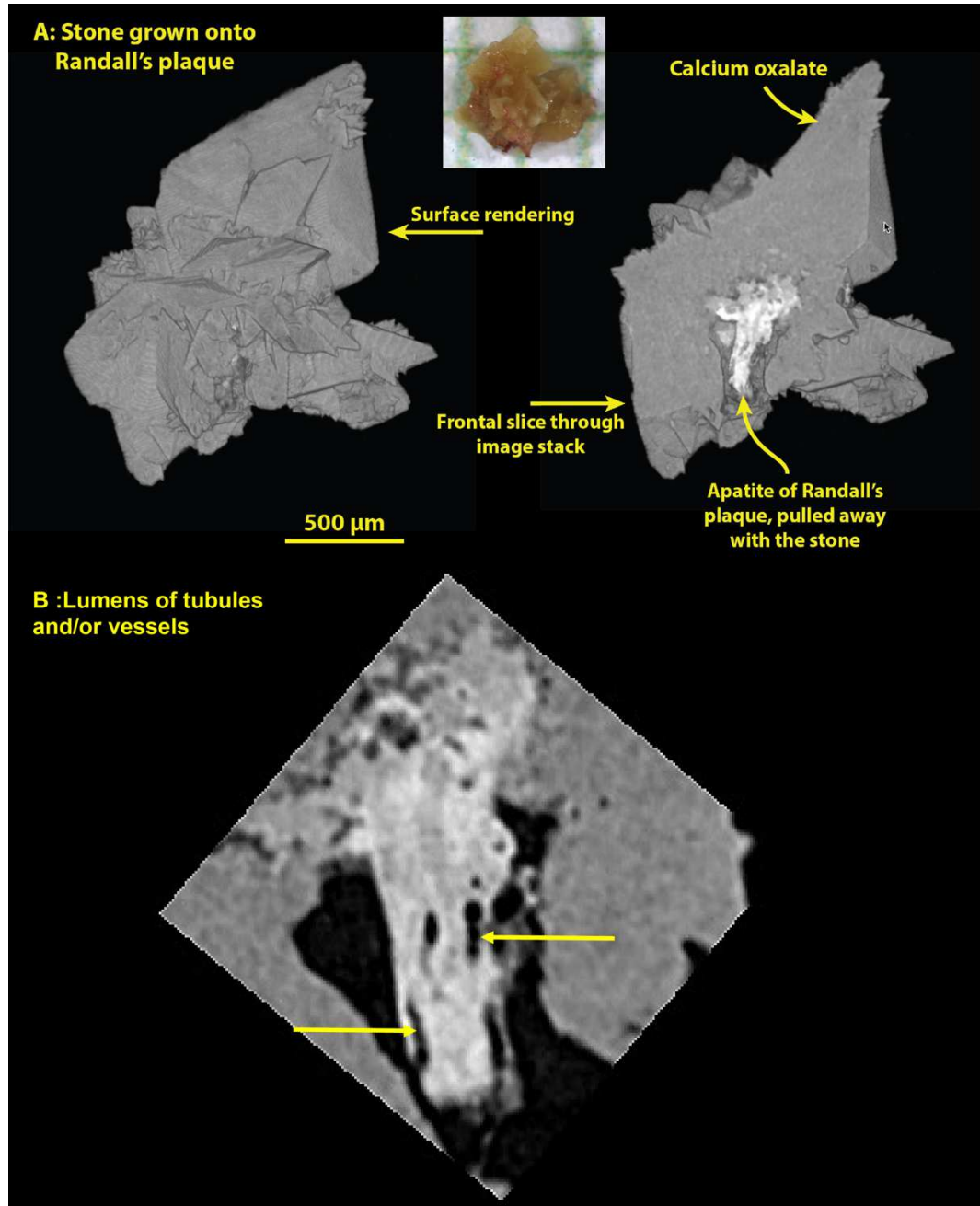
Figure 1.3: Human CaOx Stone grown on to Randall's Plaque

A. Surface rendering by micro CT reveals the microstructure of a CaOx kidney stone. A virtual frontal slice through the image stack reveals an apatite region of Randall's plaque. Evidence of the CaOx overgrowth growing on to interstitial plaque. **B.** A zoom-in of the plaque region further reveals lumens of tubules and/or vessels (arrows).
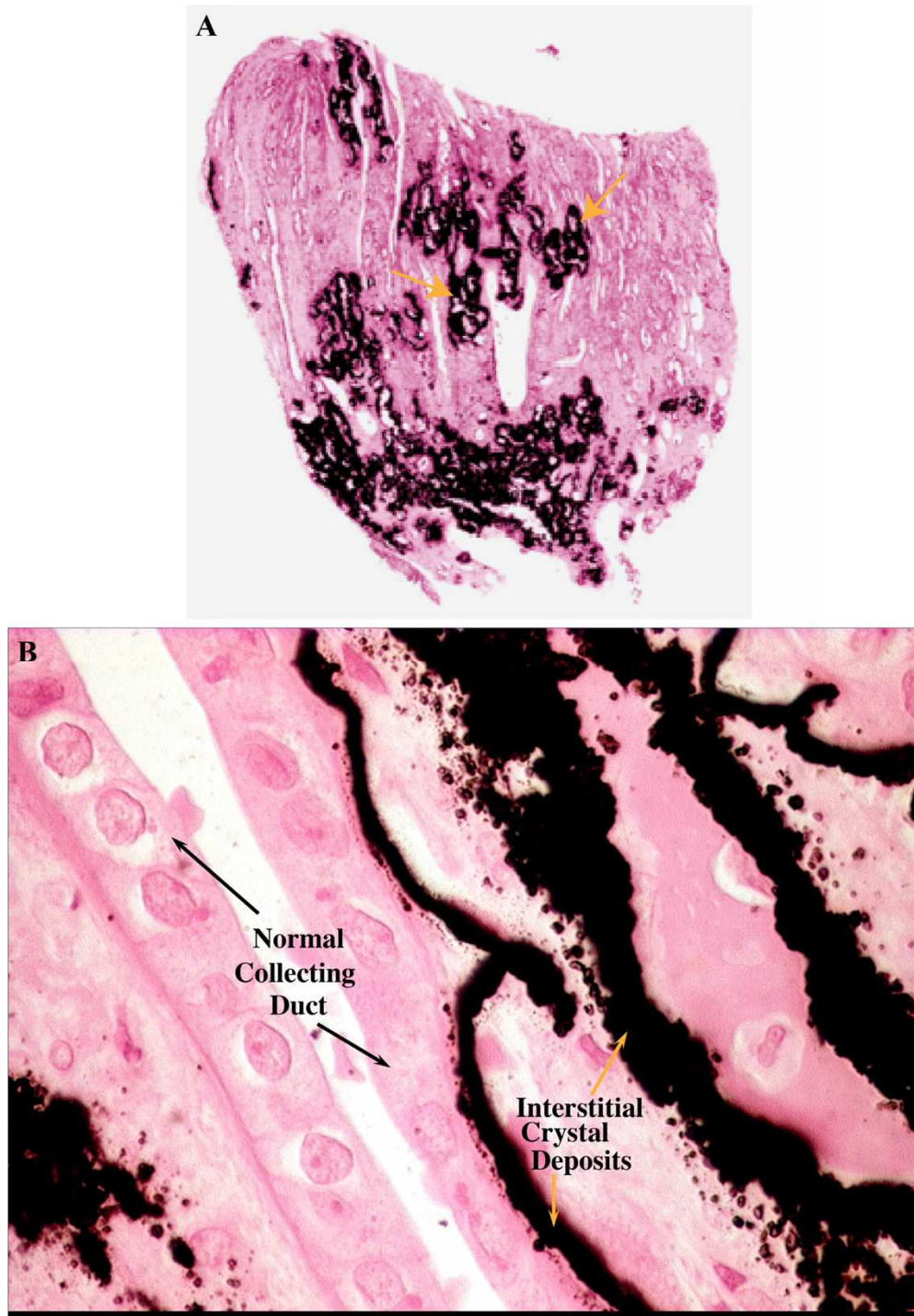
Figure 1.4: Yasue-stained section from a CaOx Stone Former

A. Low magnification microscopic image of a papillary biopsy and stained by Yasue

method to show interstitial crystal deposition (beneath the basement membranes of the

thin loops of Henle) in the CaOx stone former (yellow arrows). **B.** Note the absence of

mineral in the cells of the normal collecting duct (black arrows) (Evan, 2010).

Native fluorescence imaging of an RP stone polished to expose the Randall's plaque and CaOx monohydrate (COM) interface (Winfree, 2020).
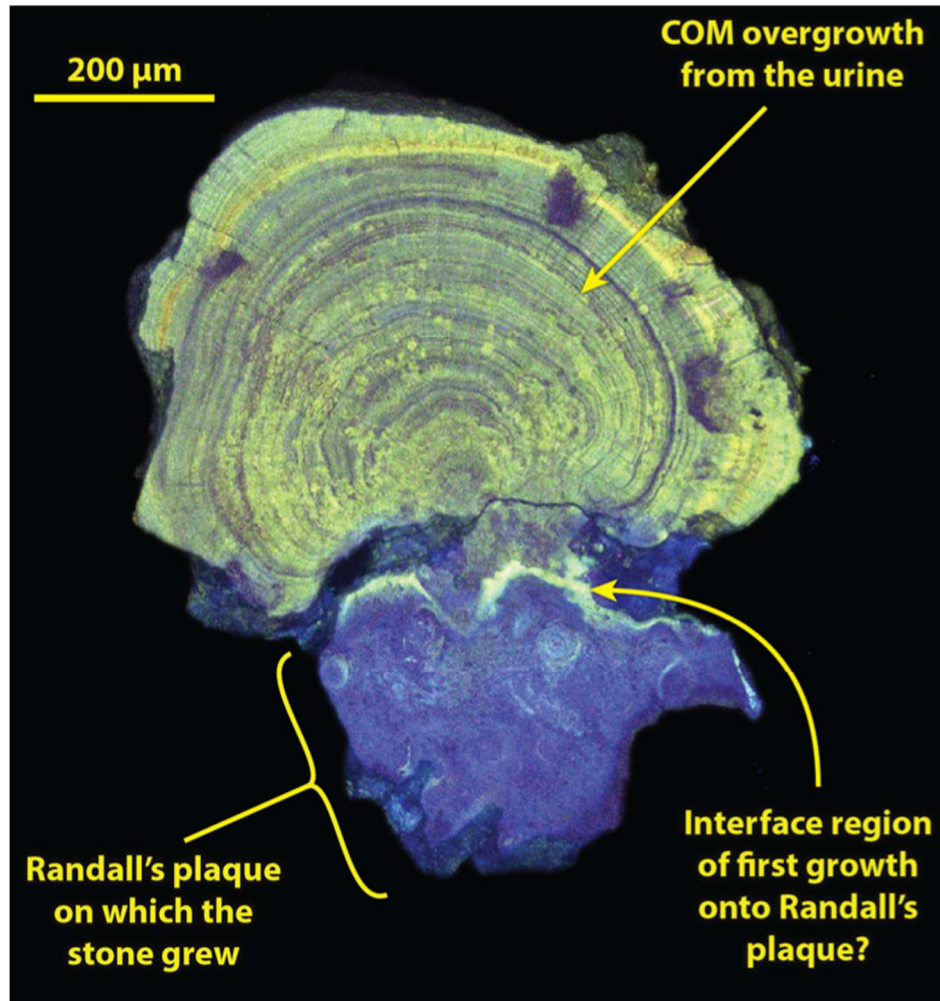
Figure 1.5: Randall's Plaque bears a unique autofluorescence signature

Chapter 2: Demineralization and Sectioning of Human Kidney Stones: A Molecular investigation revealing the Spatial Heterogeneity of the Stone Matrix

2.1 Introduction

Kidney stone prevalence continues to increase, reaching as high as 14.8%, and more than half of affected individuals will have a stone recurrence within ten years of their first episode (Khan, 2016). Health costs in the US for kidney stone treatment and management currently exceed $10 billion annually (Scales, 2016). Risk factors for nephrolithiasis—including diabetes, hypertension and obesity—are also on the rise.

Surprisingly, very little is known about the precise mechanisms of kidney stone growth. Meticulous efforts have been made to grow calcium oxalate (CaOx) stones in vitro, including control of composition and temperature over periods of weeks (Chow, 2004a) (Chow, 2004b), but the 'stones' produced consisted of fragile material that disintegrated when touched (Ananth, 2002).

The failure of inorganic solutions to produce a stone with the hardness typical of nephroliths points to some role of the organic matrix in stone formation. It has been suggested that deposition of the stone matrix is primary in forming a stone, with crystal deposition within the matrix being a secondary event (Boyce, 1968) (Boyce & Sulkin, 1956). Ultrastructural analysis of CaOx stones suggests that each mineral crystal is surrounded by a layer of matrix (Evan, 2007) (Khan & Hackett, 1993).

Proteomic analysis of CaOx kidney stone matrix has revealed the presence of over a thousand different proteins (Witzmann, 2016). How can one sort through so many possible molecules to see which ones might be fundamental for stone growth? One approach would be to find out which proteins are present in every mineral

layerhypothesizing that if a protein is fundamental to stone growth, it would necessarily always be present. The present study utilized micro CT orientation of stones during demineralization, embedment and sectioning, and subsequent analysis of matrix layers by fluorescence microscopy, immunohistochemistry, and regional proteomics using laser micro-dissection (LMD). This novel approach shows promise of being capable of distinguishing proteins that are universally present from those that occur in only some mineral layers, and thereby could identify proteins that would be candidates for possessing essential function in stone growth.

<u>2.2 Materials and Methods</u>

Stone specimens

Stones were collected during endoscopic procedures as part of an IRB-approved study (IU IRB #1010002261) or were received as cast-offs from a local stone analysis facility (Beck Analytical Services, Greenwood, IN). These stones came to us without any other patient or clinical identifiers. Stones were photographed, dried, and scanned using micro CT (Skyscan 1172 Micro CT system, Bruker-MicroCT, Kontich, Belgium) with final voxel sizes of 2-8 μm. Kidney stones reported in this paper include only those for which calcium oxalate monohydrate (COM, crystal name: whewellite) was the majority mineral. Mineral identifications were confirmed using infrared spectroscopic methods (Williams, 2010).

Kidney stone preparation and demineralization.

Kidney stones were embedded in 6-7% Knox gelatin (Kraft Foods, Northfield, IL) or HistoGel (Thermo Fisher Scientific, Waltham, Massachusetts) and scanned by micro CT to confirm orientation. Subsequently, the gel embedded stones were immersed in a 1:1 ratio of 5% paraformaldehyde (PFA) and 10% ethylenediaminetetraacetic acid (EDTA), pH 7.4, at room temperature, refreshed daily. Demineralization was deemed to be complete when the stone was invisible by micro CT (**Figure 2.1**).

Kidney stone histology

Demineralized stones were dehydrated through a series of ethanol concentrations, infiltrated, and embedded in a 1:1 mixture of Paraplast Xtra (Fisher Scientific, USA) and Peel-Away Micro-Cut (Polysciences Inc., USA). Sections were cut at 6-8 μm. Hematoxylin and eosin (H&E) and Yasue staining were used for histological analysis

(Evan, 2003). Unstained serial sections of kidney stones were also imaged by fluorescence using a Leica TCS SP8 confocal imaging system (excitation at 405 nm, 488 nm, 552 nm, and 643 nm) for native fluorescence.

Super-Resolution Auto-Fluorescence (SRAF)

SRAF imaging analyses of decalcified COM stone matrix were run in the Core Facilities of the Carl R. Woese Institute for Genomic Biology at the University of Illinois Urbana-Champaign. Images were acquired on a Zeiss LSM 880 Airyscan SRAF system (Sigavuru, 2018).

Immunostaining

Kidney stone sections were deparaffinized and rehydrated, and antigen retrieval was performed in preheated sodium citrate buffer, pH 6.0. Subsequently, sections were incubated with a sheep polyclonal antibody against human THP (THP, Millipore) and stored at room temperature overnight. THP immunoreactivity was assessed using a rabbit anti-sheep IgG secondary antibody conjugated with horseradish peroxidase (HRP) and visualized with 3,3'-diaminobenzidine tetrahydrochloride hydrate. The sections were counterstained with hematoxylin and viewed using a Leica DM3000. Sections of stones were mounted on membrane slides for the "move and cut" mode of a Leica LMD 6 microscope instrument (Micanovic, 2015).

Regional proteomics using LMD

Sections were deparaffinized and stained with either H&E or 1% methylene blue. Bulk regions of the stone matrix layers were dissected via LMD and collected in phosphate buffer. Extracted proteins were digested using Trypsin/Lysine C mix proteases and run in a Q Exactive Orbitrap High Field Liquid Chromatography/Mass Spectrometry

system. Data were searched using MaxQuant (version 1.6.10.1) and filtered using False

Discovery Rate for alpha=0.01. Hierarchical clustering analyses of these data were

conducted using the Perseus computational software (Tyanova, 2016).

2.3 Results

Micro CT visualization secures and guides proper kidney stone orientation and demineralization

Micro CT examination ensured proper stone orientation and positioning for histological sectioning. The loss of mineral density by micro CT provided a direct measure of the adequacy of demineralization. Photographic images in **Figure 2.1** shows an example of a Randall's plaque stone undergoing the process of demineralization; the stone's overall structure was maintained within the gel even after complete demineralization (**Figure 2.1C**).

Histological staining demonstrates matrix heterogeneity and confirms complete decalcification of the kidney stones

H&E and Yasue staining of kidney stone sections showed tightly packed layers in the matrix of this pure COM stone (**Figure 2.2**, H&E). Both staining methods showed heterogeneity in the density of stainable organic matrix among different layers within the stones. The absence of staining for calcium mineral in panel B (Yasue) also verified the complete demineralization of the stone indicated by micro CT.

Native fluorescence of the stone matrix reveals its molecular heterogeneity by various autofluorescent signatures

Figure 2.3 shows three different decalcified CaOx monohydrate stones taken from three different patients, imaged for native matrix fluorescence. Panel A of **Figure 2.3** shows the same stone from **Figure 2.1**, whereby the orientation of demineralized stone sections was maintained with high fidelity. The demineralized Randall's plaque displayed a unique fluorescence pattern in the far-blue region, as we have previously

described in mineralized plaque (Winfree, 2020). The CaOx surrounding the plaque region showed multiple matrix layers of differing intensities and fluorescence emission spectra, suggesting molecular heterogeneity in the composition of the matrix. The specific autofluorescent signatures of each, plaque and CaOx stone overgrowth regions, describes the unique molecular makeup of the calcified papillary interstitium and the calyceal urine-containing space. Furthermore, panels B and C show two additional CaOx stones with varied native fluorescent signatures, pointing to the molecular heterogeneity within the organic matrix of COM.

The examination of a sectioned, decalcified CaOx stone using super-resolution auto-fluorescence (SRAF) imaging (Sigavuru, 2018) is shown in **Figure 2.4**. The filamentous nature of the matrix and its heterogeneity is further revealed by the high-resolution SRAF optics (**Figure 2.4, D-H**).

Immunohistochemical staining

Kidney stone sections were also stained for Tamm-Horsfall Protein (THP), the most abundant of the urinary proteins, as shown in **Figure 2.5**. Our results consistently showed a pattern of alternating THP-rich (black arrowheads) and THP-absent layers within the stone matrix of CaOx kidney stones.

Regional proteomics using LMD

The process of LMD of a CaOx stone specimen is illustrated in **Figure 2.6A**. The average area of LMD samples for proteomic analysis was 1.64×10^6 μm^2, and these samples yielded an average of 629 distinct proteins. When concurrent proteomic analysis was performed with approximately 100 mg of CaOx stone powder, we identified 464 of those 629 proteins. Label-free quantitative analysis showed a strong correlation in

relative protein abundance between LMD and pulverized stone samples (**Figure 2.6B**),

thereby validating the LMD-based proteomics approach. Table 1 summarizes the twenty

most abundant proteins in both LMD and pulverized CaOx kidney stone samples from

the hierarchical clustering analysis from **Figure 2.6C**.

2.4 Discussion

The work described here illustrates an innovative method to study the kidney stone matrix and to explore its molecular (organic) content. Although investigators have previously demonstrated the feasibility of demineralizing and sectioning kidney stones to study the organic matrix (Chow, 2004a), we not only optimized this histological technique but extended its utility by methodically applying two novel and critical techniques: 1) micro CT was used to assess the degree of stone demineralization and, more critically, for the precise positioning and orienting of the nephroliths for histological sectioning, and 2) laser micro-dissection was used for analyzing specific regions of interest of the stone matrix. Moreover, we demonstrate the advantage of these innovative methodologies by yielding significant proteomic data with laser micro-dissected samples and demonstrate strong proteomic correlation in agreement with pulverized stone samples. The ability to apply histochemical and proteomic techniques to kidney stones enables an in-depth molecular interrogation that has not been demonstrated before and should aid in understanding the initiation and propagation of stone growth.

The organic matrix in CaOx stones appears to be heterogeneous. This is particularly apparent in the fluorescence images (Figures 2.3 and 2.4), indicating that the nature of the matrix can be different in adjacent layers. Of note, a mixed kidney stone with majority uric acid composition also demonstrated apparent heterogeneity by histologic staining and autofluorescence (**Figure 2.7**). The preliminary work with immunohistochemical analysis for THP—the most abundant of the urinary proteins (**Figure 2.5**)—showed that layers of stone matrix could be either devoid of or rich in

THP (**Figure 2.8**). This suggests, then, that THP is unlikely to be a urine protein that is essential for the growth of a stone, as it was undetectable in some layers of the stone.

The number and diversity of proteins found in these preliminary studies using LMD sections is consistent to what has previously been published for larger stone specimens (Witzmann, 2016). The presence of such a large number of different proteins in stone matrix is yet to be explained, but it is possible that many proteins in urine may become part of stone matrix in a non-specific manner. It has been proposed that certain proteins are key in the formation of a stone (Boyce, 1968), and that others may simply accumulate through long-term exposure of the stone to urine (Witzmann, 2016). If this is the case, then it will be important to sort out which proteins are key, and which are simply adventitious.

The proteomic analysis of LMD sections from demineralized stones opens the possibility of analysis of specific layers within a single stone. Such work should be able to identify proteins that are present in all stone layers. Such proteins would then be candidates for focused study of their effects on mineral deposition, perhaps using one of the modern methods that allows microscopic monitoring of mineral growth, in vitro (Singh, 2017).

2.5 Conclusions

Future studies of stone matrix will aid in describing the mechanisms of mineral and organic layer deposition. Spatial mapping of the stone proteome will undoubtedly lead to a better understanding of stone initiation including renal anchoring mechanisms (i.e. Randall's plaque and/or ductal plugging). Thus, utilization and optimization of these novel techniques can begin to unlock the mysteries of CaOx mineral initiation and propagation.
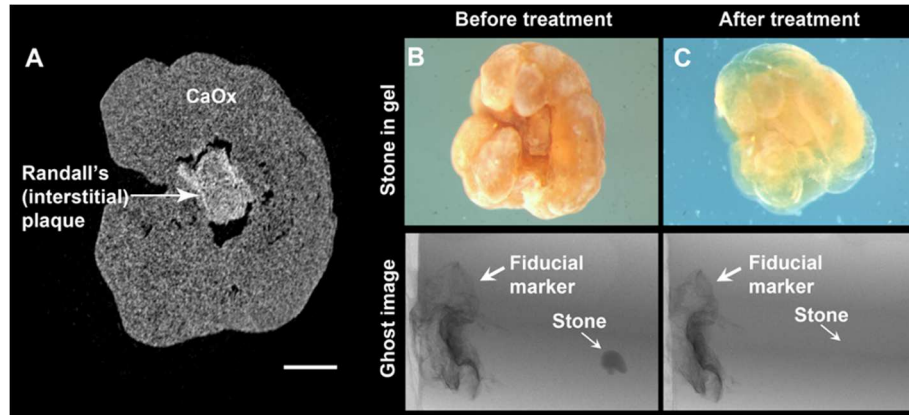
Figure 2.1: Micro CT ensures proper orientation and positioning of a Randall's plaque stone for histology and accurately assesses mineral loss

A. A Micro CT slice showing the appearance of a stone attached to Randall's (interstitial) plaque. Scale bar = 250 µm. CaOx: calcium oxalate (which, in this case, was pure CaOx monohydrate, COM). Photographic images (upper portions of panels **B** and **C**) show the stone's overall structure within a gel before and after demineralization. The lower panels of **B** and **C** show the before and after micro CT "ghost" images of a CaOx stone on Randall's plaque undergoing decalcification, with no visibility by micro CT at the end of the process. This stone came from a patient who underwent bilateral ureteroscopy for multiple renal stones. The patient was a 78-year-old male, with a history of passing stones. Urine was typical for a CaOx stone former, with multiple 24-hour collections averaging 2.9L volume, pH 6.61, Ca of 278 mg, oxalate of 35 mg, citrate >1200 mg, and a supersaturation for CaOx of 4.7 and for CaP of 1.6.
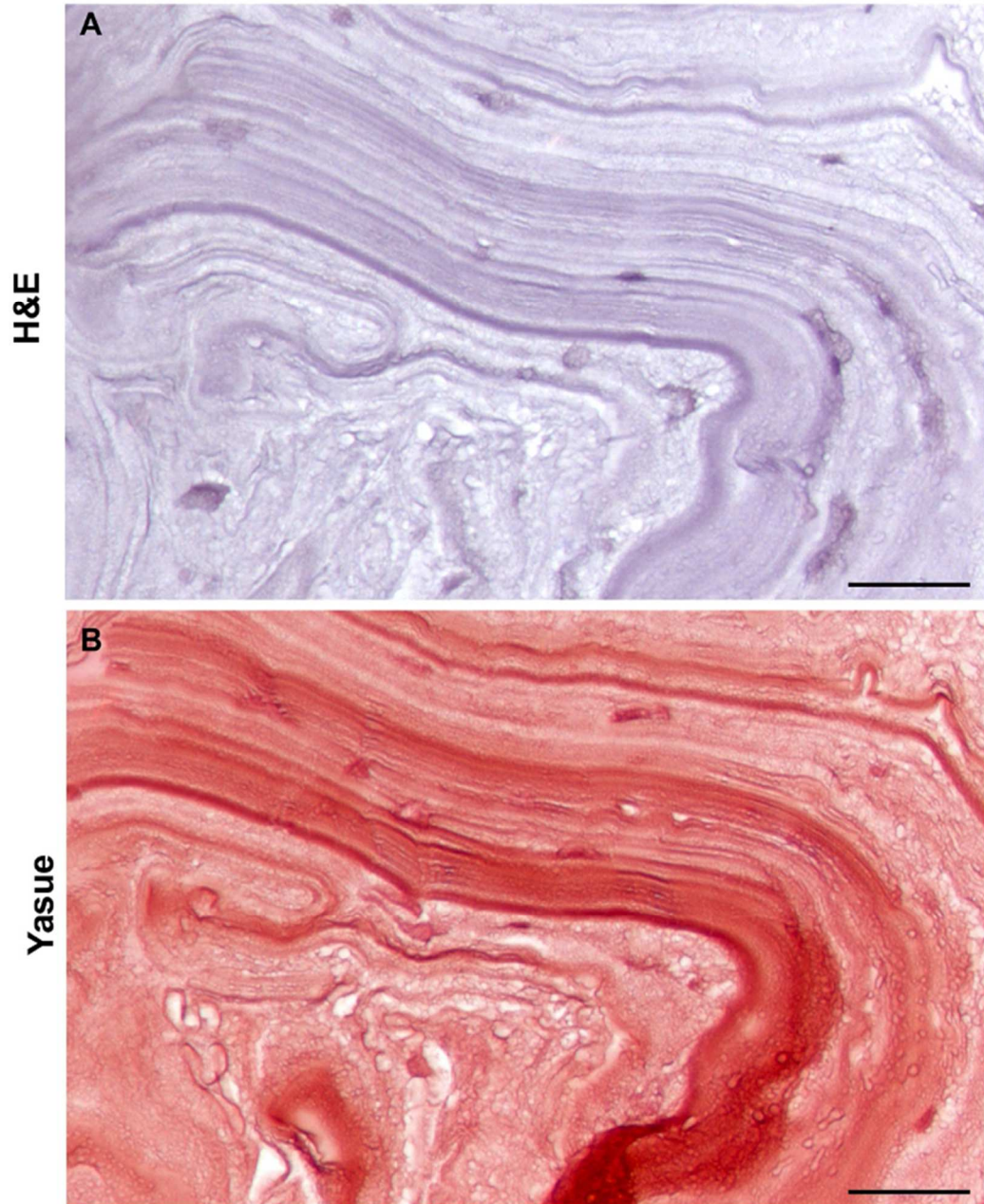
Figure 2.2: H&E and Yasue staining show stone matrix heterogeneity

A. H&E of a decalcified COM stone showed evidence of matrix heterogeneity. The various levels of staining intensities among the tightly packed layers suggests differences in organics throughout the matrix. **B**. Yasue staining also clearly depicts matrix heterogeneity. Additionally, this staining technique verifies complete demineralization of

the stone as indicated by micro CT. Scale bars = 50 µm. This specimen came to us de-

identified.
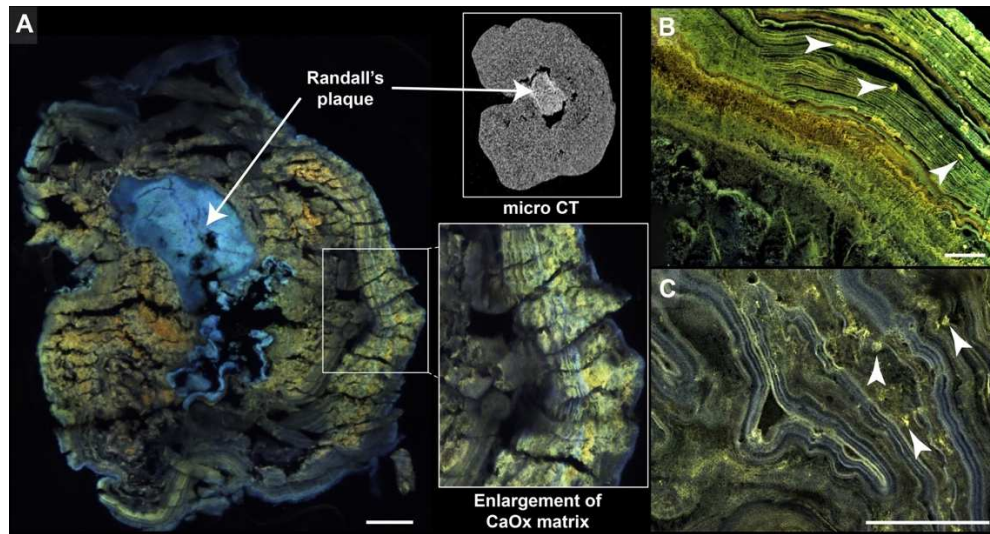
Figure 2.3: Heterogeneity of native fluorescence in stone matrices

A. The decalcified stone (from Figure 2.1) displayed fluorescence in the far-blue region in the area that used to be apatite rich (Randall's plaque). The upper right inset shows a micro CT slice of the stone prior to demineralization, in approximately the same plane as the histologic section. The lower right inset shows an enlargement of the CaOx matrix layers of differing intensities and colors. **B**. The stone matrix in this panel depicts different levels of fluorescence intensities and colors from; additionally, microscopic organic aggregates can be appreciated (white arrowheads). **C**. Fluorescent aggregates (white arrowheads) can also be seen in the matrix of this stone. Further, this stone possessed pronounced differences in fluorescence color between adjacent layers, indicating evident heterogeneity in matrix composition. Stone specimens in panels **B** and **C** are from two other patients (both de-identified). Scale bars = 100 μm.
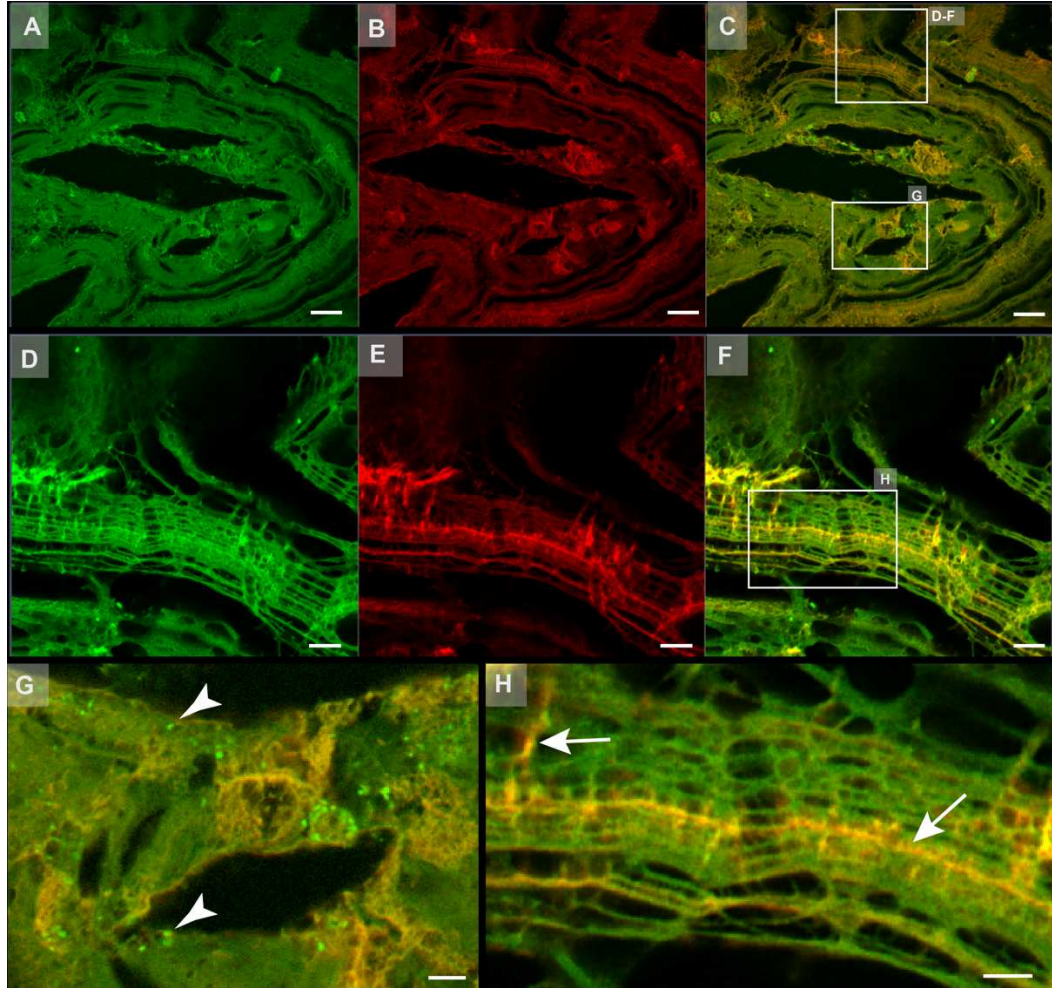
Figure 2.4: Super-resolution auto-fluorescence (SRAF) imaging renders finer resolution of the heterogeneous stone matrix

A. Low-power SRAF image of a CaOx stone matrix (blue-405 nm excitation, 420-480 nm emission channel pseudo-colored green, scale bar = 20 µm). **B**. Low-power SRAF image (red-561 nm excitation, 575-615 nm emission channel pseudo-colored red). **C**. Merged images of A and B. **D**. High-power SRAF image of D-F box in C (blue-405 nm excitation, 420-480 nm emission channel pseudo-colored green, scale bar = 5 µm). **E**. High-power image of box D-F box in C (red-561 nm excitation, 575-615 nm emission channel pseudo-colored red). **F**. Merger of D and E. **G**. Enlargement of box G in C with merged images of blue and red channels pseudo-colored green and red, respectively.

Arrowheads indicate organic aggregates entrapped within the stone matrix (scale bar = 5 µm). H. Enlargement of box H in F merged images of blue and red channels pseudo-colored green and red, respectively. Arrows indicate locations of green and red channel overlaps indicating heterogeneity within the filamentous stone matrix (scale bar = 5 µm). Although the bulk of this specimen was composed of COM, the polygonal shapes of the empty spaces in panels A through C suggest the previous presence of the dihydrate form of CaOx.
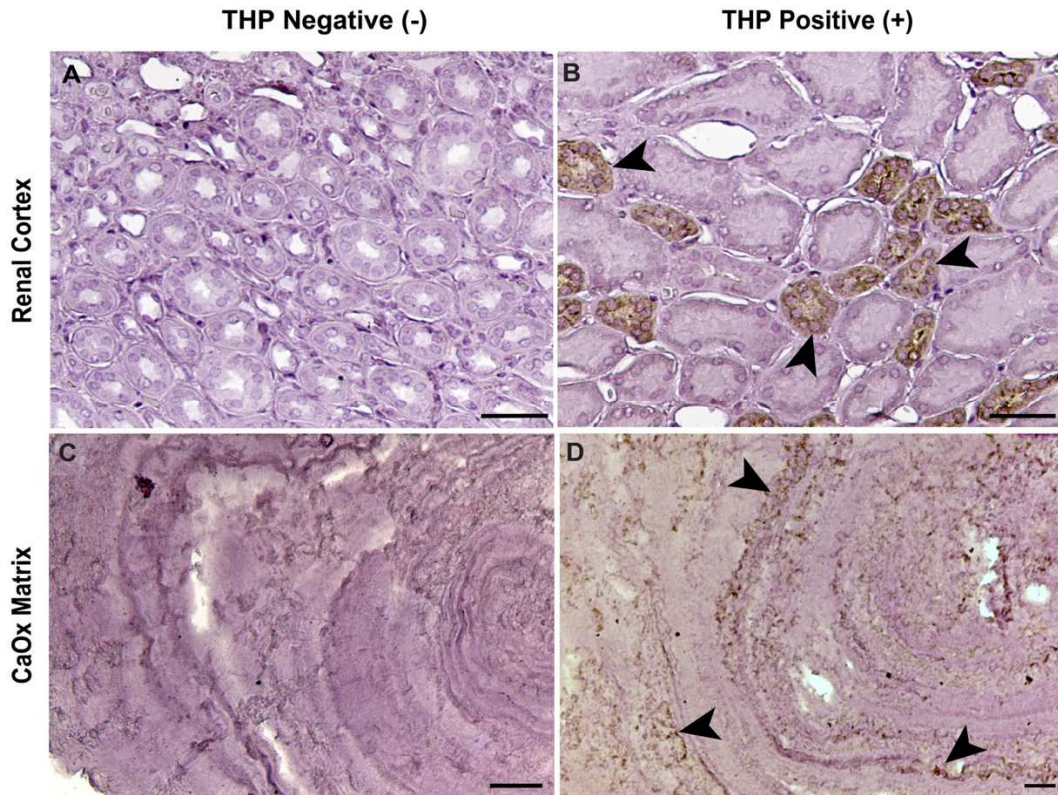
Figure 2.5: Alternating layers of THP in the stone matrix is revealed by immunohistochemistry of CaOx stone matrix

No primary antibody controls (Panels **A** and **C**). Panel **B** shows THP reactivity (black arrowheads) in the thick ascending limbs (TAL) of a human kidney section (renal cortex). Immunohistochemistry staining of CaOx stone matrix with THP shows THP-rich layers (black arrowheads) and THP-absent layers in the matrix of decalcified CaOx stones (Panel **D**). Scale bar = 50 μm. This specimen had a mixed composition, (86% calcium oxalate monohydrate [COM], 7% uric acid and 7% apatite). The patient had undergone bilateral percutaneous stone removal, and 24-hour urine analyses averaged 1.8L volume, pH of 6.10, Ca 241 mg, oxalate 49mg, citrate 747mg, with supersaturations of 8.1 for CaOx and 1.38 for CaP.
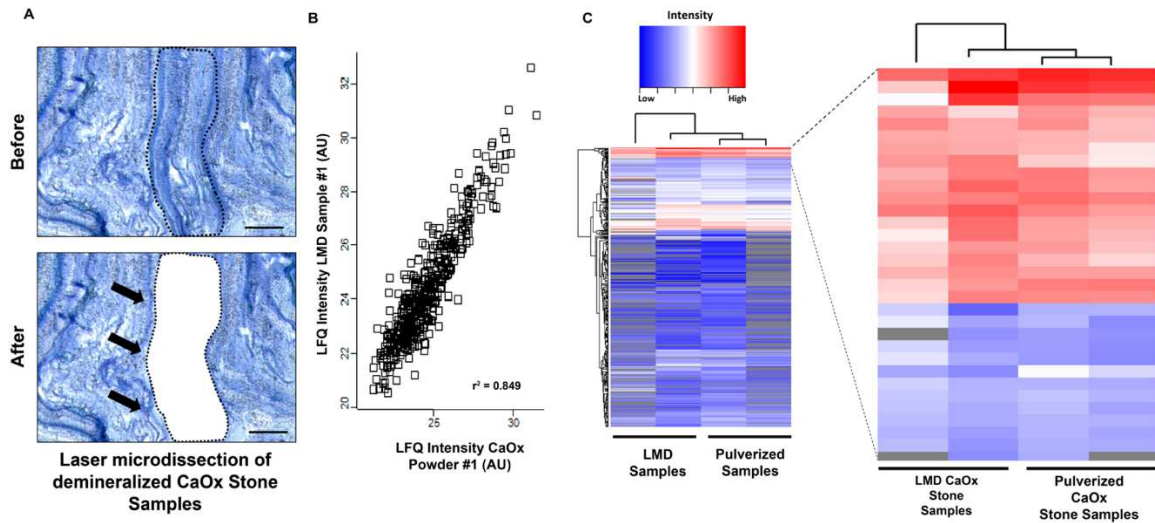
Figure 2.6: Laser microdissection facilitates the proteomic spatial mapping of CaOx stones

A. The process of laser microdissection (LMD) is illustrated in the before and after (black arrows) panels for protein extraction (scale bar = 50 µm). **B**. Proteins identified in CaOx stone powder and LMD sections plotted against one another by their relative label-free quantitation value (LFQ). AU, arbitrary units. **C**. Unsupervised hierarchical clustering highlighting the most abundant proteins identified in both LMD and pulverized CaOx stone samples.

The twenty most-abundant Proteins Identified in both LMD and Pulverized CaOx Stone Specimens
Hemoglobin subunit beta (HBB)
Hemoglobin subunit alpha (HBA2)
15-hydroxyprostaglandin dehydrogenase [NAD$^+$] (HPGD)
Fatty Acid Synthase (FAS)
Uromodulin (UMOD)
Myosin-9 (MYH9)
Osteopontin-D (SPP1)
Tubulin Beta chain (TUBB2C)
Heat shock protein HSP 90-alpha (HSP90AA1)
Tubulin alpha chain
Complement C3 (C3)
Fibrinogen alpha chain (FGA)
Vitamin K-dependent protein Z (PROZ)
Heat shock protein HSP 90-beta (HSP90AB1)
Fibrinogen gamma chain (FGG)

Table 2.1: The twenty most-abundant Proteins Identified in both LMD and Pulverized CaOx Stone Specimens

The proteins identified are listed in order of abundance based on their LFQ value by unsupervised hierarchical clustering. Note that THP (also known as uromodulin) is among the top five proteins identified.

Stained Stone Matrix　　　　**Unstained Stone Matrix**

H&E — A

Yasue — B

Native Fluorescence — C
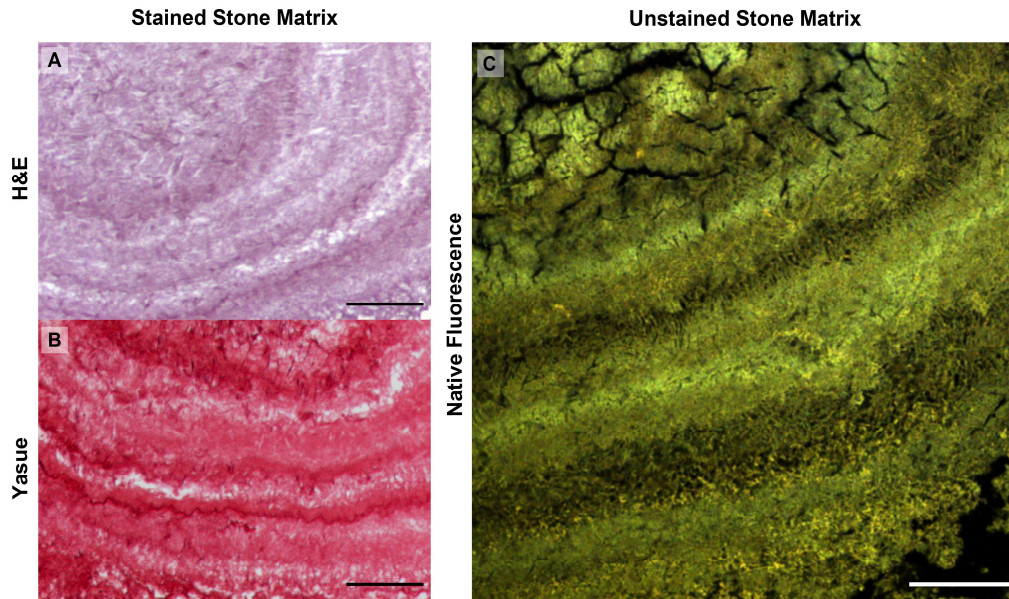
Figure 2.7. Decalcified uric acid kidney stone sections showing heterogeneity by histology staining and native fluorescence imaging

The mixed kidney stone was composed of 74% uric acid and 26% CaOx. H&E and Yasue (**A** and **B**) staining reveals nonuniformity within layers of the uric acid stone matrix. **C**. Native fluorescence imaging shows further diversity in structural composition of the matrix layers. Scale bar = 100 μm.

THP Negative (-)   **THP Positive (+)**

Uric Acid Stone Matrix
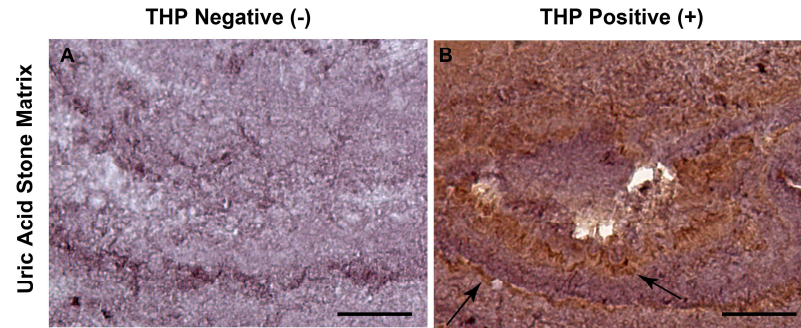
Figure 2.8. Immunohistochemistry experiments reveal alternating layers of THP of the mixed CaOx and uric acid stone matrix

A. No primary control. **B**. Mixed CaOx and Uric acid matrix contains alternating layers of THP (black arrows). Scale bar = 50 µm.

Chapter 3: Human Jackstone arms show a Protein-Rich, X-ray Lucent Core, suggesting that Proteins drive their Rapid and Linear growth

3.1 Introduction

Jackstones are rare urinary stones that contain elongated protrusions (spines, or jack arms) from their center body. These were reported in bladder stones as early as 1860 (Price, 1860) but the 'spines' in this case did not apparently contain calcium oxalate (CaOx). A later report from 1895 described CaOx stones with sharp thorny processes or spines in varying numbers, extracted from the kidney or from the bladder (Ord & Shattock, 1895). Subsequent publications on jackstones have consisted mainly of case reports (Perlmutter, 2002) (Singh, 2011) (Subasinghe, 2017) (Carneiro, 2020).

To our knowledge, there have been no reports offering a detailed analysis of jackstones or a hypothesis attempting to explain their peculiar growth and morphology. Here, we report observations on 98 jackstones from 50 human stone specimens. Using non-destructive micro-computed tomography (micro CT) and infrared spectroscopy (IR), we report the predominant mineral composition in these stones and highlight novel findings concerning the cores of the jack arms. This paper aims to provide a comprehensive view of the nature of jackstones, their mineral and organic composition, as well to propose a potential molecular hypothesis to explain their peculiar morphology (Canela, 2021).

3.2 Materials and Methods

Source of urinary stones

Jackstones were identified as having protrusions from the body of the stone that were longer than they were wide. Most of the jackstones in this study were found in specimens discarded by a local stone analysis facility (Beck Analytical Services, Greenwood, IN). These specimens were marked as being of human origin but came to us without any other identifiers. We also found 3 jackstones among patients from an ongoing study of stone formers, all of which were consented for approved study (IRB protocol #101000226). These stones were of renal origin, collected during percutaneous nephrolithotomy procedures. Finally, we include one large, renal jackstone that was taken via robotic pyelolithotomy, as a case study.

Micro-computed tomographic imaging (micro CT)

Stones, all dried in air at room temperature, were scanned using a Skyscan 1172 micro CT system (Bruker-MicroCT, Kontich, Belgium) at 60kVp, 0.5-mm Al filter, for a final voxel size of 6-13 μm (Williams, 2010). The one exception to this procedure was a very large renal jackstone, which was scanned using a Skyscan 1176 micro CT system with a 33 μm voxel size. Image stacks from micro CT were viewed using Image J (Schindelin, 2012).

Spectroscopic verification of mineral

Following micro CT reconstructions, small portions of each specimen were taken using a sharp blade. Stone portions were ground with potassium bromide and analyzed using Fourier-transform infrared (FT-IR) spectroscopy using the traditional pellet method (Williams, 2010) on a Bruker Alpha-T Spectrometer.

44

Demineralization and histologic section

Jackstones were subjected to a demineralization process previously described [9]. Briefly, selected jack arms were mounted in HistoGel (Thermo Fisher Scientific, Waltham, Massachusetts) and rescanned by micro CT to verify orientation. The jack arms were then demineralized using a 1:1 ratio of 5% paraformaldehyde (PFA) and 10% ethylenediaminetetraacetic acid (EDTA), pH 7.4, over several nights at room temperature with the solution being replaced daily. Micro CT was used to track the demineralization process and the process was complete when the jack arm was invisible by micro CT (Canela, 2021).

The demineralized jackstones were dehydrated through a series of graded ethanol concentrations and then embedded in paraffin. Serial sections were cut at 6-8 μm for histology and immunohistochemistry analysis. Deparaffinized and unstained serial sections of jack arms were imaged for native fluorescence on a Leica TCS SP8 confocal imaging system (excitation at 405, 488, 552, and 643) (Canela,2021) (Winfree, 2021).

Immunohistochemistry

Paraffin-embedded human kidney and jackstone arm sections were deparaffinized and rehydrated. For antigen retrieval, slides were incubated in a preheated sodium citrate buffer solution (10mM sodium citrate, 0.05% Tween 20, pH 6.0) for 60 minutes. Following antigen retrieval, sections were treated with sheep polyclonal antibody against human Tamm-Horsfall protein (THP, Millipore) at a 1:200 dilution and stored at room temperature overnight. THP immunoreactivity was assessed using rabbit anti-sheep IgG secondary antibody conjugated with horseradish peroxidase (HRP) and visualized with 3,3'-diaminobenzidine tetrahydrochloride hydrate (DAB) (Sigma-Aldrich). The sections

were counterstained with hematoxylin and viewed under a Leica DM3000 microscope (Leica Microsystems). Optical densities were measured using mean gray values obtained from color deconvolution images of DAB-labeled tissue in Image J (Crowe and Yue, 2019) (Seyed, 2017). Squares of fixed area (1296 μm^2) were measured for average gray value over core and shell regions using a fixed spatial grid to reduce selection bias.

Statistics

Data are presented as mean ± standard deviation. For optical densities, multiple measurements were grouped using nesting by patient specimen and tested for effect of region (core or shell) using standard linear regression modelling in JMP Pro 15 (SAS Institute, Inc, Cary, NC).

3.3 Results

A total of 98 jackstones were identified in 50 patient specimens (**Table 3.1**), with an average of 2.0±0.4 jackstones per patient specimen (range of 1-14 jackstones per specimen). The jackstones had on average 4.2±0.4 arms (range 1-14 arms per stone), and the arms were on average 1.5±0.1 mm in diameter (range 0.5-6.3 mm, measured at the midpoint along length of each arm). The major mineral in all of these specimens was calcium oxalate, and primarily of the monohydrate form (COM).

The one-arm jackstone in **Figure 3.1** illustrates the findings typical for the 98 jackstones. Panel A shows a photomicrograph of the jackstone on millimeter paper and panel B a slice through the micro CT image stack. The radiolucent center in the body of this stone was not uncommon in the 98 jackstones we examined (seen in 42 of the 98 jackstones) but the radiolucency along the core of the arm was seen in every arm of every jackstone (**Tables 3.1 and 3.2**). It was also typical that a 'bulb' of radiolucency marked the base of each jack arm (arrowhead in **Figure 3.1B**). The radiolucent core of jack arms also frequently contained thin layers of mineral that spanned the radiolucent core.

The mineral layers within the radiolucent core were sometimes composed of apatite (which is seen easily using micro CT [Williams, 2010] [Williams, 2017]), as in **Figure 3.1B**, where they are seen as white layers along the core of the jack arm. In other jackstones, there was little apatite within the radiolucent core. For example, one of the jack arms in the renal stone illustrated in **Figure 3.2** showed no apatite by micro CT, and the other arms showed only one or two layers of apatite scattered along the axis of each arm. However, all of these jack arms did have thin layers of calcium oxalate spanning the

47

radiolucent core, all curved with their convex surface pointing toward the tip of the jack arm.

The three study patients in which jackstones were found (including the stone in **Figure 3.2**) were typical of recurrent CaOx stone formers (**Table 3.2**). Briefly, all three patients were undergoing percutaneous stone removal, and all had considerable stone burdens and multiple stones. Only one jackstone was found in each patient. All patients showed ductal plugging and dilated ducts in their renal papillae (Borofsky, 2016) (Rivera, 2016). The patients showed no signs of urinary tract infection. Serum and urine values were unremarkable. One patient showed endoscopic signs of medullary sponge kidney in some calyces, but the jackstone was found in the renal pelvic space.

Figure 3.3 (A-C) shows the largest jackstone in this study. This stone originated from a kidney with substantial hydronephrosis and was collected during a robotic pyelolithotomy procedure. The specimen included 9 non-jackstones, all of which were smooth surfaced, and rather round, with some flattened surfaces suggesting they likely had been packed together. None of these 9 stones showed any evidence of jack arm growth by micro CT. This was typical for the specimens in which we had multiple stones; the non-jackstones tended to be CaOx type Id (**Figure 3.3C**) (Daudon, 2020) and showed no hint of arm formation by micro CT.

In 55% (54/98) of the jackstones studied, the thickness of the jack arm shell tapered with distance from the stone body. This tapering is consistent with the radial growth of the jack arm being faster than the rest of the stone, such that the newly formed tip of the arm would be younger than the rest of the stone and thus have a thinner deposition of CaOx. In most of the specimens (56 of 98) layers could be observed in the

stone to extend from the stone body only partway out onto the jack arms (as in **Figure 3.1B**), suggesting that when those layers were deposited, the arm was of shorter length. Layers above this (presumably newer layers) extended out further onto the jack arms. (We note that all stones showed growth layers visible by microscope upon dissection, but the resolution of the micro CT was not sufficient to discern growth layers in some of the pure COM stones.) These observations together argue that the shape of the jackstone could be accounted for by the arm length growing at a faster radial rate than the stone body.

Three jack arms were also studied in histologic section following demineralization. **Figure 3.4** shows such a section imaged for native fluorescence. Note that the relatively protein-poor shell of the arm delaminated as mineral was removed, while the higher protein content of the core allowed it to fix more readily. The core of the arms showed greater magnitude of native fluorescence than did the shell, which is consistent with the core containing a larger quantity of organic material. This higher content of organic material—which always has a low X-ray attenuation value—would explain the low X-ray attenuation of the cores in jack arms.

A few sections were also stained for THP, as shown in **Figure 3.5**. The cores of the jack arms showed on average a 1.6-fold enrichment of THP staining in comparison to the shell regions ($p<0.0001$).

3.4 Discussion

We have shown that jackstone arm protrusions consist of x-ray lucent cores surrounded by classic layers of COM extending outward from the body of the stone. The jackstones included in this study bear at least one protrusion that was longer than it was wide.

The shape of the jackstone is remarkable. Arms extend out from the stone body typically at right angles to the stone surface. One way this shape could be achieved would be by having the entire stone grow on a star-shaped template. With this hypothesis, the mystery of the jackstone morphology would be explained by the initial formation of a template with arms, perhaps from aggregation of urinary proteins. The observations in this study do not support this hypothesis. While the jack arms invariably contained a core of X-ray lucent material, this core did not extend into the center of the stone body; rather, our results suggest that an X-ray lucent core of the jack arm typically began as a mass of X-ray lucent material deposited on to the early surface of a stone of typical shape (a nascent jackstone calculus), thus allowing growth of the jack arm from there.

The radial growth of the jack arms is indicated by two observations. First, in stones in which layers were distinctly visible by micro CT, it was common for early layers on the stone body to be contiguous only partway out onto the jack arms. Then, layers outside this would be contiguous further out on the jack arms. This appearance strongly suggests that the tips of the jack arms grew out at a radial rate faster than did the body of the stone. Similarly, the thickness of the shell regions on jack arms (as well as the total arm diameter) tended to diminish with length away from the stone body, which also is consistent with the tips of the arms being younger than the arm bases.

Jackstones invariably had straight arms. This is a remarkable observation; for example, the renal stone in **Figure 3.3** would certainly not have had unlimited volume in which to grow, even within a hydronephrotic kidney, and the non-jackstones collected with it showed flattened sides that suggest that they had been packed together. The jackstone in **Figure 3.1** is from a specimen that included 14 jackstones and 25 non-jackstones, and all of the non-jackstones showed flattened sides. This suggests that all of these stones had been packed together rather tightly, and yet the jack arms were remarkably straight, with their directional growth apparently unaffected by the presence of closely packed stones on all sides. Contrarily, the renal stone in **Figure 3.2** was constrained within a calyx of normal size, its arms extended straight out from the stone body and apparently formed singly. These observations raise the possibility that the deposition of a particular composition of matrix may serve as the initiation site for the growth of a jack arm. It is plausible that protein aggregates with specific macromolecular adsorption capabilities preferentially bind to certain areas on the crystal surfaces of nascent jackstone calculi (Boyce, 1968) (Leal, 1977) (Khan, 1983) (Khan & Hackett, 1984) (Khan, 1993). However, the differences between jackstones that grow among other packed calculi and those that grow without packed stones remain unknown. Of note, the micro CT studies on the non-jackstones did not show radiolucency cores. Further, infrared studies of the non-jackstones confirmed the same major mineral type as in the jackstones in all cases.

How is it that the jack arm grows more rapidly than the stone body? Our findings are consistent with the hypothesis that the core of the jack arm becomes surrounded by layers of mineral that allow for the addition of new organic material (probably protein)

from the urine only at the tip of the jack arm, and that the addition of this material at the tip of the jack arm would then drive its linear growth (**Figure 3.6**). A possible driver of this directionality might be physical abrasion, either with other stones or with the wall of the urinary space. If a mass of protein were to deposit onto the surface of a stone and then be coated by a thin layer of calcium oxalate, the most likely place for abrasion to remove mineral from the mineral-coated mass would be at the point most distant from the body of the stone (i.e. tip of the jack arm). This, then, would be the place where more protein would bind to the existing protein mass, extending its dimensions away from the stone body. Subsequently, addition of another layer of mineral would thicken the mineral on the unabraded sides of the initial protein mass, while leaving the tip farthest from the stone body most susceptible to repeated abrasion damage. With such a cycle, protein(s) from the urine that preferentially bound to the existing protein core—which episodically would have the thin mineral covering its tip abraded away—would extend the protein core away from the stone body.

The organic nature of the X-ray lucent core of the jack arm is supported by some of our additional observations. IR analysis typically showed richer protein levels in core samples as opposed to shell pieces. Microscopic imaging of demineralized histological sections of jack arms demonstrated an intensely fluorescent core compared with the outer shell of compact COM layers. The fluorescence of the core is consistent with an enrichment of organic material in this area in comparison to the surrounding COM layers. Furthermore, immunohistochemistry studies using THP showed supportive results (**Figure 3.5**). THP is a unique glycoprotein exclusively expressed in the kidney, specifically in the distal renal tubular cells lining the thick ascending limbs (Jaggi, 2007)

(El-Achkar, 2013). Proteomic studies on urinary stones have also demonstrated the abundance of THP in pulverized and LMD stone samples (Canela, 2021) (Witzmann, 2016) (Wesson, 2019). We undertook this part of the study simply to see if a very abundant urine (and stone) protein would show any differential distribution between jack arm core and shell. Our results demonstrated that THP showed greater signal in the radiolucent core of jack arms than in the mineral-rich shell. However, our immunohistochemistry experiments could not test whether THP was enriched relative to other proteins and is thus, a critical caveat in our study.

Another inherent limitation to our study is that most of our calculi came to us unidentified. Thus, we are unable to provide a precise report on the number of jackstones originating from either bladder or kidney. However, based on the analyses conducted on the known renal jackstones and comparing them to the others in our collection, we were unable to detect inner structural or compositional differences.

3.5 Conclusion

We studied a large collection of human jackstones and found that they were composed of COM but that the jack arms invariably contained a radiolucent core that was rich in organic material, apparently protein. Micro CT visualization of growth layers showed that the jack arms grew at a faster radial rate than their respective bodies, with the jack arms extending in a straight direction. We propose that there are proteins in the core of the jack arms that drive this peculiar growth. Discovery of these proteins could provide clues as to how urinary stones, in general, grow in size.
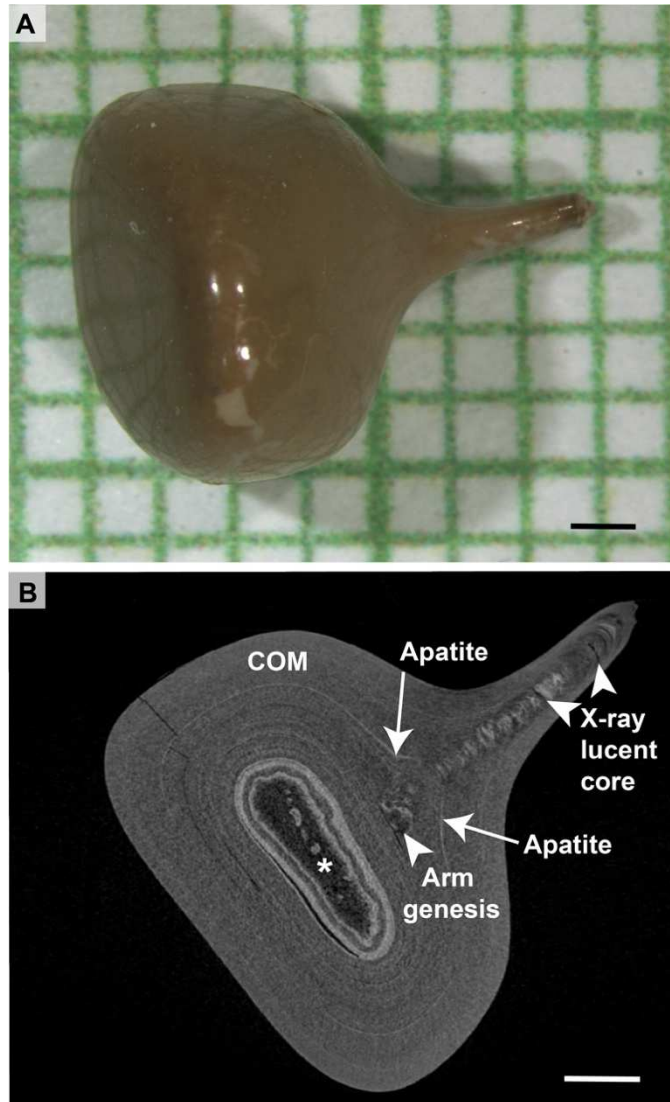
Figure 3.1: Jackstones possess radiolucent cores within their distinctive arm protrusions

A. Representative jackstone with one arm protrusion on millimeter (mm) paper. **B**. Micro CT slice showing the center of the stone and core of the jack arm. The center of this stone has an X-ray lucent region (dark) which probably indicates a protein-rich, mineral-poor region (white asterisk). This dark region is surrounded by layers of apatite which then give way to nearly pure calcium oxalate monohydrate (COM) appearing in light gray by micro CT. The beginning of the jack arm apparently is the X-ray lucent area marked with

55

a white arrowhead (Arm genesis). The core of the jack arm (white arrowheads) has

alternating dark regions (protein-rich) and X-ray bright lines (apatite), and both the

enrichment of protein and the presence of apatite were verified by infrared spectroscopy

(FT-IR). Layering of this stone, seen most easily in the apatite layer indicated by the

white arrows, moves from body of stone out onto the jack arm, indicating that the arm

grew at a faster rate than did the body of the stone. This stone was 1 of 14 jackstones in a

patient specimen that included an additional 25 non-jackstones. Note the flattened surface

of the stone opposite to the jack arm, suggesting that this stone was packed rather tightly

among the other stones as they grew. Scale bars = 1 mm
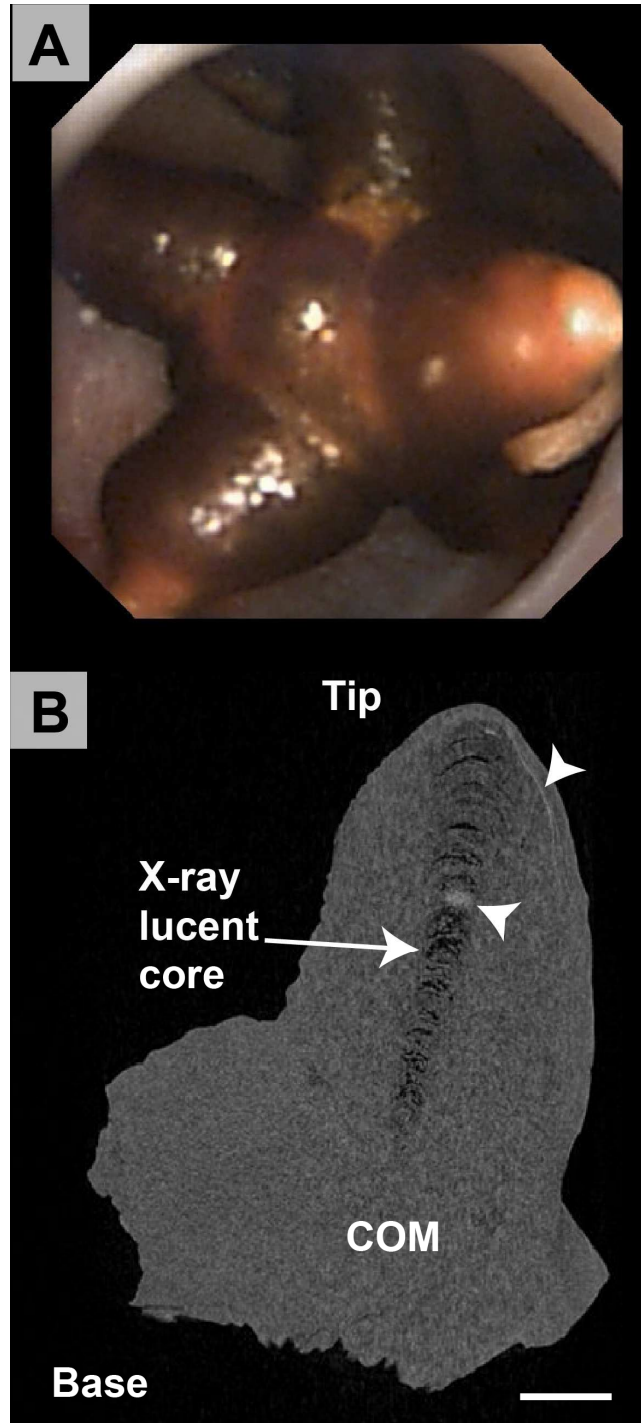
Figure 3.2: Jackstone found in a renal calyx of a stone patient

A. Ureteroscopic view of a seven-arm jackstone in a renal calyx; the calyx is

approximately 1 cm across. **B**. Micro CT image slice of one of the arms from A, which

shows a radiolucent core (white arrow) and minimal traces of apatite (white arrowheads)

within what is predominantly calcium oxalate monohydrate (COM) mineral. Scale bar = 500 μm
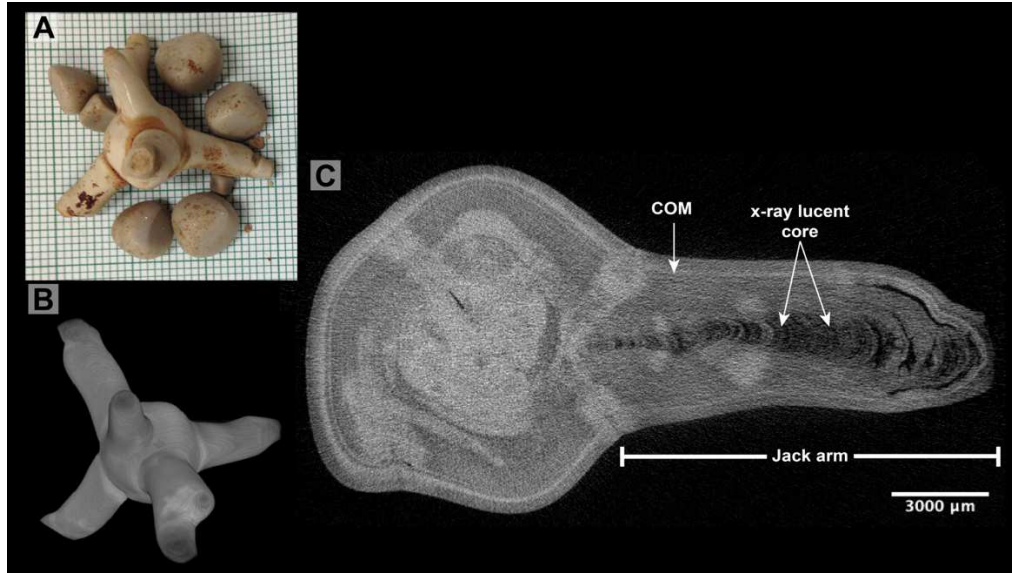
Figure 3.3: Very large renal jackstone taken during robotic pyelolithotomy

A. Photomicrograph of entire stone specimen on mm paper. The jackstone is about 3 cm wide; none of the smaller stones collected in the same region of the kidney showed jack arms. **B.** Surface rendering of jackstone, from micro CT (rotated up and slightly to the left in comparison to orientation in A to show all 5 arms). **C.** Slice through micro CT image stack to show the characteristics of one of the jack arms.
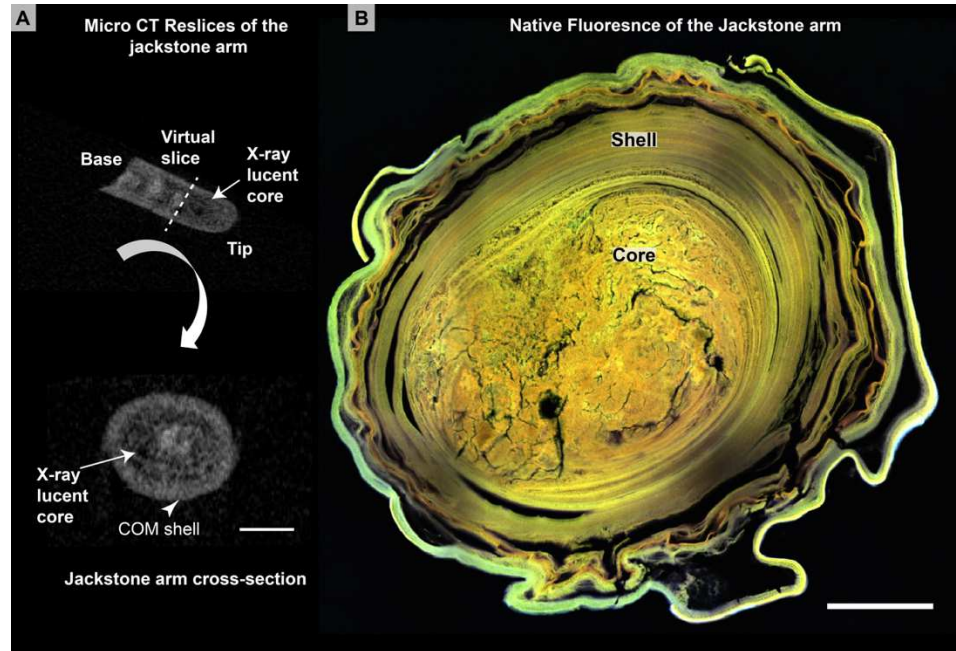
Figure 3.4: Cross-section of a jackstone arm using micro CT and fluorescent microscopic methods

A. Micro CT of the jackstone arm before demineralization and sectioning alongside its virtual cross section. Scale bar = 500 μm. **B.** A maximum projection image showing the native fluorescence of the jackstone arm cross-section; a core region glows brilliantly with autofluorescence compared to the shell region. The disaggregation of layers, especially in the shell, is apparently due to a lack of adequate protein for fixation as mineral was removed. The core of the arm showed less collapse, which also points to it having a richer protein content than in the COM shell. The highly bright outer regions outlining the cross section may possibly be depicting a higher protein content in those areas or, more likely, an edge artifact. Scale bar = 200 μm
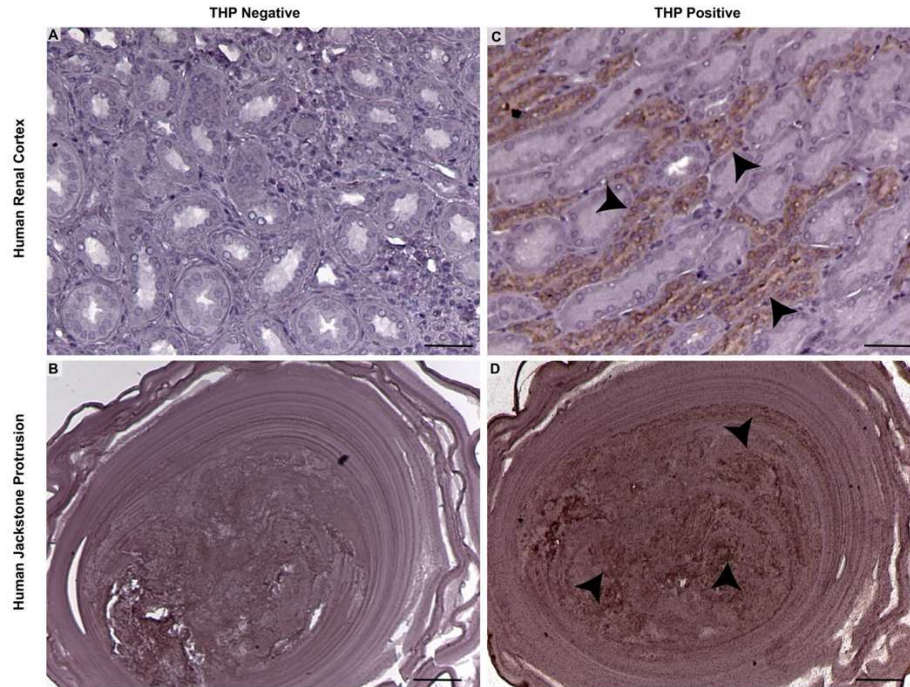
Figure 3.5: Immunohistochemistry showed that THP content was richer in the jackstone core region than in the COM shell

Negative controls (**A & C**, scale bars = 50 µm) of human renal tissue and a demineralized jackstone cross-section showed no positive reaction with the secondary antibody in the absence of antibody to Tamm-Horsfall protein (THP). Panel **C** shows a successful positive control of THP in human renal tissue, with thick ascending limbs staining brown for THP (black arrowheads). Panel **D** shows THP aggregation (black arrowheads) in the core of the jackstone protrusion (**B & D**, scale bars = 100 µm). All samples were counterstained with hematoxylin. Note that immunohistochemistry experiments did not show distinction between an inner and outer core as in Figure 3.4.
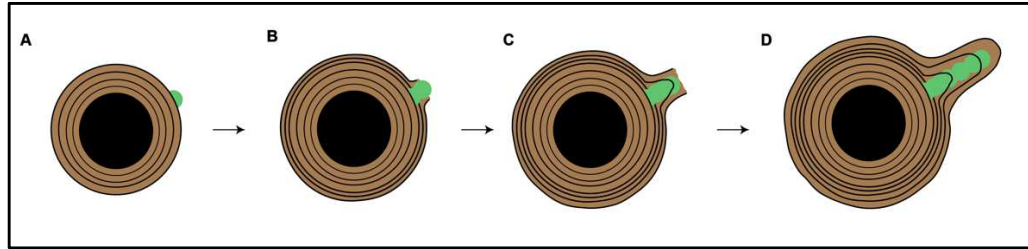
Figure 3.6: Hypothesis for growth of a jackstone arm

A. The initial deposition of specific urine protein aggregates (green mass) on to the surface of a calcium oxalate monohydrate (COM) stone. **B** and **C.** Preferential binding of additional urine protein aggregates permits the laying down of additional and nascent COM layers around the stone and the protein aggregate, allowing for arm growth and extension. **D.** As more urine proteins deposit on to the protrusion, more COM layers are laid allowing the arm to grow at a faster rate than the stone body.

Jackstone Specimen Data

Specimen	Number of Jackstones	Average # of Arms	Average arm diameter (µm)	Predominant Mineral Type
6238	1	10	1362	COM
16162	1	3	1517	COM
25961	2	2	755	COM
29638	1	1	1424	COM
40107	1	6	1078	COM
41165	1	6	818	COM
41222	1	3	1611	COM
48658	1	3	1465	COM
66118	1	2	1902	COM
69008	1	14	928	COM
98287	1	3	1334	COM
99835	1	3	1063	COM
100828	1	6	1271	COM
100860	1	2	700	COM
101277	1	1	3698	COM
101763	1	1	2320	COM
104304	1	3	1846	COM
118247	1	10	1712	COM
123451	1	2	1295	COM

130934	2	4	1675	COM
141335	1	1	1083	COM
146118	1	5	1382	COM
146193	1	5	752	COM
147033	1	8	1046	COM
149268	2	3	987	COM
157517	1	12	2097	COM
105308	1	1	3639	COM
143180	3	2	1024	COM
144902	2	1	1128	COM
158364	5	4	1259	COM
26346	1	5	724	COM
40502	1	5	500	COM
41966	1	6	919	COM
4593	2	3	1663	COM
5612	1	3	1421	COM
588092	1	3	2526	COM
89601	1	4	1125	COM
93642	1	2	1044	COM
KRP296b	1	7	1647	COM
KRP384	1	4	857	COM
KRP385B	1	2	1893	COM
P1301	14	2	928	COM

P1302	1	11	6295	COM
P1315	4	4	1032	COM
P1316	2	4	1019	COM
P1352	1	5	4649	COM
P1364	6	4	797	COM
P1370	9	2	1912	COM
P1386	8	5	690	COM
P1400	1	2	1463	COM

Table 3.1: Jackstone Specimen Data

List of the jackstone specimens studied by micro CT. The average number of arms and

average arm diameter are listed in the table above. The jackstones appeared to be

composed, predominantly, of calcium oxalate monohydrate (COM) by micro CT.

Clinical and Surgical Data on Patients with Jackstones

	Patient 1 (Figure 3.2)	Patient 2 (KRP384 in Table 3.1)	Patient 3 (KRP385 in Table 3.1)
Age	71	67	62
Sex	F	F	M
Body mass index	47	19	46
Age at first stone	63	16	39
Number of procedures	4	6	3
Hypertension	Yes	no	No
Diabetes	Yes	no	No
Medullary sponge	no	Yes	No
Surgery	perc	perc	perc
Number of jackstones	1	1	1
Number of stones removed	21	17	6
Volume of stones/kidney (mm^3)	196	139	360

Stones on Randall's plaque	0	0	0
Stone apatite % (by volume)	18	6	0.1
Plugging score (average)	1	2	0.67
Pitting score (average)	0	0.33	0
LoC score (average)	0	0.17	0.33
RP score (average)	0.67	0	0.33
% plugging (average)	0.8%	2.1%	2.3%
% Randall's plaque (average)	0.8%	0.0%	0.5%
#papillae with dilated ducts/kidney	1	5	1
Stone culture	—	no growth	no growth
Urine culture	—	no growth	no growth
Serum creatinine (mg/dL)	0.9	0.9	1.1

Serum calcium (mg/dL)	9.4	9.8	9.2
Serum uric acid (mg/dL)	6.5	4.2	6.8
24-hour urine volume (L)	2.1	2.2	1.2
24-hour urine pH	5.8	5.7	5.4
24-hour urine citrate (mg)	672	193	484
24-hour urine calcium (mg)	293	130	101
24-hour urine oxalate (mg)	44	31	53
24-hour urine sodium (mEq)	238	114	197
24-hour urine CaOx supersaturation	8.6	5.1	7.3
24-hour urine brushite supersaturation	0.8	0.2	0.4

Table 3.2: Clinical and Surgical Data on Patients with Jackstones

Perc, percutaneous nephrolithotomy. Stone voluments, percent apatite, and Randall's plaque identification done by micro CT (Williams, 2015). Papillary scores (Plugging, etc.) by Borofsky method (Borofsky, 2016). Papillary plugging and plaque surface area percentages as in Rivera et al. (Rivera, 2016).

Chapter 4: Collagen fibrils and cell nuclei are entrapped within Randall's Plaque but not in CaOx matrix overgrowth: A microscopic inquiry into Randall's Plaque Stone Pathogenesis

4.1 Introduction

It is estimated that one-in-eleven people in the United States will have a kidney stone event in their lifetime, and more than half of those individuals will have stone recurrence within ten years of their first episode (Scales, 2016). Kidney stones have been associated with an increased risk of end-stage renal failure, chronic kidney disease and metabolic syndrome (Hung CT, 2020) (Johri, 2010). Currently, there are limited treatments or preventative measures for kidney stone disease (Moe OW 2011 and Khan, 2021).

Approximately 80% of all kidney stones are composed of calcium oxalate (CaOx), yet very little is known about the precise mechanisms underlying CaOx stone formation (Worcester 2010) (Williams & McAteer, 2013) (Bird & Khan, 2017). Previous research suggests that as many as half of all CaOx patients grow their stones on interstitial Randall's plaque (Daudon 2015, Linnes 2013). Randall's plaque is commonly described as the calcium phosphate deposition in the renal papillary interstitium (Randall 1937 and Evan 2003). Though the growth of CaOx stone on Randall's plaque was described decades ago, the actual process by which CaOx stone formation occurs on Randall's plaque remains unknown. It is widely accepted that part of this process involves the breaching of the renal papillary epithelium, exposing interstitial calcium phosphate plaque to urinary proteins (Evan 2007 and Khan 2015); but the mechanisms by which this breach occurs remains elusive. When urinary molecules come in direct contact

with the interstitial plaque, the plaque can serve as a nucleation site for overgrowth of CaOx. As a result, CaOx stone layers grow onto Randall's plaque and the nascent stone remains anchored to the renal papilla and probably can grow episodically (Williams 2017). As CaOx stones grow larger, they can cause symptoms while they remain anchored to the papilla or when they detach and become lodged in the renal calyceal space, pelvis, or ureter (Cifuentes, 1987).

Study of the interface where urinary molecules deposit onto exposed Randall's plaque has been very limited. Evan et al. describe sections of two stones taken as biopsy specimens (where stones were still anchored to papillary tissue); one of these was demineralized and studied using electron microscopy and the other was partially demineralized and studied using light and infrared microscopy methods (Evan, 2007). Sethmann et al. studied the plaque overgrowth region of a cleaved stone using scanning electron microscopy (Sethmann, 2017). The observations from these studies were largely focused on the minerals found within this region.

We conducted an interrogation on Randall's plaque stones using recently developed methodologies that enable controlled orientation of a nephrolith during decalcification and sectioning (Canela, 2021). The objective of this work is to describe the microenvironment of Randall's plaque that had nucleated stone growth, explore its molecular composition and to differentiate interstitial plaque from CaOx overgrowth (Canela, 2021).

4.2 Materials and Methods

Randall's plaque stone source

Randall's plaque stones were collected from patients during surgery (percutaneous nephrolithotomy or stone removal by ureteroscopy) (**Table 4.1**). A standard protocol for the study of kidney stone patients approved by the Indiana University (IU) Institutional Review Board (IRB) committee (IRB protocol #1010002261) was followed throughout the present study.

Micro CT imaging

Dry Randall's plaque stones were photographed and scanned using micro-computed tomographic (micro CT) imaging to verify and determine the presence of plaque and stone mineral composition. The stones were scanned using a Skyscan 1172 micro-CT system (Bruker-MicroCT, Kontich, Belgium) at 60kVp, 0.5-mm Al filter, for a final voxel size of 4-8 μm (Williams 2021).

Demineralization

Randall's plaque stones were embedded in HistoGel (Thermo Fisher Scientific, Waltham, Massachusetts) along with a fiducial marker and rescanned by micro CT to confirm stone orientation (Canela, 2021). The embedded stones were then fixed and demineralized with 5% paraformaldehyde (PFA) and 10% ethylenediaminetetraacedic acid, pH 7.2-7.4. Demineralization was carried out at room temperature on a shaker at low speed, and the solution was replaced daily. Micro CT was used throughout this process to track the demineralization and to confirm its completion (Canela, 2021). After stones became transparent by micro CT, they were kept in 5% PFA, at 4ºC, prior to histological processing and sectioning.

Staining and imaging of demineralized stones

Decalcified stones were dehydrated through a series of graded ethanol concentrations and then embedded in paraffin. Paraffinized and unstained (label-free) sections of stones were imaged by fluorescence on a Leica TCS SP8 imaging system; and multiphoton excitation at 910 nm for second harmonic generation (SHG) imaging was used for collagen detection (Ferkowicz, 2021). Subsequent staining of human renal tissue and demineralized stone sections were deparaffinized, permeabilized with 0.05% Triton X-100 and stained using 7-aminoactinomycin D (7-AAD) (Thermo Fisher Scientific, Itasca, Illinois, USA) or 4',6-diamindino-2-phenylindole (DAPI) (Vector Laboratories, Burlingame, CA, USA) for DNA detection. Additional sections were stained by routine hematoxylin & eosin (H&E) methods. Observations were all done in triplicate, except where noted.

Immunofluorescence

Immunofluorescence imaging was also used for detection of vimentin (VIM) and the leukocyte common antigen or cluster of differentiation 45 (CD45) in kidney cortical and Randall's plaque stone sections. Paraffin-embedded slides of kidney and stone sections were deparaffinized, rehydrated with graded ethanol concentrations and then incubated in preheated sodium citrate buffer solution (10mM sodium citrate, 0.05% Tween 20, pH 6.0) or in Antigen Unmasking Solution (REF# H-3300) (Vector Laboratories) for 1 hour. Sections were blocked in 10% normal donkey serum for at least 1 hour at room temperature, followed by primary antibody or conjugated-primary antibody incubation at room temperature overnight. Antibodies used included Anti-Vimentin Antibody (Santa Cruz Biotechnology, Inc., Dallas, TX; SC-66002), and

purified anti-human CD45 Antibody (BioLegend, San Diego, CA; cat# 304002) conjugated to Alexa Fluor ® 488. Sections were then washed with phosphate-buffered saline with 0.05% Tween 20. Vimentin treated sections were probed with Alexa® dye-conjugated secondary antibody, anti-mouse-647 and washed again with phosphate buffered saline with 0.05% Triton X. Vimentin treated sections were counterstained with DAPI; CD45 treated sections were counterstained with 7-AAD. Following final washes with phosphate-buffered saline, sections were mounted with glass coverslips using ProLongTM Glass Antifade Mountant, (Thermo Fisher Scientific, Waltham, MA; REF# P36980).

Micro CT analyses of our Randall's plaque (RP) stone specimens showed moderate x-ray attenuation in the spaces of lumens of vessels and/or tubules (Williams 2017). **Figure 4.1A** shows a 3D reconstruction using micro CT of a Randall's plaque stone (Patient 1 from **Table 4.1**) before demineralization (**Figure 4.1** panel A). The same stone was embedded in HistoGel and completely demineralized in panel B (**Figure 4.1B**). RP orientation was achieved with the aid of fiducial markers despite the loss of mineral and protein in both plaque and organic matrix during treatment. No mineral was detectable by micro CT after the demineralization treatment, yet the overall structure of the stone was retained.

The demineralized unstained sections of Randall's plaque stones were analyzed by autofluorescence. The results consistently showed that the plaque region that was apatite-rich exhibited endogenous fluorescence in the far-blue spectrum (**Figure 4.1C**, white arrowhead) as opposed to the CaOx overgrowth which appeared mostly with yellow and green fluorescence range (Winfree 2020). Notice the artifactual void between the outer edge of the stone and the remainder of the overgrowth (white arrows); it appears that most of the organic matrix from the CaOx overgrowth region had pulled away from the gel, perhaps as a result of the dehydration process before paraffin embedment.

Figure 4.2 (panels A and B) shows two additional Randall's plaque stones. Each panel shows different slice orientations of demineralized Randall's plaque along with its corresponding higher magnification in the image inset (**Figure 4.2A** and **4.2C**). The two Randall's plaque stone sections were examined for fibrillar collagen using SHG imaging. Both Randall's plaque stones demonstrated collagen enrichment exclusively within areas

of decalcified Randall's plaque by SHG (**Figures 4.2B** and **4.2D**). Stones analyzed by SHG showed variability in the amount of surface area covered by collagen. From the six different Randall's plaque stones assessed using SHG imaging, all six consistently showed collagen fibrillary bundles exclusively in regions of Randall's Plaque.

Following confirmation of the autofluorescence pattern and presence of collagen within demineralized Randall's plaque stones, sections were tested for the presence of cell nuclei. Traditional hematoxylin and eosin (H&E) and staining with 7-AAD or DAPI revealed cell nuclei in areas of demineralized Randall's plaque but not in the regions of CaOx matrix overgrowth (**Figure 4.3**). **Figure 4.3** shows three examples of the cell nuclei observed in our demineralized Randall's plaque stones. The first section (**Figure 4.3A**) is an example of the same Randall's plaque stone shown in **Figure 4.2A** and **Figure 4.2B**. This plaque region presented with a highly enriched area of cell nuclei. **Figure 4.3B** shows a different Randall's plaque stone showing cell nuclei on the edge of the plaque region. The 7-AAD positivity was observed exclusively in the area that was highly-auto fluorescent in the RP blue-channel but not in the CaOx overgrowth region. The cell nuclei in panel A appear to be in close proximity to one another and oval in shape. The Randall's plaque stone section from patient 2 showed markedly less 7-AAD positivity (**Figure 4.3B**); the nuclei were few in number, found only at the edge of the plaque, and appeared not as close to each other as the former example. The third section in **Figure 4.3C** shows an enlarged region of cell nuclei stained with DAPI in a Randall's plaque stone from patient 4. These nuclei also appear relatively close together in proximity as opposed to those in **Figure 4.3B**.

Subsequent to our cell nuclei discovery in plaque, we sought to begin the characterization of these plaque-entrapped cells. **Figure 4.1** shows plaque nuclei staining positive for either vimentin or CD45. In **Figure 4.4A** and **4.4B**, we show DAPI positive nuclei with variable vimentin expression in a Randall's plaque stone section. Additionally, **Figure 4.4D** and **4.4E** depict 7-AAD positive cell nuclei with CD45 positive expression in a Randall's plaque stone section.

The data presented in this paper offer a novel method to study plaque and stone formation. By performing high resolution imaging of human Randall's plaque (RP) stone samples, we offer a direct inquiry and exploration into the microenvironment of RP to unravel important details concerning RP and CaOx stone pathogenesis.

Ultrastructural analysis on Randall's plaque suggests that calcium phosphate deposition in the papillary interstitium becomes intimately associated with type I collagen fusing into a "syncytium" of mineral (Evan et al, 2008 and Khan, 2016). Our results with SHG imaging to detect fibrillar collagen support the idea that collagen and cellular products play a role in plaque formation. We propose complex processes by which calcium phosphate mineralization traps surrounding collagen (now mineralized) along with interstitial cells (yet to be defined), papillary epithelial cells or a mix of different cell types. As calcium phosphate plaque progresses toward the calyceal space, the plaque contacts urine supersaturated for CaOx (Khan, 2016), initiating the formation of a nascent CaOx stone growing anchored to Randall's plaque.

SHG imaging for collagen detection has its limitations. SHG cannot be used for the imaging of all types of collagens (Sugita, 2021). Collagens I and II readily provide strong SHG signal while type III collagens show very weak SHG signal (Chen X, 2012) (Sugita, 2021). Interestingly, certain regions within plaques from our stone sections analyzed did not provide strong SHG signals (e.g., **Figure 4.2B**), indicating the possible presence of collagen type III associated with RP (or other types of collagens [type IV, VI, XV] associated with renal fibrosis) or, inexplicably, the complete absence of collagen in

some regions of mature RP (Alexakis C, 2005) (Mozes MM, 1999) (Uchio K, 1999) (Muona A, 2002) (Groma V, 1998).

Our identification of preserved nuclei with ordinary morphology in plaque is an important finding that would be nearly impossible without the methods described. Indeed, our findings highlight, for the first-time in stark resolution, cell nuclear structures in stone associated RP but not always intimately associated with the collagen detected by SHG. Earlier studies investigating the mucoprotein matrix of urinary calculi, but not of Randall's plaque stones, suggest the presence of preserved cell nuclei within the matrix of decalcified calcium phosphate urinary stones (Boyce, 1956). Boyce and Sulkin affirmed that smooth muscle cells, fibroblasts, lymphocytes, monocytes and transitional epithelial cells were present in their decalcified calcium phosphate stone samples. The cell nuclei identified in this study focused on CaOx stones having grown on to RP (interstitial calcium phosphate) and anchored to the renal papilla.

In Randall's plaque stones analyzed for nuclei (from six different patients), we identified the presence of nuclei in variable quantities. Nuclei were observed lining the edges of the plaque (presumably the tissue side) and not always congregating within the CaOx stone matrix. Interestingly, stones showing strong SHG signal did not always correlate with strong nuclear positivity. In the case of the stone shown in **Figure 4.2D**, we detected high fibrillar collagen throughout the plaque. But when the same stone was tested for the presence of nuclei, only a relatively low number were detected and on the edge of the plaque (**Figure 4.3D**). It is plausible that the mineralized plaque environment impacts the correlation of collagen fibers and cellular proliferation, but the question remains as to how this occurs. An alternative view is the possibility that cell death

(apoptosis and/or necrosis) may not be a prerequisite for the normal process of the formation of fully mineralized Randall's plaque; instead, it might be a secondary response following mineralization. Perhaps, during the pre-mineralization phase, papillary cells respond to local injury signals by initiating a set of complex molecular cascades that, in combination with mineral imbalance, promote ectopic mineralization (Evan, 2003) (Taguchi, 2017) (Khan, 2021).

Indeed, our immunofluorescence data offers support to previously proposed theories on RP genesis. First, the localization of vimentin (**Figure 4.4B**) supports the idea that mesenchymal-like cells are present in the RP stones (derived from the mineralized papilla). If mesenchymal-like cells play a role in the mineralization of the papillary interstitium, how did they get there? Are mesenchymal-like cells native to the connective tissue environment of the papillary interstitium or are there active epithelial-to-mesenchymal transitions (EMT) actively occurring in the renal papilla (Gambaro, 2008) (Convento, 2017) (Convento, 2019) (Leggett, 2021)? Researchers on RP genesis hypothesize that tubular epithelial cells in the kidney acquire a bone-like or an osteogenic phenotype (upregulation of BMP2, BMP7, collagen, OPN, MGP, OPG and vimentin [VIM]) during the extracellular remodeling that occurs in calcification and, likely in the development of RP (Yiu, 2015) (Khan, 2015) (Joshi, 2015). Alternatively, if some of the RP nuclei are epithelial cells, are we identifying mesenchymal-derived cells that stem from an EMT occurring during the pre-mineralization phase (Gambaro, 2004) (Thiery, 2006) (Joshi, 2015) (Khan, 2015)? Thus far, our data only support the presence of VIM+ or CD45+ nuclei, and collagen in RP stones. Does the identification of CD45 provide

additional support for the presence of mesenchymal cells or an osteogenic-like phenotype?

CD45, or previously the leukocyte common antigen, detection is commonly used for the localization of all leukocytes or cells of hematopoietic origin, including osteoclasts (Shivtiel S, 2008) (Hermiston ML, 2003). A role has been attributed to immune cells and inflammation in connection to RP genesis and CaOx stone formation as well as extensive quality reviews (Khan, 2014) (Taguchi, 2017) (Tang, 2019) (Khan, 2021). Our CD45 (**Figure 4.4D**) immunofluorescence study suggest that some of our RP stone nuclei appear to retain the common leukocyte antigen signature. An important question remains: are these cells residents of the renal papilla or are they migrating (infiltrating) to the papilla as a response to localized injury? Further, if these cells retain an immune cell function, are they contributing to the maintenance of crystallization or to promoters of crystallization? If not, is it possible that these CD45+ cell nuclei may be evidence of an osteogenic-like cell phenotype contributing to extracellular (collagen) remodeling and calcification? Here we can only speculate and emphasize the need for future studies investigating the role of immune cell activity and/or osteogenic-like transformations in the development of RP and CaOx stone formation. In essence, we can at present only provide data supporting the identification of cell nuclei with some VIM+ and CD45+ nuclei. The true nature of cells and their role within plaque are yet to be determined and warrant further investigation.

A major limitation to this report rests upon the fact that our data do not offer a complete story as to how these constituents (collagen, nuclei) contribute to the direct production of plaque in the renal papilla and if they have a direct role in the formation of

the CaOx stone matrix. Our findings support the predominant theories or hypotheses of RP genesis and CaOx stone formation. Although we tested for a few biomarkers (VIM and CD45) for cell characterization, we have yet to confidently affirm the presence of a specific cell type or types embedded within RP stones. Another caveat from our study is that we only tested a limited number of RP stones for our immunofluorescent studies (n = 2 RP stones for CD45 and n = 3 RP stones for VIM). However, this work illustrates an important feature of RP stones (the presence of VIM+ or CD45+ cells) by outlining the fundamental principles of properly handling RP stones for demineralization and innovative testing using imaging and molecular biology techniques. We believe that these methods will be important in future studies on RP development and CaOx kidney stone formation.
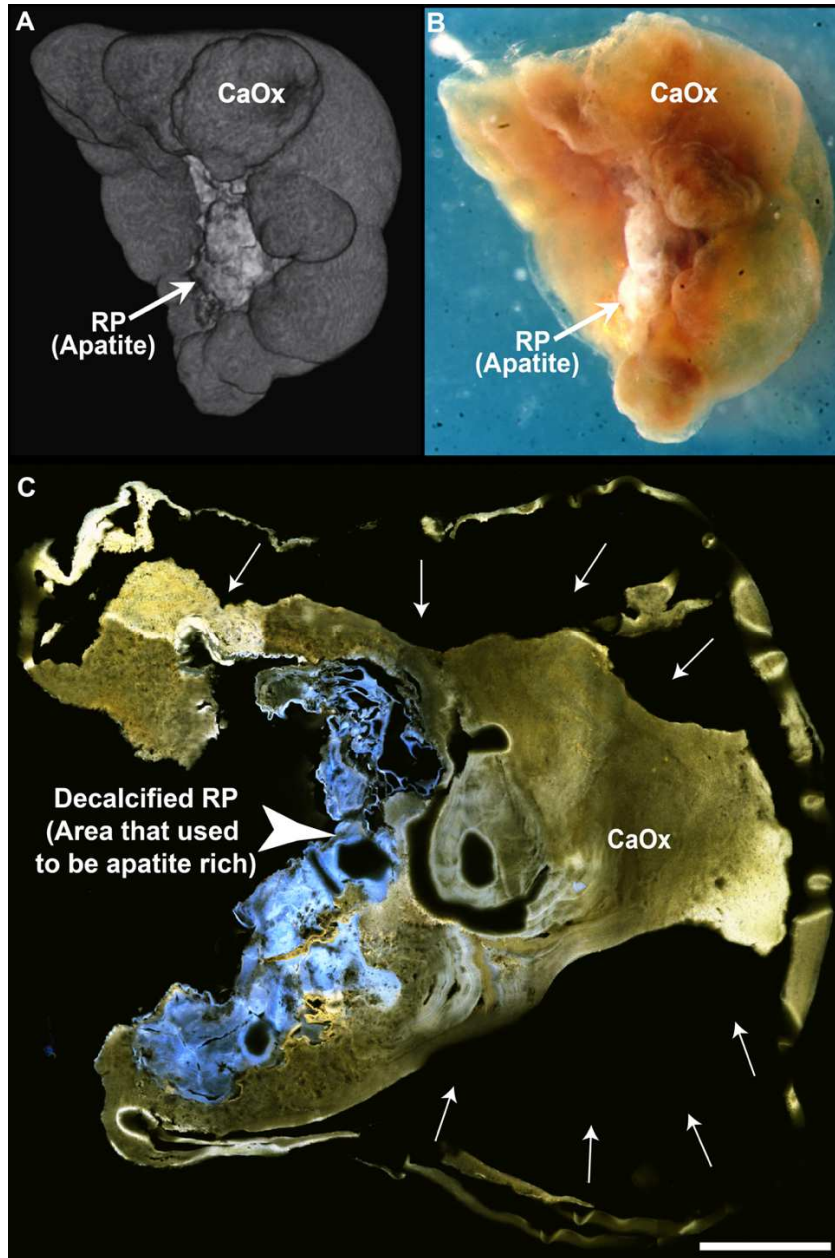
Figure 4.1: Demineralization of a Randall's Plaque (RP) stone

A. A 3-D reconstruction of calcium oxalate (CaOx) stone surface growing on RP using

micro-CT before the demineralization treatment. **B.** The same RP stone from 1A

suspended in gel and completely demineralized. Note that the structure of the stone is

completely retained, even though no mineral was detectable by micro-CT. **C.** This

section, in maximum intensity z-projection, shows RP in blue (arrowhead) and the CaOx

matrix in the green-yellow range. An artifactual void between the outer edge of the stone and the edge of the CaOx overgrowth can be seen (white arrows) indicating that shrinkage of CaOx matrix away from original boundary has occurred (probably during the dehydration process before paraffin embedment). Scale bar = 250 μm.
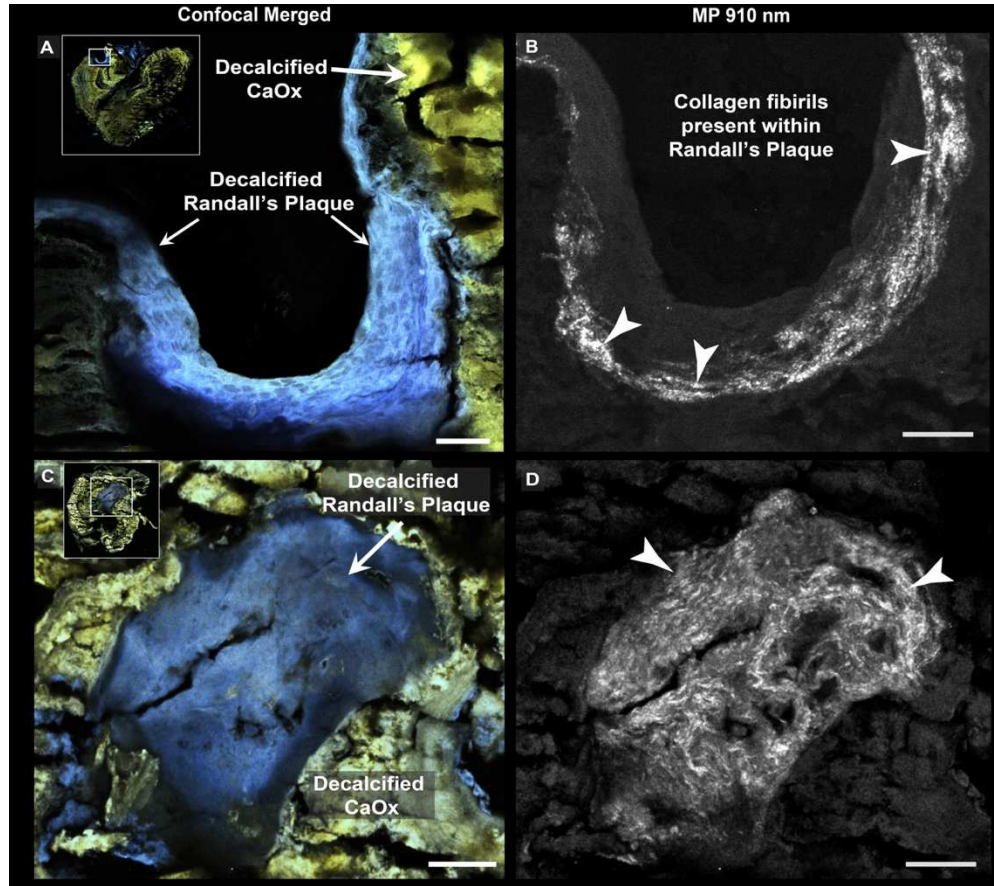
Figure 4.2: Second harmonic generation (SHG) of decalcified Randall's Plaque shows collagen fibrils

A. Autofluorescence in region of demineralized Randall's plaque (stone different from the one in in Figure 1). Spaces of apparent cell nuclei in plaque are seen. **B.** Second harmonic generation (SHG) visualization of collagen fibrils (arrowheads) in specimen shown in A. SHG shows collagen fibers in part of Randall's plaque but not throughout the entire plaque region. Region of plaque devoid of SHG signal is indicated by an asterisk. **C.** Randall's plaque stone from patient 2 (**Table 4.1**), histologically sectioned through a different plane, showing a plaque region (in blue) and the surrounding CaOx matrix. **D.** SHG of section C shows that collagen fibrils (arrowheads) were observed coursing throughout the plaque section (scale bars = 25 μm).
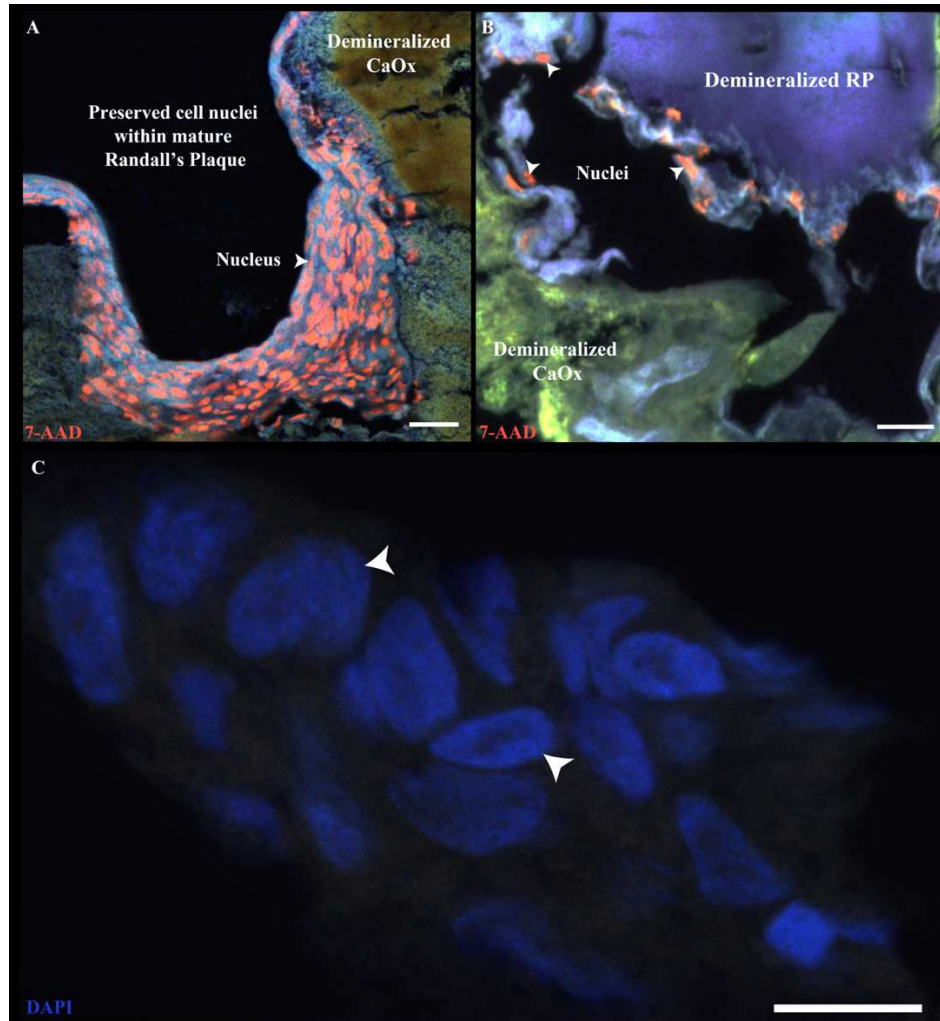
Figure 4.3: Cell nuclei in demineralized Randall's plaque stain with 7-AAD or DAPI

A. A specific region of a demineralized Randall's plaque stone (patient 1) shows enriched cell nuclei positivity with 7-AAD (white arrowhead, nucleus). **B.** A Randall's plaque stone section from patient 2 displaying a few cell nuclei at the edge of the demineralized plaque, presumably from the tissue side. Notice the quantitative differences between the numerous nuclei in A and sparser nuclear region in B (scale bar = 25 µm). **C.** Enlarged region of cell nuclei in plaque stained with DAPI from patient 4. This stone section was quenched with 50mM NH_4Cl to reduce native fluorescence from the stone (scale bar = 5 µm).
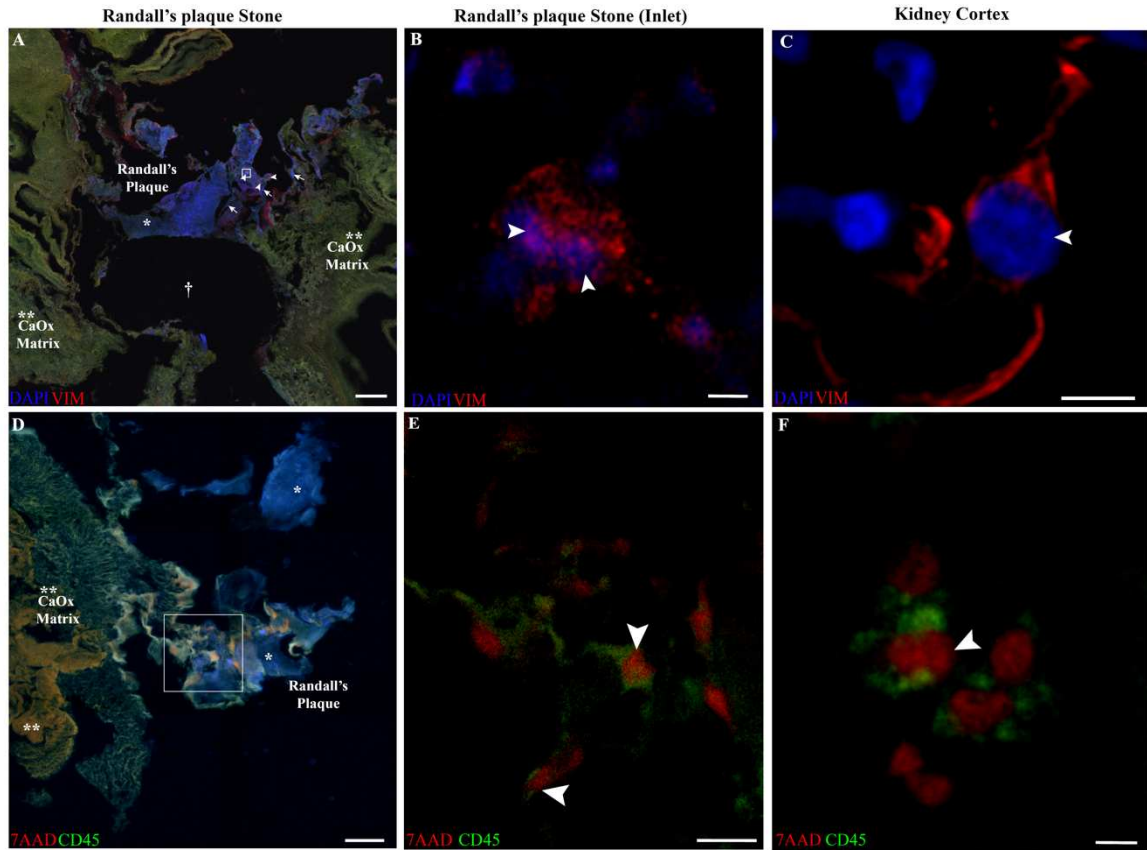
Figure 4.4: Entrapped cell nuclei from Randall's plaque stones express vimentin or CD45

A. Randall's plaque stone section showing nuclei positivity with both DAPI and VIM (white arroheads) (scale bar = 100 µm). **B.** Inlet of A (scale bar = 5 µm). **C.** A cortical section of human kidney showing DAPI (blue) and VIM positivity (red) (scale bar = 5 µm). **D.** Randall's plaque stone with 7-AAD (red) positive nuclei with variable CD45 (green) positive expression (scale bar = 25 µm). **E.** Inlet of D (scale bar = 5 µm). **F.** A cortical section of human kidney showing 7-AAD (red) positive nuclei (white arrowhead) and CD45 expression (green).

Clinical and surgical data on patients with Randall's plaque stones

	Patient 1	Patient 2	Patient 3	Patient 4	Patient 5	Patient 6
Age	56	78	66	63	32	25
Sex	M	M	M	F	M	M
Body mass index	—	33	23	20	19	22
Age at first stone	28	37	65	12	22	25
Hypertension	No	No	No	No	No	No
Diabetes	No	No	Yes	No	No	Yes
Surgery	URS	URS	URS	Perc	Perc	URS
Stone culture	—	—	No growth	—	No growth	—
Urine culture	—	Positive	No growth	Positive	No growth	—
Serum creatinine (mg/dL)	—	1.33	1.1	0.79	1.1	0.9
Serum calcium (mg/dL)	—	9.6	8.5	9.5	9.8	9.3
Serum uric acid (mg/dL)	—	5.3	4.5	3.2	6.6	5.9
24-hour urine volume (L)	3.1	2.87	2.49	1.75	2.5	2.8
24-hour urine pH	5.5	6.61	5.8	6.1	6.36	6.18
24-hour urine citrate (mg)	2059	1587	1324	265	604	374
24-hour urine calcium (mg)	100	278	122	123	172	157
24-hour urine oxalate (mg)	71	35	58	8	58	32
24-hour urine sodium (mEq)	—	226	107	36	185	143
24-hour urine CaOx supersaturation	2.85	4.66	5.2	1.21	5.4	3.33
24-hour urine CaP supersaturation	—	1.55	0.5	1.37	1.22	0.68
7-AAD or DAPI positivity	+, Figure 4.3A	+, Figure 4.3B	+	+, Figure 4.4C	+	+

VIM or CD45	+ CD45, +VIM	—	+ CD45, +VIM Figure 4.4D (CD45)	+VIM, Figure 4.4A	—	—

Table 4.1: Clinical and Surgical Data on Patients with Randall's Plaque Stones

Chapter 5: Spatial Transcriptomics of the Human Kidney Papilla reveals signaling pathways of Leukocyte Activation, Response to Oxidative Stress, Ossification and Extracellular Structure Organization associated with Nephrolithiasis

5.1 Introduction

Nephrolithiasis (kidney stone disease) is common and, on the rise (Scales, 2012) (Sorokin, 2017). The recurrence rate of nephrolithiasis is reported to be at least 50% within the first 5-10 years of the first stone episode (Khan, 2017) (Tasian, 2017). Stone disease has been previously described as a complex disease having a multifactorial etiology affected by both genetic and environmental factors (Coe, 2010) (Howles, 2020). Despite important efforts by researchers to describe its pathophysiology, the precise mechanisms contributing to kidney stone pathogenesis remain incomplete (Khan, 2021).

Multiple theories have been proposed to describe stone disease formation (Coe, 2010) (Khan 2021). A predominant view of stone disease is the pathway involving idiopathic calcium oxalate (CaOx) stone formation on to interstitial apatite plaques (Randall, 1937) (Evan, 2006) (Williams, 2013) accompanied by urine CaOx supersaturation (Coe, 1992). This theory proposes that the deposition of calcium phosphate (apatite) in the renal papillary interstitium, specifically in the basement membrane of the loop of Henle, is in part due to hypercalciuria accompanied by a decrease in urine volume and pH of idiopathic CaOx stone patients (Kuo, 2003) (Evan, 2006). The interstitial apatite (plaque) is then exposed to the supersaturated urine (likely due to papillary injury by unknown mechanisms). The exposed plaque serves as a nidus for CaOx crystals and urinary proteins which give way to the initiation and propagation of a nascent CaOx stone (Evan, 2007).

Experimental studies investigating plaque and stone formation suggest that stone disease may be driven by inflammation, oxidative stress (reactive oxygen species [ROS]), immune cell activity, components of the extracellular matrix, and osteogenic-like changes in the kidney papilla (Taguchi, 2017) (Khan, 2012) (Joshi, 2015) (Khan, 2016) (Khan 2021). However, clinical data to support these findings (immune cells, inflammation, osteogenic changes, etc.) are limited (Khan, 2021). Thus, it is challenging for researchers and clinicians to identify specific biomarkers for the identification of the early stages of stone disease, and for the development of efficient therapies for the treatment of de novo or recurrent kidney stone formers.

The advent of spatially resolved transcriptomics has, more recently, lent its capabilities to conduct direct and novel inquiries of diseased and non-diseased tissue (Ståhl, 2016) (Moncada, 2020) (Raghubar, 2020). Moreover, the integration of spatial and single-cell transcriptomics has allowed for the direct identification of intracellular tissue dynamics and the uncovering of critical gene transcripts in diseased tissue (Ferreira, 2021) (Longo, 2021).

The aim of our study was to identify molecular signatures unique to stone disease by spatial transcriptomics of the human kidney papilla. Differentially expressed genes (DEGs) and enriched pathways in stone forming papillae relative to reference tissue were identified. Supervised annotation of specific regions of the stone forming papillae provided us with a platform to further analyze the molecular effectors potentially involved in stone disease tissue. Our spatial transcriptomics data provides new data aimed to describing the potential role of biological, molecular, and cellular pathways involved in the development and progression of stone disease.

<u>5.2 Materials and Methods</u>

Biopsy protocol

Idiopathic CaOx patients undergoing percutaneous nephrolithotomy (for stone removal) had biopsy specimens taken from selected papillae during surgery (Evan, 2003). These procedures were part of the institutional review board (IRB) of Indiana University. Informed consent was obtained from all participants in this study. Additionally, a human reference (non-stone former) nephrectomy (without histological evidence of renal pathology) was obtained from the Biopsy Biobank Cohort of Indiana (Eadon, 2020)

Slide preparation and mRNA extraction & sequencing

Papillary tissues were frozen on dry ice in optimal cutting temperature (OCT) medium following extraction. Frozen 10 µm sections were mounted onto etched frames of the specialized Visium spatial slides with capture areas as instructed by 10x Genomics protocols (Visium Spatial Protocols—Tissue Preparation Guide, Document Number CD=G000240 Rev A, 10x Genomics). Tissue sections were fixed with methanol, subsequently stained with hematoxylin and eosin (H&E) and imaged by bright-field microscopy. Microscopic images were acquired according to protocols described by 10x Genomics protocols (Technical Note - Visium Spatial Gene Expression Imaging Guidelines, Document Number CG000241, 10x Genomics). Stained tissues were permeabilized and mRNA was extracted and bound to oligonucleotides on the capture areas on the Visium slides (Visium Spatial Gene Expression Reagent Kits, Document Number CD000239, Rev D, 10x Genomics [2020, October]). cDNA libraries were prepared and sequenced utilizing the NovaSeq 6000 Sequencing system by Illumina.

Data Visualization

Gene expression mapping for spatial transcriptomic was achieved using 10x

Genomics Space Ranger). with Human reference, GRCh38 (GENCODE v32/Ensembl

98) provided by 10x Genomics. Cell Ranger processes data for alignment with barcodes

within the 55 μm spots relative to the positioning of the stained tissue. The alignments

are achieved using graph-based clustering algorithms and compiled into files for

visualization by the 10x Genomics Loupe Browser (10x Genomics Loupe Browser

5.0.0.). The Loupe Browser visualizes mapping of the RNA-sequencing counts to

specific histological locations (55μm spots) and allows interactive functions for regional

comparisons (such as marker gene analysis) (Ferreira, 2021).

Comparison analysis within tissues were performed using the Loupe Browser;

DEG comparisons across samples were performed using R and the R packages

ReactomePA and ClusterProfiler as previously described in Ferreira et al. (Ferreira,

2021).

Immunofluorescent Staining and Imaging

The immunofluorescence staining analysis and imaging conducted here closely

follows the methods outlined by Makki et al. (Makki, 2020). Images were acquired using

a Leica SP8 confocal microscope. Collected z-stack images were constructed and stitched

using the Leica LAS X software.

5.3 Results

  Our data show, for the first time, transcriptomic maps of stone-forming and non-stone forming renal papillae. These spatial transcriptomic maps allow us to observe the co-localization of specific gene transcript signatures throughout the renal papilla and to identify those that are differentially expressed when comparing normal to diseased tissue. **Figure 5.1** outlines a workflow starting from the biopsies of kidney papillae, spatial transcriptomics, to future validation methods of potential candidate biomarkers for stone disease.

  Further, bioinformatic methodologies allowed us to perform bulk transcriptomic comparisons across tissues (e.g., non-stone reference papilla vs. stone-forming papilla). **Figure 5.2** compares total gene expression between a non-stone reference papilla and three different stone-forming papillae (Reference vs. Stone 1, Reference vs. Stone 2, etc.), along with their respective enriched functional pathways (**Figure 5.2**). The comparisons consistently show multiple upregulated genes in the stone-forming papilla such as IGKC, IGHA1, FOS, ATF3, JUN, SOD2, SPP1, MMP7, MGP, TNFRSF11B, and CCL2; in contrast, we observe significant downregulation of APOD, GPX3 and HIF3A in the stone-forming papillae when compared to reference papillum. Some of the pathways include neutrophil mediated immunity, antigen processing and presentation of peptide antigen, myeloid cell differentiation, response to reactive oxygen species, regulation of ossification, and extracellular matrix organization. In **Figure 5.3**, we show the spatial and relative gene expression maps of MMP7 in reference and stone tissues.

Figure 5.4 shows supervised clustering based on the characterization of mineral deposits on to consecutive tissues of a stone former papillary specimen. DEGs and their respective enriched pathways are displayed (**Figure 5.4**).

For preliminary validation of oxidative damage to stone papillary tissue (response to oxidative stress, inflammation, and macrophage activation), we sought to test for p-c-JUN and CD68. **Figure 5.5** shows preliminary immunofluorescent staining to validate the DEGs and pathways identified in stone forming papillae.

Spatial transcriptomics has allowed us to map the molecular signature of the stone forming papilla. This molecular map of spatially resolved transcriptomics in the papillae provides us with tools to discern some of the mysteries about the pathogenesis of kidney stone disease.

Initial analyses compared the bulk transcriptomic signatures between stone and non-stone papillae (**Figure 5.2**). Thus far, our data shows upregulated genes, in stone forming papillae, that are of particular interest to us, given their association with pathways of inflammation and the immune response, reactive oxygen species (ROS), extracellular remodeling, and calcification or ossification. Moreover, these genes have great relevance to stone disease given the protein composition of the kidney stone matrix (Merchant, 2008) (Canales, 2009) (Kaneko, 2011) (Okumura, 2013) (Witzmann, 2018) (Wesson, 2019). Proteins encoded by genes S100A8, S100A9, MGP, SSP1, LTF, APCS and LYZ have been consistently found in the stone matrix and are found to be upregulated in the stone former papillae analyzed in the current study. Consistent with previous hypotheses (Khan, 2021), the stone forming papillae showed several consistently enriched pathways when compared to the non-stone forming papillum. These pathways include leukocyte mediated immunity (GO:0002443), response to oxidative stress (GO:0006979), ossification (GO:0001503) and extracellular structure organization (GO:0043062). More specifically the differentially expressed genes identified in the renal papillae correlated with significantly enriched pathways such as: neutrophil mediated immunity, neutrophil activation, myeloid cell differentiation, response to reactive oxygen species, osteoblast differentiation and extracellular matrix organization. These data

confirm the previously reported ideas that papillary kidney stone formation involves

inflammation, the immune system, ROS and ossification-like events (Merchant, 2008)

(Khan, 2017) (Taguchi, 2017) (Khan, 2014) (Joshi, 2015) (Khan, 2021).

The spatial transcriptomic profiles of stone forming papillae have been unknown.

Taguchi et al. explored genome wide gene expression on renal papillary Randall's

Plaques (RP) and non-RP, and showed upregulation of LCSN2, IL11, and PTGS1 in the

RP patient tissue (Taguchi, 2017). Our work here expands on these findings by spatially

resolving our transcriptomic data on to stone forming papillary tissue. We paid particular

attention to MMPs since they were significantly increased in the CaOx papillae.

Furthermore, matrix metalloproteinase (MMP) expression and activity have been shown

to be increased in tissue injury and inflammatory diseases processes, and have been

shown to modulate leukocyte influx, and play critical roles in extracellular remodeling

(Manicone, 2008) (Bulow, 2019). Additionally, MMPs such as MMP7 and MMP9 have

important roles in monocyte and macrophage activity as well as association to

atherosclerotic plaque progression (Newby, 2015).

In our comparisons, MMP9 (compare MMP9 in reference tissue to CaOx1 tissue

sections) and MMP7 (compare MMP7 in reference tissue to CaOx1,2,3 tissue sections)

appeared to be differentially expressed in the stone forming papillae (**Figure 5.2**). In

Figure 5.3 we show the relative gene expression of MMP7 in reference tissue and three

CaOx renal papillary tissue. MMP7 appears to be localized specifically to the renal

tubular epithelia in the reference tissue as previously reported (Zhou, 2017) (Fu, 2019).

However, in all three CaOx tissues, MMP7 appears to be spread out throughout the tissue

and not specifically limited by the tubular signatures. This points to the likelihood of these CaOx stone tissues showing sparse inflammatory/immune and tissue damage.

Data in **Figure 5.4** show how we manually annotated stone tissue papillae for gene expression analysis. Specific regions of the stone papillum were designated as either non-mineralized, contiguous to mineralized and mineralized regions. Our transcriptomic data suggests that as we move from the non-mineralized area to regions close to and, the mineralized tissue, we see more injury and immune gene profiles. Genes such as SSP1, LYZ, CHIT1, MMP9 tend to be consistently expressed near areas of mineralization within the stone forming papilla. This suggests too, that even within the stone forming papillum, we can organize the tissue into regions of relative injury by spatial transcriptomics. When comparing the non-mineralized region to the mineralized regions, some of the enriched pathways that are significant include the regulation of expression of SLITs and ROBOs (perhaps in leukocyte chemotaxis) (Tong, 2019), myeloid homeostasis, myeloid cell differentiation, and Fc gamma receptor mediated phagocytosis.

The preliminary imaging studies validate our initial studies by spatial transcriptomics on the reference and stone papillae. The CaOx stone papilla shown in **Figure 5.5** exhibits positivity to the injury ROS marker, phosphorylated c-JUN, and the macrophage activation marker, CD68. The reference papillum shown in **Figure 5.5** tested negative for both phosphorylated c-JUN negative and CD68.

Altogether, the studies and data presented here shows that spatial transcriptomic technology allowed us to map the molecular signature of the stone forming papillae. We present molecular and spatial data in support for leukocyte activation, response to oxidative stress, ossification and extracellular structure organization in kidney stone

papillae. Additionally, more studies are needed to validate some of the data presented here, including the MMP7 data. These studies are promising given the potential for translation into clinical applications.
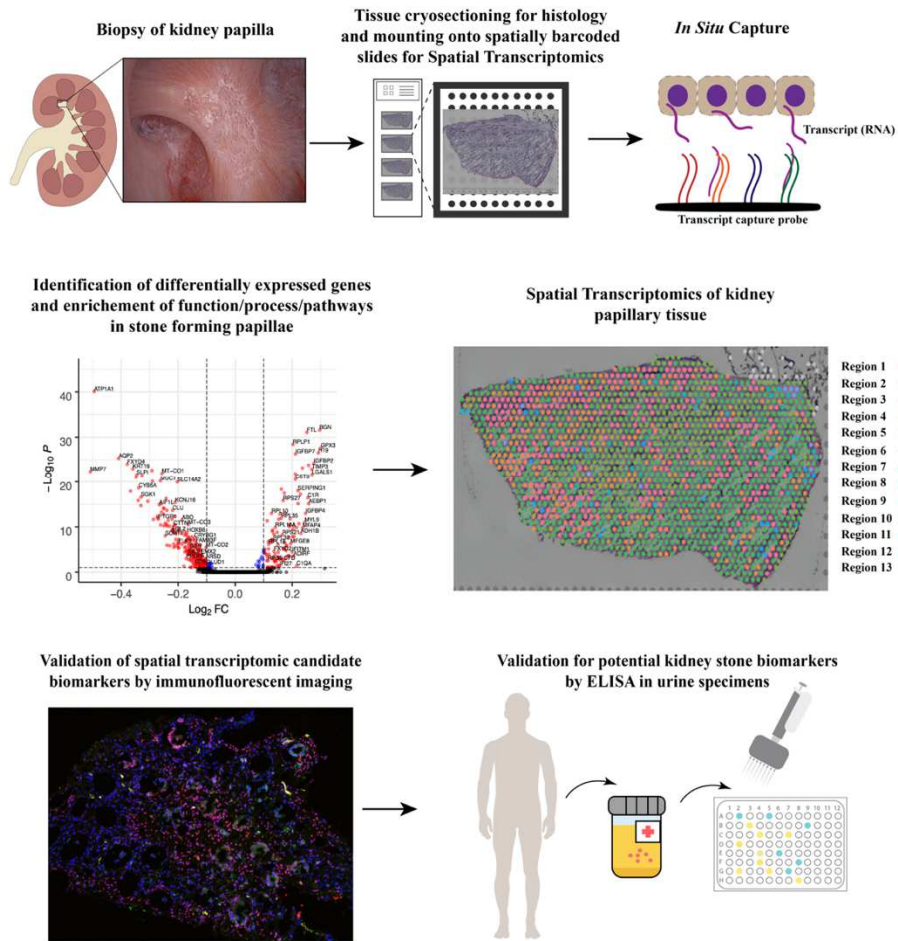
Figure 5.1: Schematic from spatial transcriptomics to the targeting of urine markers for kidney stone diseases

Illustrated are the ways that renal papillary biopsies were obtained, tissue sectioning, and mounting on a bead array that allows in situ capture of RNA from specific spots in the tissue section. The transcriptomic data from these beads are then analyzed (middle row) by both unsupervised and supervised clustering and in accord with histologic location based on the section. Genes that are indicated as differentially expressed in diseased tissue can then be looked for in urine.
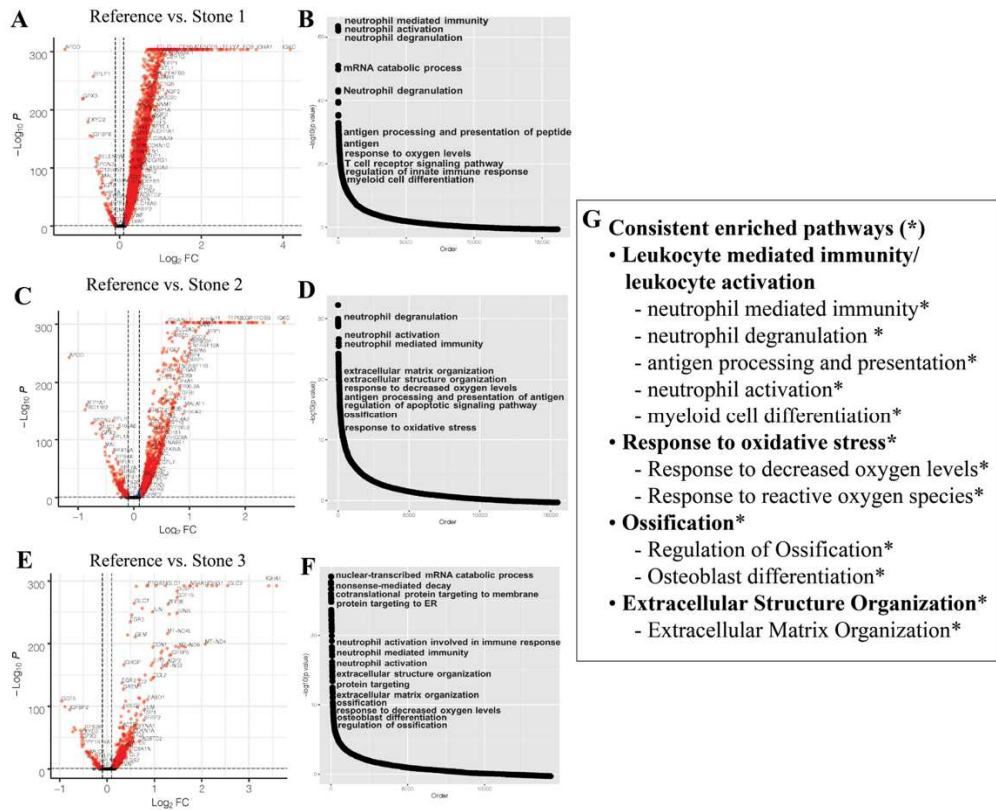
Figure 5.2: Comparative bulk analysis between reference and stone papillae

Comparative analyses between reference papillum and three CaOx stone papillae. **A**, **C**, and **E** show volcano plots displaying differentially expressed genes per bulk comparison along with their respective enriched pathways (**B**, **D**, **F**) **G.** Parental and child terms of the consistently enriched pathways throughout the bulk comparisons.

Figure 5.3: MMP7 is consistently upregulated in stone tissue biopsies

The relative gene expression of MMP7 in a reference papillary section shows a specific, spatial co-localization (namely in the kidney tubules). The CaOx stone sections show a more dispersed signal of MMP7 throughout the tissue and not localized as seen in the reference tissue sections.
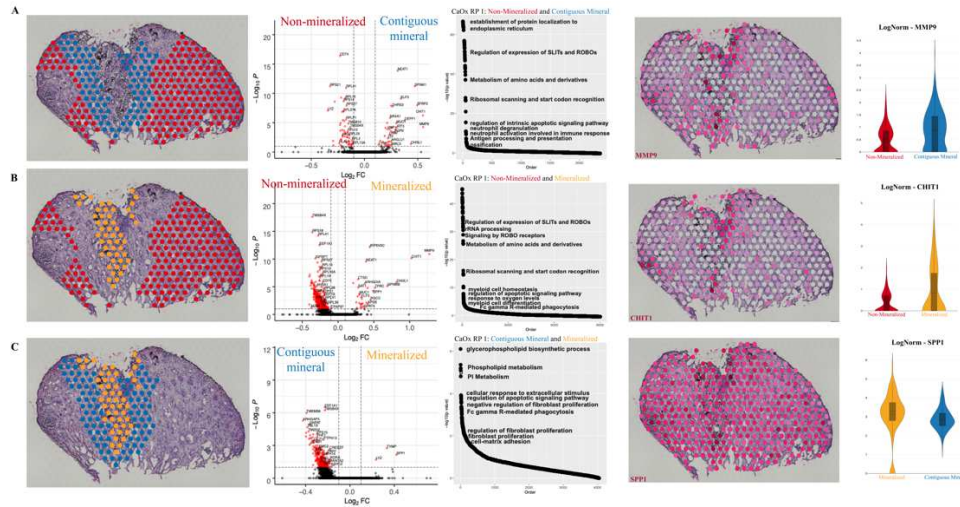
Figure 5.4: Areas contiguous to mineral and within mineral show upregulated genes such as MMP9, CHIT1 and SPP1

CaOx stone kidney papilla sections were manually annotated into non-mineral, contiguous to mineral, and mineral categories for transcriptomic comparisons. **A.** Comparison between the non-mineralized region and contiguous to mineral region. Volcano plot displaying differentially expressed genes are shown along with enriched pathways. A violin plot is shown displaying the spatial map of MMP9 and its respective LogNorm value in its category. **B**. Comparison between non-mineralized and mineralized regions. Volcano plot displaying differentially expressed genes are shown along with enriched pathways. A violin plot is shown displaying the spatial map of CHIT1 and its respective LogNorm value in its category. **C.** Comparison between the contiguous mineral and mineralized regions. Volcano plot displaying differentially expressed genes are shown along with enriched pathways. A violin plot is shown displaying the spatial map of SPP1 and its respective LogNorm value in its category.
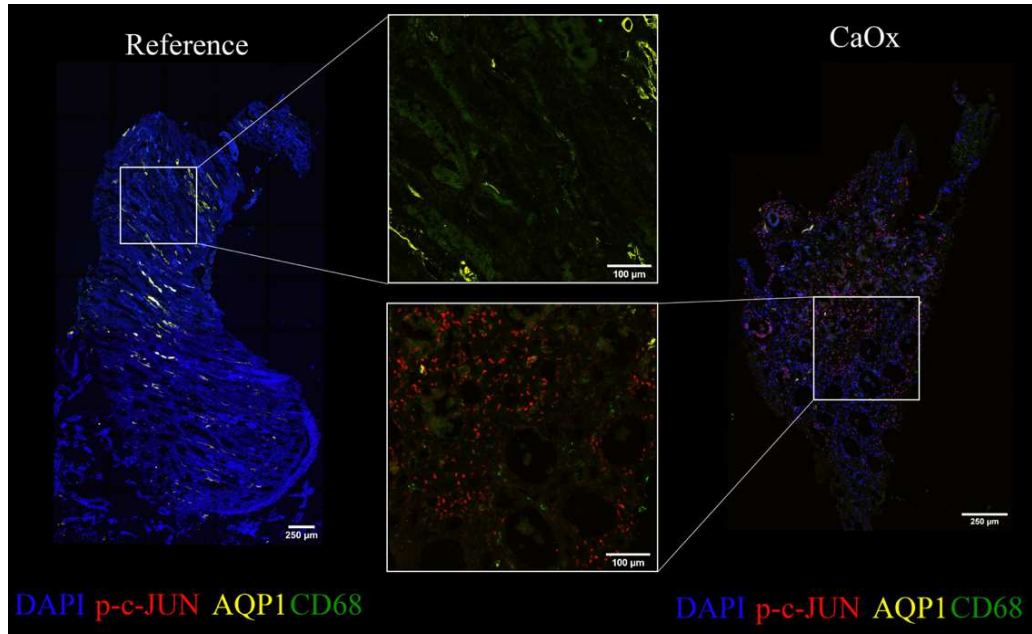
Figure 5.5: Validation of injury and immune cell activation in CaOx kidney stone papilla

Immunofluorescence imaging of reference and CaOx kidney stone papillae for p-c-JUN, AQP1 and CD68. Reference papilla is p-c-JUN negative and CD68 negative. CaOx kidney stone papilla shows positivity for both phosphorylated-c-JUN (red) and CD68 (green).

Chapter 6: Summary and Future Directions

The work presented here describes novel and innovative techniques in the direct study of kidney stone matrix, Randall's plaque stones and papillary biopsies. In the aim to further understand the pathophysiology of nephrolithiasis, we report unique methodologies, testable hypotheses and new discoveries in the field of kidney stone research. However, a complete mechanistic process describing the pathogenesis of kidney stone development and Randall's plaque remains unclear.

6.1. Demineralization and Sectioning of Human Kidney Stones: A Molecular investigation of the Stone Matrix

The aim of this project was to develop an innovative methodology to study kidney stone matrix and to explore its molecular content. Pioneering work led by previous investigators demonstrated the feasibility of demineralizing and sectioning kidney stones to explore the organic matrix in kidney stones (Boyce, 1956) (Khan & Hackett, 1993). Indeed, much of the work described in Chapter 2 takes inspiration from their pioneering work.

Our efforts not only demineralized and studied CaOx stones histologically. The methodology optimized the then current histological technique and extended its utility by methodically applying two novel and critical techniques. The first technique used micro CT to assess the degree of stone demineralization and for the precise positioning and orienting of the stones for histological sectioning and imaging. Secondly, we successfully applied the use of laser micro-dissection for the study of specific regions of interest in CaOx stone matrix. These techniques were essential for proteomic analyses of specific regions of interest.

We demonstrate the feasibility of yielding significant proteomic data with laser micro-dissected samples. The proteomic yield of laser micro dissected stone samples showed strong proteomic correlation with powdered CaOx stones. Proteins identified in the micro dissected stone samples included those associated with the regulation of acute inflammatory response, cellular response to oxidative stress, macrophage differentiation and reactive oxygen species metabolic processes. Those proteins include uromodulin, osteopontin, complement c3, fibrinogen alpha chain, vitamin K-dependent protein Z, mannan-binding lectin serine protease 2, protein S100 A8, protein S100 A9 and hundreds of others. The demonstration of successfully applying histochemical and proteomic techniques to kidney stones enables an in-depth molecular interrogation that is novel to better understanding the molecular processes dictating kidney stone formation.

The heterogeneity of CaOx stone matrix provided insight into stone development. The fluorescence signatures in CaOx stone matrices indicated that the composition of matrix need not be constant in adjacent layers. This observation led us to test the co-localization of uromodulin or THP—the most abundant of the urinary proteins. Our data showed that layers of CaOx stone matrix could be either devoid of or enriched in THP. These findings suggest that THP is unlikely a urine protein that is essential for the propagation of a stone given that it was untraceable in some of layers analyzed.

Future Directions

Future molecular studies of stone matrix will likely aid in describing mechanisms of mineral and organic layer deposition. Of particular interest, spatial mapping of the stone proteome will undoubtedly lead to a better understanding of stone growth, including renal anchoring mechanisms such as Randall's plaque. For instance,

microdissection of bulk regions of demineralized Randall's plaques, plugs or bone in kidney stones would provide an invaluable molecular understanding regarding the underpinnings of plaque, and plug growth as well as the crystal promotors of stone growth. A spatial map or atlas of different kidney stone anchoring types can be developed to compare and contrast the various mechanisms that may be contributing to the genesis of stone formation. Comparisons across and within stone types (plaque vs. plug) would add to our understanding of stone disease etiology. Thus, future utilization and optimization of these novel methodologies can begin to unlock some of the many mysteries of CaOx stone disease.

6.2 Human Jackstone arms show a Protein-Rich and X-ray Lucent Core

Jackstone calculi are rare stones occurring in kidney stone patients. We sought to investigate jackstone morphology and their mineral composition. We posited that if this rare, enigmatic, form of calculi development bears directional growth, then it may serve as a basis to understand general stone growth and formation.

In Chapter 3, we reported a total of 98 jackstones in 50 patient specimens. The predominant mineral in all specimens was calcium oxalate, and primarily of the monohydrate form (COM). Micro CT analyses on jackstones revealed that their arm protrusions consisted of x-ray lucent cores encapsulated by typical layers of COM. The X-ray lucent core appeared to be extending outward from the body surface of the stone towards the arm protrusion. While the jackstone arms always contained a core of X-ray lucent material, this core did not extend into the center of the stone body. Our data suggested that an X-ray lucent core of the jackstone arm typically began as a mass of X-ray lucent material on the surface of a typical stone (a nascent jackstone without arms).

From this point on, that initial mass on the surface of the stone serves a nidus for the growth and extension of the jack arm.

From the data presented in Chapter 3, we deduced the following hypothesis for the jackstone growth phenomenon. Briefly, if a mass of protein were to deposit onto the surface of a stone and then be coated by a thin layer of CaOx, this then, would be the place where more protein would bind to the pre-existing protein mass, extending its dimensions away from the stone body. Subsequently, addition CaOx layers would thicken on unabraded sides of the initial protein mass, while leaving the tip most susceptible to repeated abrasion damage (from either surrounding stones or the urinary space). With such a cycle, urinary proteins that preferentially bound to the existing protein core would extend the protein core farther away from the stone body resulting in a jackstone arm.

The exploration of the organic nature of the X-ray lucent cores was investigated using current IR methods and the innovative methodologies outlined in Chapter 2. Infrared spectroscopy (IR) analysis typically showed richer protein levels in core samples of jackstone arms as opposed to jackstone shell pieces. Additionally, we applied our demineralization methods to jackstone arms along with the careful orienting techniques for proper microscopic imaging. Microscopic imaging of the demineralized jackstone arms demonstrated an intense fluorescence at the core compared with the outer shell of compact COM layers. The fluorescence of the core is consistent and in agreement with an enrichment of organic material in this area in comparison to the surrounding COM layers. Furthermore, immunohistochemistry studies using THP (uromodulin) showed supportive results. We undertook this part of the study simply to see if a very abundant urinary and

stone protein would show any differential distribution between jack arm core and shell. The immunohistochemistry staining showed that THP had greater signal in the radiolucent core of jack arms than in the mineral-rich shell. These immunohistochemistry experiments could not test whether THP was enriched relative to other proteins.

Future Directions

We studied a large collection of human jackstones. Jackstone calculi were invariantly composed of COM and each contained at least one arm with a radiolucent core that was organic-rich, and apparently composed of protein matrix. Although we proposed a mechanism for jackstone growth, more studies are needed to verify and to test this and other hypotheses. Our hypothesis states that the protein-rich matrix core of a jack arm might preferentially bind more protein from the urine and resist deposition of CaOx, such that the arm grows in a linear manner and at a faster rate than the bulk of the stone. This hypothesis thus predicts an enrichment of certain urine proteins in the core of the jack arm; a theory that is testable by appropriate proteomic analysis. One potential way to test this is to apply the laser microdissection techniques outlined in Chapter 2. If core and shell sections were laser microdissected and each analyzed by proteomics, we would then be able to differentiate the two regions by protein composition. It could be possible that the jack arm cores may be enriched or differentially expressing specific protein signatures that drive general CaOx stone growth. These findings may aid not only in the additional explanation of jackstone growth but may be useful other types of urinary stones. Moreover, if a set of specific proteins are identified as candidates for kidney stone growth, those protein candidates may be used in future studies that will greatly impact our understanding of urinary stone growth: 1) candidate proteins can be co-localized and

thus, validated in immunohistochemistry experiments on jackstone calculi sections as a set of proof-of-principle studies. Furthermore, these proteins may be targeted in urine of stone patients as a potential biomarker for stone disease. 2) Those protein candidates identified as promotors or propagators of stone formation in jackstone cores may be tested singly and, in combination in 'stone farms' for the growth or artificial CaOx kidney stones in vitro (Ananth, 2002) (Chow, 2004).

6.3 Collagen Fibrils and Cell Nuclei are entrapped within Randall's Plaque Kidney Stones

Kidney stones with evidence of having grown on to Randall's plaque (RP) were studied in the same way that generic CaOx stones and jackstones were analyzed in Chapters 2 and 3, respectively. Briefly, we extended the capabilities of micro CT to trace mineral content and to orient the RP stones as they decalcified. Complete demineralization was achieved without disrupting the RP stone structure. We confirmed the positioning of plaque and CaOx matrix by autofluorescence techniques in microscopy previously shown by Winfree and colleagues (Winfree, 2020).

The strengths of the methods described rest on the ability to orient the plaque-stone "tissue" accurately and precisely for analysis by conventional histology and imaging techniques which led to some exciting discoveries. Studying demineralized RP stones using native fluoresnce microscopy allows us to efficiently explore the molecular signatures associated with RP. SHG imaging facilitated the detection of collagen in plaque without the use of transmission and scanning electron microscopy (Khan 2012). We undertook this part of the study as a proof-of-principle to demonstrate that these molecular interrogation methods were applicable to the demineralized plaque-stone

sections. Although these findings are not novel or surprising, these results give clear indications of how they lend their functionality to investigate plaque and stone as tissue. Furthermore, these techniques allowed us to discover cell nuclei in areas of Randall's plaque; a finding that to our knowledge, had never been described in the kidney stone literature.

The identification of cell nuclei in RP stones would have been nearly impossible without the optimized methodologies described in Chapter 2. Aside from the exciting discovery of cells in RP stones, we conducted immunofluorescent studies to test for vimentin and CD45. Vimentin was co-localized in a few cells of in RP stones. These findings offer support to the idea that mesenchymal-like cells may play an active role in the mineralization of the renal papilla (Gambaro, 2004) (Khan, 2016). The studies targeting CD45 also showed some positivity of the common leukocyte antigen in cells entrapped by RP in stones, suggesting that an immune cell population may be playing a more direct role in plaque-stone pathogenesis than previously thought (Zhang, 2021). Alternatively, CD45+ nuclei may suggest that an osteogenic-like phenotype or myeloid calcifying cells may be contributing to renal papillary extracellular remodeling and calcification (Fadini, 2012). Although these findings are novel and exciting for the field, the true nature of the cells and their role within plaque are yet to be determined and warrant further investigation.

Future Directions

We have shown that collagen and cells are entrapped within the plaque region of RP stones. Further, we provide evidence of a mesenchymal-like and immune cell types present in RP stones. To expand on this work, it would be informative to screen for more

proteins that may aid in the full characterization of the collagen and cells discovered in the work described in Chapter 4. For collagen detection, it would be important to verify that SHG is identifying collagen I, II or if other collagens are present and not detected by SGH (collagen type III, IV, VI, XV). Additional immunofluorescence experiments with the fibroblast marker antibody (ER-TR7) or protein S1004 would strengthen our findings of RP cells expressing vimentin. These experiments would put to rest the question of whether or not these cells are indeed fibroblasts; or if a different mesenchymal-like cell type is present in RP. Furthermore, characterizing the CD45+ cells in RP would be of great importance to decipher the role immune cells may play in plaque and stone development. Another test to consider would include a panel of targeting CD68, MARCO, CCL2, CSF1, and myeloperoxidase (MPO), CD15 and CD33 by immunofluorescence. These studies would strengthen the CD45+ findings presented here and begin to specify the type of immune cell presence in RP stones (CD45+CD68+, M1 macrophages and CD15+CD33+, neutrophils).

To further expand on this work, additional experiments with osteoblast and osteoclast markers would be needed, given that osteogenesis has been proposed as a mechanisms of RP formation (Evan 2018). These studies targeting osteoblast/osteoclast markers will either strengthen our CD45+ observations for an osteogenic phenotype, challenge the notion that immune cells are present in RP or show that both cell types occupy the RP environment. Evan el al. did not find bone gene expression in regions of human Randall's plaques (Evan, 2015) (Evan, 2018). But Mezzabotta et al. did observe expression of osterix (Sp7) in a cell culture of a human kidney with medullary sponge disease (Mezzabotta, 2015) (Evan, 2018). Thus, testing for the receptor activator of

nuclear factor κ β (RANK or TNFRSF11A) by immunofluorescence may provide an interesting avenue in the exploration of an osteogenic phenotype in the cells entrapped within RP stones.

Finally, expanding LMD technology on to demineralized RP stones would expand on the specific molecular (proteomic) signatures present in plaque and different from CaOx matrix. Utilizing the LMD-proteomics techniques, one can microdissect the RP region and run various proteomic analyses on RP. These studies would provide a specific molecular signature of the plaque and would further differentiate it from the stone matrix. Furthermore, LMD proteomic analyses on RP regions would also allow for bioinformatic analyses on the enriched molecular pathway associated with proteins identified in plaque versus those identified in stone matrix.

6.4 Spatial Transcriptomics of the Human Kidney Papilla in the context of CaOx Stone Formation

Spatial transcriptomics has allowed us to begin constructing a molecular atlas of the kidney stone forming papilla. In Chapter 5 we describe how kidney papillary biopsies were obtained and handled for histological sectioning and for the spatial sequencing of tissue according to Visium spatial transcriptomic protocols. Comparative analysis between reference and stone papillae showed major differences in differentially expressed genes (DEGs). Stone papillae consistently showed genes such as ATF3, JUN, CCL2, SPP1, VIM, MMP7 and MGP to be upregulated when compared to the reference sample. Pathways associated with leukocyte activation, response to oxidative stress, ossification and extracellular structure organization were significantly enriched for those DEGs when comparing CaOx versus the non-stone reference. Moreover, when mapping

genes related to inflammation, such as MMP7, one can see a more disperse expression throughout the CaOx papillae and a more localized expression of MMP7 in the reference. This, coupled with the bulk comparisons performed, show that CaOx papillary tissues have higher signatures of inflammation throughout as opposed to the non-stone reference.

The interrogation of a stone forming papillum via spatial transcriptomics led to interesting observations. Briefly, supervised spatial analyses comparing regions within the mineral, near mineral (contiguous) and away (non-mineralized) from mineral showed that areas closer to the mineral burden expressed higher upregulated genes related to injury, oxidative stress, inflammation, repair, and extracellular remodeling than did areas that were designated non mineral. Of particular interest, genes such as MMP9 and SPP1 tended to be enriched in those regions that were calcified. Moreover, validation studies using immunofluorescent imaging supported these findings, where c-JUN and CD68 were both co-localized to CaOx papillary tissue but not in non-stone reference samples. These data indicate that the stone forming papilla expresses injury markers relative to the reference non-forming papilla.

Future Directions

Although these findings support previous explanations of immune and inflammatory involvement in stone disease, more studies are needed to formulate a complete solidified story about how immune cells are contributing to papillary mineralization. One way to add to these data is to integrate single nuclear transcriptomics (snRNA) to these spatial transcriptomic data. This type of analysis will allow us to position cell types to the areas of mineral/plaque burden and, perhaps, co-localize specific immune and connective tissue cells (e.g. macrophages, fibroblasts). Furthermore, a

comparative analysis in the cell types between stone and non-stone papillae will lead to a better understanding on their role in mineral or plaque pathogenesis. Additionally, comparing different anatomical regions (thin limbs, collecting ducts, interstitium) between stone papillae and reference tissues would also be of importance as to how and where mineralization initiations in the stone forming papillae. Do thin limbs in the CaOx stone forming papillae express genes of inflammation, injury, ROS and osteogenesis? Does the interstitium express upregulated genes involved in extracellular remodeling, immune cell activity and osteogenesis? This area of investigation deserves more attention.

These initial analyses we present point to the possibility of selecting potential biomarkers that can used in a clinical setting. If future studies validate some of the specific genes we present and validate their products (proteins) in CaOx stone papillary tissue, it would be worth analyzing them in urine. A set of experiments using enzyme-linked immunosorbent assay (ELISA) of non-stone and stone patient urine samples would serve as an additional layer of validation for some of the data presented by spatial transcriptomics. These tools would be invaluable for kidney stone patients in the clinical setting and may serve to screen disease state and progression, and perhaps may lead to therapeutic targets to prevent nephrolithiasis.

6.5 Concluding Remarks

The research projects detailed above highlight the complexity of kidney stone disease etiology and the innovative methodologies needed to study nephrolithiasis. The bulk of work presented here did not rely on animal models of nephrolithiasis since no reliable animal model currently exists. Instead, we relied on the meticulous direct study

on CaOx kidney stones surgically extracted from patients. We analyzed their mineral and organic material and pieced together experiments for an understanding of kidney stone formation. We relied heavily on micro CT, IR, traditional histology, immunohistochemistry and immunofluorescence microscopy. Further, we applied the use of "omics" technology to study proteins (proteomics) in the stone matrix and gene expression (transcriptomics) signatures in the kidney papillae. Our limited knowledge on the pathophysiology of kidney stone formation led us to develop innovative methods to study kidney stones. Our optimized demineralization methods coupled with fluoresnce microscopy led to the discovery of cell nuclei in regions of Randall's plaque stones. The identification of cell nuclei also led us to discover immune- and mesenchymal-like signatures in those cells which may help us better understand the pathophysiology of kidney stone disease. In toto, these results show that 1) the kidney stone CaOx matrix is heterogenous and particular regions of the matrix exhibit proteins associated with inflammation, ROS and the immune response ; 2) jackstone calculi have a radiolucent core that is rich in protein and likely drive their rapid and linear growth; 3) collagen and cell nuclei are entrapped in plaque of RP stones and 4) kidney papillae of stone formers reveal signaling pathways of leukocyte activation, response to oxidative stress, ossification and extracellular remodeling. These findings may potentially serve as initial steps to develop biomarkers and to begin investigating future therapeutic targets for non-invasive treatment or prevention of kidney stone diseases.

References

1. Ananth, K., Kavanagh, J. P., Walton, R. C., & Rao, P. N. (2002). Enlargement of calcium oxalate stones to clinically significant size in an in-vitro stone generator. *BJU Int, 90*(9), 939-944. doi:10.1046/j.1464-410x.2002.03027.x

2. Bird, V. Y., & Khan, S. R. (2017). How do stones form? Is unification of theories on stone formation possible? [Cómo se forman las piedras? Es posible la unificación de las teorías sobre la formación de las piedras?]. *Archivos espanoles de urologia, 70*(1), 12-27. Retrieved from https://pubmed.ncbi.nlm.nih.gov/28221139

3. https://www.ncbi.nlm.nih.gov/pmc/articles/PMC5683182/

4. Blazquez-Medela, A. M., Guihard, P. J., Yao, J., Jumabay, M., Lusis, A. J., Bostrom, K. I., & Yao, Y. (2015). ABCC6 deficiency is associated with activation of BMP signaling in liver and kidney. *FEBS Open Bio, 5*, 257-263. doi:10.1016/j.fob.2015.03.009

5. Boonla, C., Tosukhowong, P., Spittau, B., Schlosser, A., Pimratana, C., & Krieglstein, K. (2014). Inflammatory and fibrotic proteins proteomically identified as key protein constituents in urine and stone matrix of patients with kidney calculi. *Clin Chim Acta, 429*, 81-89. doi:10.1016/j.cca.2013.11.036

6. Borofsky, M. S., Paonessa, J. E., Evan, A. P., Williams, J. C., Jr., Coe, F. L., Worcester, E. M., & Lingeman, J. E. (2016). A Proposed Grading System to Standardize the Description of Renal Papillary Appearance at the Time of Endoscopy in Patients with Nephrolithiasis. *J Endourol, 30*(1), 122-127. doi:10.1089/end.2015.0298

7. Boyce, W. H. (1968). Organic matrix of human urinary concretions. *Am J Med, 45*(5), 673-683. doi:10.1016/0002-9343(68)90203-9

8. Boyce, W. H., & Garvey, F. K. (1956). The amount and nature of the organic matrix in urinary calculi: a review. *J Urol, 76*(3), 213-227. doi:10.1016/s0022-5347(17)66686-2

9. Boyce, W. H., & Sulkin, N. M. (1956). Biocolloids of urine in health and in calculous disease. III. The mucoprotein matrix of urinary calculi. *J Clin Invest, 35*(10), 1067-1079. doi:10.1172/JCI103361

10. Bulow, R. D., & Boor, P. (2019). Extracellular Matrix in Kidney Fibrosis: More Than Just a Scaffold. *J Histochem Cytochem, 67*(9), 643-661. doi:10.1369/0022155419849388

11. Canales, B. K., Anderson, L., Higgins, L., Ensrud-Bowlin, K., Roberts, K. P., Wu, B., . . . Monga, M. (2010). Proteome of human calcium kidney stones. *Urology, 76*(4), 1017 e1013-1020. doi:10.1016/j.urology.2010.05.005

12. Canales, B. K., Anderson, L., Higgins, L., Slaton, J., Roberts, K. P., Liu, N., & Monga, M. (2008). Second prize: Comprehensive proteomic analysis of human calcium oxalate monohydrate kidney stone matrix. *J Endourol, 22*(6), 1161-1167. doi:10.1089/end.2007.0440

13. Canela, V. H., Bledsoe, S. B., Lingeman, J. E., Gerber, G., Worcester, E. M., El-Achkar, T. M., & Williams, J. C., Jr. (2021). Demineralization and sectioning of human kidney stones: A molecular investigation revealing the spatial heterogeneity of the stone matrix. *Physiol Rep, 9*(1), e14658. doi:10.14814/phy2.14658

14. Canela, V. H., Bledsoe, S. B., Worcester, E. M., Lingeman, J. E., El-Achkar, T. M., & Williams, J. C., Jr. (2021). Collagen fibrils and cell nuclei are entrapped within Randall's plaques but not in CaOx matrix overgrowth: A microscopic inquiry into Randall's plaque stone pathogenesis. *Anat Rec (Hoboken)*. doi:10.1002/ar.24837

15. Canela, V. H., Dzien, C., Bledsoe, S. B., Borofsky, M. S., Boris, R. S., Lingeman, J. E., . . . Williams, J. C., Jr. (2021). Human jackstone arms show a protein-rich, X-ray lucent core, suggesting that proteins drive their rapid and linear growth. *Urolithiasis*. doi:10.1007/s00240-021-01275-1

16. Carneiro, C., Cunha, M. F., & Brito, J. (2020). Jackstone Calculus. *Urology, 137*, e6-e7. doi:10.1016/j.urology.2019.12.021

17. Chen, L., Hsi, R. S., Yang, F., Sherer, B. A., Stoller, M. L., & Ho, S. P. (2017). Anatomically-specific intratubular and interstitial biominerals in the human renal medullo-papillary complex. *PLoS One, 12*(11), e0187103. doi:10.1371/journal.pone.0187103

18. Chen, Q., Shou, P., Zheng, C., Jiang, M., Cao, G., Yang, Q., . . . Shi, Y. (2016). Fate decision of mesenchymal stem cells: adipocytes or osteoblasts? *Cell Death Differ, 23*(7), 1128-1139. doi:10.1038/cdd.2015.168

19. Childs, M. A., Mynderse, L. A., Rangel, L. J., Wilson, T. M., Lingeman, J. E., & Krambeck, A. E. (2013). Pathogenesis of bladder calculi in the presence of urinary stasis. *J Urol, 189*(4), 1347-1351. doi:10.1016/j.juro.2012.11.079

20. Chow, K., Dixon, J., Gilpin, S., Kavanagh, J. P., & Rao, P. N. (2004a). Citrate inhibits growth of residual fragments in an in vitro model of calcium oxalate renal stones. *Kidney Int, 65*(5), 1724-1730. doi:10.1111/j.1523-1755.2004.00566.x

21. Chow, K., Dixon, J., Gilpin, S., Kavanagh, J. P., & Rao, P. N. (2004b). A stone farm: development of a method for simultaneous production of multiple calcium oxalate stones in vitro. *Urol Res, 32*(1), 55-60. doi:10.1007/s00240-003-0379-1

22. Chuang, T. F., Hung, H. C., Li, S. F., Lee, M. W., Pai, J. Y., & Hung, C. T. (2020). Risk of chronic kidney disease in patients with kidney stones-a nationwide cohort study. *BMC Nephrol, 21*(1), 292. doi:10.1186/s12882-020-01950-2

23. Ciftcioglu, N., Vejdani, K., Lee, O., Mathew, G., Aho, K. M., Kajander, E. O., . . . Stoller, M. L. (2008). Association between Randall's plaque and calcifying nanoparticles. *Int J Nanomedicine, 3*(1), 105-115. doi:10.2147/ijn.s2553

24. Cifuentes Delatte, L., Minon-Cifuentes, J., & Medina, J. A. (1987). New studies on papillary calculi. *J Urol, 137*(5), 1024-1029. doi:10.1016/s0022-5347(17)44352-7

25. Coe, F. L., Evan, A., & Worcester, E. (2005). Kidney stone disease. *J Clin Invest, 115*(10), 2598-2608. doi:10.1172/jci26662

26. Convento, M., Pessoa, E., Aragao, A., Schor, N., & Borges, F. (2019). Oxalate induces type II epithelial to mesenchymal transition (EMT) in inner medullary collecting duct cells (IMCD) in vitro and stimulate the expression of osteogenic and fibrotic markers in kidney medulla in vivo. *Oncotarget, 10*(10), 1102-1118. doi:10.18632/oncotarget.26634

27. Convento, M. B., Pessoa, E. A., Cruz, E., da Gloria, M. A., Schor, N., & Borges, F. T. (2017). Calcium oxalate crystals and oxalate induce an epithelial-to-mesenchymal transition in the proximal tubular epithelial cells: Contribution to oxalate kidney injury. *Sci Rep, 7*, 45740. doi:10.1038/srep45740

28. Crowe, A. R., & Yue, W. (2019). Semi-quantitative Determination of Protein Expression using Immunohistochemistry Staining and Analysis: An Integrated Protocol. *Bio Protoc, 9*(24). doi:10.21769/BioProtoc.3465

29. Daudon, M., Bazin, D., & Letavernier, E. (2015). Randall's plaque as the origin of calcium oxalate kidney stones. *Urolithiasis, 43 Suppl 1*, 5-11. doi:10.1007/s00240-014-0703-y

30. Daudon M, W. J., Jr. (2020). Characteristics of Human Kidney Stones. In F. L. Coe, E. Worcester, J. E. Lingeman, & A. P. Evan (Eds.), *Kidney Stones* (pp. 77-97): Jaypee Medical Publishers.

31. Denu, R. A., Nemcek, S., Bloom, D. D., Goodrich, A. D., Kim, J., Mosher, D. F., & Hematti, P. (2016). Fibroblasts and Mesenchymal Stromal/Stem Cells Are Phenotypically Indistinguishable. *Acta Haematol, 136*(2), 85-97. doi:10.1159/000445096

32. Douenias, R., Rich, M., Badlani, G., Mazor, D., & Smith, A. (1991). Predisposing factors in bladder calculi. Review of 100 cases. *Urology, 37*(3), 240-243. doi:10.1016/0090-4295(91)80293-g

33. Eadon, M. T., Schwantes-An, T. H., Phillips, C. L., Roberts, A. R., Greene, C. V., Hallab, A., . . . Moorthi, R. N. (2020). Kidney Histopathology and Prediction of Kidney Failure: A Retrospective Cohort Study. *Am J Kidney Dis, 76*(3), 350-360. doi:10.1053/j.ajkd.2019.12.014

34. El-Achkar, T. M., McCracken, R., Liu, Y., Heitmeier, M. R., Bourgeois, S., Ryerse, J., & Wu, X. R. (2013). Tamm-Horsfall protein translocates to the basolateral domain of thick ascending limbs, interstitium, and circulation during recovery from acute kidney injury. *Am J Physiol Renal Physiol, 304*(8), F1066-1075. doi:10.1152/ajprenal.00543.2012

35. Evan, A. P., Coe, F. L., Lingeman, J., Bledsoe, S., & Worcester, E. M. (2018). Randall's plaque in stone formers originates in ascending thin limbs. *Am J Physiol Renal Physiol, 315*(5), F1236-F1242. doi:10.1152/ajprenal.00035.2018

36. Evan, A. P., Coe, F. L., Lingeman, J. E., Shao, Y., Sommer, A. J., Bledsoe, S. B., . . . Worcester, E. M. (2007). Mechanism of formation of human calcium oxalate renal stones on Randall's plaque. *Anat Rec (Hoboken), 290*(10), 1315-1323. doi:10.1002/ar.20580

37. Evan, A. P., Lingeman, J. E., Coe, F. L., Parks, J. H., Bledsoe, S. B., Shao, Y., . . . Grynpas, M. (2003). Randall's plaque of patients with nephrolithiasis begins in basement membranes of thin loops of Henle. *J Clin Invest, 111*(5), 607-616. doi:10.1172/JCI17038

38. Evan, A. P., Weinman, E. J., Wu, X. R., Lingeman, J. E., Worcester, E. M., & Coe, F. L. (2010). Comparison of the pathology of interstitial plaque in human ICSF stone patients to NHERF-1 and THP-null mice. *Urol Res, 38*(6), 439-452. doi:10.1007/s00240-010-0330-1

39. Evan, A. P., Worcester, E. M., Coe, F. L., Williams, J., Jr., & Lingeman, J. E. (2015). Mechanisms of human kidney stone formation. *Urolithiasis, 43 Suppl 1*(0 1), 19-32. doi:10.1007/s00240-014-0701-0

40. Fadini, G. P., Rattazzi, M., Matsumoto, T., Asahara, T., & Khosla, S. (2012). Emerging role of circulating calcifying cells in the bone-vascular axis. *Circulation, 125*(22), 2772-2781. doi:10.1161/CIRCULATIONAHA.112.090860

41. Ferkowicz, M. J., Winfree, S., Sabo, A. R., Kamocka, M. M., Khochare, S., Barwinska, D., . . . Kidney Precision Medicine, P. (2021). Large-scale, three-dimensional tissue cytometry of the human kidney: a complete and accessible pipeline. *Lab Invest, 101*(5), 661-676. doi:10.1038/s41374-020-00518-w

42. Fleisch, H. (1978). Inhibitors and promoters of stone formation. *Kidney Int, 13*(5), 361-371. doi:10.1038/ki.1978.54

43. Fu, H., Zhou, D., Zhu, H., Liao, J., Lin, L., Hong, X., . . . Liu, Y. (2019). Matrix metalloproteinase-7 protects against acute kidney injury by priming renal tubules for survival and regeneration. *Kidney Int, 95*(5), 1167-1180. doi:10.1016/j.kint.2018.11.043

44. Gambaro, G., Abaterusso, C., Fabris, A., Ruggera, L., Zattoni, F., Del Prete, D., . . . Anglani, F. (2009). The origin of nephrocalcinosis, Randall's plaque and renal stones: a cell biology viewpoint. *Arch Ital Urol Androl, 81*(3), 166-170. Retrieved from https://www.ncbi.nlm.nih.gov/pubmed/19911679

45. Gambaro, G., D'Angelo, A., Fabris, A., Tosetto, E., Anglani, F., & Lupo, A. (2004). Crystals, Randall's plaques and renal stones: do bone and atherosclerosis teach us something? *Journal of nephrology, 17*(6), 774-777. Retrieved from https://www.ncbi.nlm.nih.gov/pubmed/15593050

46. Gambaro, G., Fabris, A., Abaterusso, C., Cosaro, A., Ceol, M., Mezzabotta, F., . . . Anglani, F. (2008). Pathogenesis of nephrolithiasis: recent insight from cell biology and renal pathology. *Clin Cases Miner Bone Metab, 5*(2), 107-109. Retrieved from https://www.ncbi.nlm.nih.gov/pubmed/22460990

47. Gay, C., Letavernier, E., Verpont, M. C., Walls, M., Bazin, D., Daudon, M., . . . de Frutos, M. (2020). Nanoscale Analysis of Randall's Plaques by Electron Energy Loss Spectromicroscopy: Insight in Early Biomineral Formation in Human Kidney. *ACS Nano, 14*(2), 1823-1836. doi:10.1021/acsnano.9b07664

48. Giachelli, C. M. (2004). Vascular calcification mechanisms. *J Am Soc Nephrol, 15*(12), 2959-2964. doi:10.1097/01.ASN.0000145894.57533.C4

49. Giachelli, C. M. (2005). Inducers and inhibitors of biomineralization: lessons from pathological calcification. *Orthod Craniofac Res, 8*(4), 229-231. doi:10.1111/j.1601-6343.2005.00345.x

50. Grupp, C., Lottermoser, J., Cohen, D. I., Begher, M., Franz, H. E., & Muller, G. A. (1997). Transformation of rat inner medullary fibroblasts to myofibroblasts in vitro. *Kidney Int, 52*(5), 1279-1290. doi:10.1038/ki.1997.453

51. Hermiston, M. L., Xu, Z., & Weiss, A. (2003). CD45: a critical regulator of signaling thresholds in immune cells. *Annu Rev Immunol, 21*, 107-137. doi:10.1146/annurev.immunol.21.120601.140946

52. Howles, S. A., & Thakker, R. V. (2020). Genetics of kidney stone disease. *Nat Rev Urol, 17*(7), 407-421. doi:10.1038/s41585-020-0332-x

53. Howles, S. A., Wiberg, A., Goldsworthy, M., Bayliss, A. L., Gluck, A. K., Ng, M., . . . Furniss, D. (2019). Genetic variants of calcium and vitamin D metabolism in kidney stone disease. *Nat Commun, 10*(1), 5175. doi:10.1038/s41467-019-13145-x

54. Iwanaga, J., Singh, V., Ohtsuka, A., Hwang, Y., Kim, H. J., Morys, J., . . . Tubbs, R. S. (2021). Acknowledging the use of human cadaveric tissues in research papers: Recommendations from anatomical journal editors. *Clin Anat, 34*(1), 2-4. doi:10.1002/ca.23671

55. Jaggi, M., Nakagawa, Y., Zipperle, L., & Hess, B. (2007). Tamm-Horsfall protein in recurrent calcium kidney stone formers with positive family history: abnormalities in urinary excretion, molecular structure and function. *Urol Res, 35*(2), 55-62. doi:10.1007/s00240-007-0083-7

56. Johri, N., Cooper, B., Robertson, W., Choong, S., Rickards, D., & Unwin, R. (2010). An update and practical guide to renal stone management. *Nephron Clin Pract, 116*(3), c159-171. doi:10.1159/000317196

57. Joshi, S., Clapp, W. L., Wang, W., & Khan, S. R. (2015). Osteogenic changes in kidneys of hyperoxaluric rats. *Biochim Biophys Acta, 1852*(9), 2000-2012. doi:10.1016/j.bbadis.2015.06.020

58. Khan, S. R. (2021). Inflammation and injury: what role do they play in the development of Randall's plaques and formation of calcium oxalate kidney stones? *Comptes Rendus Chimie*(Online First), 1-19. doi:https://doi.org/10.5802/crchim.93

59. Khan, S. R., & Canales, B. K. (2015). Unified theory on the pathogenesis of Randall's plaques and plugs. *Urolithiasis, 43 Suppl 1*, 109-123. doi:10.1007/s00240-014-0705-9

60. Khan, S. R., Canales, B. K., & Dominguez-Gutierrez, P. R. (2021). Randall's plaque and calcium oxalate stone formation: role for immunity and inflammation. *Nat Rev Nephrol, 17*(6), 417-433. doi:10.1038/s41581-020-00392-1

61. Khan, S. R., Finlayson, B., & Hackett, R. L. (1983). Stone matrix as proteins adsorbed on crystal surfaces: a microscopic study. *Scan Electron Microsc*(Pt 1), 379-385. Retrieved from https://www.ncbi.nlm.nih.gov/pubmed/6635558

62. Khan, S. R., & Hackett, R. L. (1984). Microstructure of decalcified human calcium oxalate urinary stones. *Scan Electron Microsc*(Pt 2), 935-941. Retrieved from https://www.ncbi.nlm.nih.gov/pubmed/6385225

63. Khan, S. R., & Hackett, R. L. (1993). Role of organic matrix in urinary stone formation: an ultrastructural study of crystal matrix interface of calcium oxalate monohydrate stones. *J Urol, 150*(1), 239-245. doi:10.1016/s0022-5347(17)35454-x

64. Khan, S. R., Pearle, M. S., Robertson, W. G., Gambaro, G., Canales, B. K., Doizi, S., . . . Tiselius, H. G. (2016). Kidney stones. *Nat Rev Dis Primers, 2*, 16008. doi:10.1038/nrdp.2016.8

65. Khan, S. R., Rodriguez, D. E., Gower, L. B., & Monga, M. (2012). Association of Randall plaque with collagen fibers and membrane vesicles. *J Urol, 187*(3), 1094-1100. doi:10.1016/j.juro.2011.10.125

66. Kolbach-Mandel, A. M., Mandel, N. S., Cohen, S. R., Kleinman, J. G., Ahmed, F., Mandel, I. C., & Wesson, J. A. (2017). Guaifenesin stone matrix proteomics: a protocol for identifying proteins critical to stone formation. *Urolithiasis, 45*(2), 139-149. doi:10.1007/s00240-016-0907-4

67. Kriz, W., & Kaissling, B. (2008). Structural Organization of the Mammalian Kidney. *Seldin and Giebisch's The Kidney, 1*, 479-563. doi:10.1016/B978-012088488-9.50023-1

68. Leal, J. J., & Finlayson, B. (1977). Adsorption of naturally occurring polymers onto calcium oxalate crystal surfaces. *Invest Urol, 14*(4), 278-283. Retrieved from https://www.ncbi.nlm.nih.gov/pubmed/64463

69. Leggett, S. E., Hruska, A. M., Guo, M., & Wong, I. Y. (2021). The epithelial-mesenchymal transition and the cytoskeleton in bioengineered systems. *Cell Commun Signal, 19*(1), 32. doi:10.1186/s12964-021-00713-2

70. Lemley, K. V., & Kriz, W. (1991). Anatomy of the renal interstitium. *Kidney Int, 39*(3), 370-381. doi:10.1038/ki.1991.49

71. Letavernier, E., Bazin, D., Daudon, M. (2016). Randall's plaque and kidney stones: Recent advances and future challenges. *Comptes Rendus Chimie, 19*(11-12), 1456-1460.

72. Letavernier, E., Bouderlique, E., Zaworski, J., Martin, L., & Daudon, M. (2019). Pseudoxanthoma Elasticum, Kidney Stones and Pyrophosphate: From a Rare Disease to Urolithiasis and Vascular Calcifications. *Int J Mol Sci, 20*(24). doi:10.3390/ijms20246353

73. Letavernier, E., Kauffenstein, G., Huguet, L., Navasiolava, N., Bouderlique, E., Tang, E., . . . Martin, L. (2018). ABCC6 Deficiency Promotes Development of Randall Plaque. *J Am Soc Nephrol, 29*(9), 2337-2347. doi:10.1681/ASN.2017101148

74. Lieske, J. C., Mehta, R. A., Milliner, D. S., Rule, A. D., Bergstralh, E. J., & Sarr, M. G. (2015). Kidney stones are common after bariatric surgery. *Kidney Int, 87*(4), 839-845. doi:10.1038/ki.2014.352

75. Lieske, J. C., Rule, A. D., Krambeck, A. E., Williams, J. C., Bergstralh, E. J., Mehta, R. A., & Moyer, T. P. (2014). Stone composition as a function of age and sex. *Clin J Am Soc Nephrol, 9*(12), 2141-2146. doi:10.2215/CJN.05660614

76. Linnes, M. P., Krambeck, A. E., Cornell, L., Williams, J. C., Jr., Korinek, M., Bergstralh, E. J., . . . Lieske, J. C. (2013). Phenotypic characterization of kidney stone formers by endoscopic and histological quantification of intrarenal calcification. *Kidney Int, 84*(4), 818-825. doi:10.1038/ki.2013.189

77. Makki, M. S., Winfree, S., Lingeman, J. E., Witzmann, F. A., Worcester, E. M., Krambeck, A. E., . . . El-Achkar, T. M. (2020). A Precision Medicine Approach Uncovers a Unique Signature of Neutrophils in Patients With Brushite Kidney Stones. *Kidney Int Rep, 5*(5), 663-677. doi:10.1016/j.ekir.2020.02.1025

78. Manicone, A. M., & McGuire, J. K. (2008). Matrix metalloproteinases as modulators of inflammation. *Semin Cell Dev Biol, 19*(1), 34-41. doi:10.1016/j.semcdb.2007.07.003

79. Melo Ferreira, R., Sabo, A. R., Winfree, S., Collins, K. S., Janosevic, D., Gulbronson, C. J., . . . Eadon, M. T. (2021). Integration of spatial and single-cell transcriptomics localizes epithelial cell-immune cross-talk in kidney injury. *JCI Insight, 6*(12). doi:10.1172/jci.insight.147703

80. Merchant, M. L., Cummins, T. D., Wilkey, D. W., Salyer, S. A., Powell, D. W., Klein, J. B., & Lederer, E. D. (2008). Proteomic analysis of renal calculi indicates an important role for inflammatory processes in calcium stone formation. *Am J Physiol Renal Physiol, 295*(4), F1254-1258. doi:10.1152/ajprenal.00134.2008

81. Micanovic, R., Khan, S., & El-Achkar, T. M. (2015). Immunofluorescence laser micro-dissection of specific nephron segments in the mouse kidney allows targeted downstream proteomic analysis. *Physiol Rep, 3*(2). doi:10.14814/phy2.12306

82. Modlin, M. (1980). A history of urinary stone. *S Afr Med J, 58*(16), 652-655. Retrieved from https://www.ncbi.nlm.nih.gov/pubmed/6999641

83. Moe, O. W., Pearle, M. S., & Sakhaee, K. (2011). Pharmacotherapy of urolithiasis: evidence from clinical trials. *Kidney Int, 79*(4), 385-392. doi:10.1038/ki.2010.389

84. Morrison, S. J., Csete, M., Groves, A. K., Melega, W., Wold, B., & Anderson, D. J. (2000). Culture in reduced levels of oxygen promotes clonogenic sympathoadrenal differentiation by isolated neural crest stem cells. *J Neurosci, 20*(19), 7370-7376. Retrieved from https://www.ncbi.nlm.nih.gov/pubmed/11007895

85. Newby, A. C. (2015). Metalloproteinases promote plaque rupture and myocardial infarction: A persuasive concept waiting for clinical translation. *Matrix Biol, 44-46*, 157-166. doi:10.1016/j.matbio.2015.01.015

86. Oliver, J. A., Klinakis, A., Cheema, F. H., Friedlander, J., Sampogna, R. V., Martens, T. P., . . . Al-Awqati, Q. (2009). Proliferation and migration of label-retaining cells of the kidney papilla. *J Am Soc Nephrol, 20*(11), 2315-2327. doi:10.1681/ASN.2008111203

87. Oliver, J. A., Maarouf, O., Cheema, F. H., Martens, T. P., & Al-Awqati, Q. (2004). The renal papilla is a niche for adult kidney stem cells. *J Clin Invest, 114*(6), 795-804. doi:10.1172/JCI20921

88. Ord WM, S. S. (1895). On the microscopic structure of urinary calculi of oxalate of lime. *Transactions of the Pathological Society of London*(46), 91-132.

89. PC, P. (1860). Fourteen calculi removed from the bladder of a man aged 72, by the operation of lithotomy; curious form of the larger stones. *Transactions of the Pathological Society of London*(11), 166-168.

90. Perlmutter, S., Hsu, C. T., Villa, P. A., & Katz, D. S. (2002). Sonography of a human jackstone calculus. *J Ultrasound Med, 21*(9), 1047-1051. doi:10.7863/jum.2002.21.9.1047

91. Randall, A. (1937). The Origin and Growth of Renal Calculi. *Ann Surg, 105*(6), 1009-1027. doi:10.1097/00000658-193706000-00014

92. Rivera, M., Cockerill, P. A., Enders, F., Mehta, R. A., Vaughan, L., Vrtiska, T. J., . . . Krambeck, A. E. (2016). Characterization of Inner Medullary Collecting Duct Plug Formation Among Idiopathic Calcium Oxalate Stone Formers. *Urology, 94*, 47-52. doi:10.1016/j.urology.2016.05.026

93. Sakhaee, K., Maalouf, N. M., Kumar, R., Pasch, A., & Moe, O. W. (2011). Nephrolithiasis-associated bone disease: pathogenesis and treatment options. *Kidney Int, 79*(4), 393-403. doi:10.1038/ki.2010.473

94. Scales, C. D., Jr., Smith, A. C., Hanley, J. M., Saigal, C. S., & Urologic Diseases in America, P. (2012). Prevalence of kidney stones in the United States. *European urology, 62*(1), 160-165. doi:10.1016/j.eururo.2012.03.052

95. Scales, C. D., Jr., Tasian, G. E., Schwaderer, A. L., Goldfarb, D. S., Star, R. A., & Kirkali, Z. (2016). Urinary Stone Disease: Advancing Knowledge, Patient Care, and Population Health. *Clin J Am Soc Nephrol, 11*(7), 1305-1312. doi:10.2215/CJN.13251215

96. Schindelin, J., Arganda-Carreras, I., Frise, E., Kaynig, V., Longair, M., Pietzsch, T., . . . Cardona, A. (2012). Fiji: an open-source platform for biological-image analysis. *Nat Methods, 9*(7), 676-682. doi:10.1038/nmeth.2019

97. Schure, R., Costa, K. D., Rezaei, R., Lee, W., Laschinger, C., Tenenbaum, H. C., & McCulloch, C. A. (2013). Impact of matrix metalloproteinases on inhibition of mineralization by fetuin. *J Periodontal Res, 48*(3), 357-366. doi:10.1111/jre.12015

98. Sethmann, I., Wendt-Nordahl, G., Knoll, T., Enzmann, F., Simon, L., & Kleebe, H. J. (2017). Microstructures of Randall's plaques and their interfaces with calcium oxalate monohydrate kidney stones reflect underlying mineral precipitation mechanisms. *Urolithiasis, 45*(3), 235-248. doi:10.1007/s00240-016-0925-2

99. Seyed Jafari, S. M., & Hunger, R. E. (2017). IHC Optical Density Score: A New Practical Method for Quantitative Immunohistochemistry Image Analysis. *Appl Immunohistochem Mol Morphol, 25*(1), e12-e13. doi:10.1097/PAI.0000000000000370

100. Shah, J., & Whitfield, H. N. (2002). Urolithiasis through the ages. *BJU International, 89*(8), 801-810. doi:https://doi.org/10.1046/j.1464-410X.2002.02769.x

101. Shivtiel, S., Kollet, O., Lapid, K., Schajnovitz, A., Goichberg, P., Kalinkovich, A., . . . Lapidot, T. (2008). CD45 regulates retention, motility, and numbers of hematopoietic progenitors, and affects osteoclast remodeling of metaphyseal trabecules. *J Exp Med, 205*(10), 2381-2395. doi:10.1084/jem.20080072

102. Singh, K. J., Tiwari, A., & Goyal, A. (2011). Jackstone: A rare entity of vesical calculus. *Indian J Urol, 27*(4), 543-544. doi:10.4103/0970-1591.91449

103. Singh, R., Sivaguru, M., Fried, G. A., Fouke, B. W., Sanford, R. A., Carrera, M., & Werth, C. J. (2017). Real rock-microfluidic flow cell: A test bed for real-time in situ analysis of flow, transport, and reaction in a subsurface reactive transport environment. *J Contam Hydrol, 204*, 28-39. doi:10.1016/j.jconhyd.2017.08.001

104. Sivaguru, M., Saw, J. J., Williams, J. C., Jr., Lieske, J. C., Krambeck, A. E., Romero, M. F., . . . Fouke, B. W. (2018). Geobiology reveals how human kidney stones dissolve in vivo. *Sci Rep, 8*(1), 13731. doi:10.1038/s41598-018-31890-9

105. Sivaguru, M., Saw, J. J., Wilson, E. M., Lieske, J. C., Krambeck, A. E., Williams, J. C., . . . Fouke, B. W. (2021). Human kidney stones: a natural record of universal biomineralization. *Nature Reviews Urology, 18*(7), 404-432. doi:10.1038/s41585-021-00469-x

106. Song, J., Czerniak, S., Wang, T., Ying, W., Carlone, D. L., Breault, D. T., & Humphreys, B. D. (2011). Characterization and fate of telomerase-expressing epithelia during kidney repair. *J Am Soc Nephrol, 22*(12), 2256-2265. doi:10.1681/ASN.2011050447

107. Sorokin, I., Mamoulakis, C., Miyazawa, K., Rodgers, A., Talati, J., & Lotan, Y. (2017). Epidemiology of stone disease across the world. *World J Urol, 35*(9), 1301-1320. doi:10.1007/s00345-017-2008-6

108. Subasinghe, D., Goonewardena, S., & Kathiragamathamby, V. (2017). Jack stone in the bladder: case report of a rare entity. *BMC Urol, 17*(1), 40. doi:10.1186/s12894-017-0230-6

109. Taguchi, K., Hamamoto, S., Okada, A., Unno, R., Kamisawa, H., Naiki, T., . . . Yasui, T. (2017). Genome-Wide Gene Expression Profiling of Randall's Plaques in Calcium Oxalate Stone Formers. *J Am Soc Nephrol, 28*(1), 333-347. doi:10.1681/ASN.2015111271

110. Tang, P. M., Nikolic-Paterson, D. J., & Lan, H. Y. (2019). Macrophages: versatile players in renal inflammation and fibrosis. *Nat Rev Nephrol, 15*(3), 144-158. doi:10.1038/s41581-019-0110-2

111. Taylor, E. R., & Stoller, M. L. (2015). Vascular theory of the formation of Randall plaques. *Urolithiasis, 43 Suppl 1*, 41-45. doi:10.1007/s00240-014-0718-4

112. Tong, M., Jun, T., Nie, Y., Hao, J., & Fan, D. (2019). The Role of the Slit/Robo Signaling Pathway. *J Cancer, 10*(12), 2694-2705. doi:10.7150/jca.31877

113. Tyanova, S., Temu, T., Sinitcyn, P., Carlson, A., Hein, M. Y., Geiger, T., . . . Cox, J. (2016). The Perseus computational platform for comprehensive analysis of (prote)omics data. *Nat Methods, 13*(9), 731-740. doi:10.1038/nmeth.3901

114. Vanslambrouck, J., Li, J., & Little, M. H. (2011). The renal papilla: an enigma in damage and repair. *J Am Soc Nephrol, 22*(12), 2145-2147. doi:10.1681/ASN.2011100984

115. Vermooten, V. (1942). The Origin and Development in the Renal Papilla of Randall’s Calcium Plaques. *Journal of Urology, 48*(1), 27-37. doi:doi:10.1016/S0022-5347(17)70680-5

116. Vezzoli, G., Arcidiacono, T., & Citterio, L. (2019). Classical and Modern Genetic Approach to Kidney Stone Disease. *Kidney Int Rep, 4*(4), 507-509. doi:10.1016/j.ekir.2019.01.006

117. Wesson, J. A., Kolbach-Mandel, A. M., Hoffmann, B. R., Davis, C., & Mandel, N. S. (2019). Selective protein enrichment in calcium oxalate stone matrix: a window to pathogenesis? *Urolithiasis, 47*(6), 521-532. doi:10.1007/s00240-019-01131-3

118. Williams, J. C., Jr., Lingeman, J. E., Coe, F. L., Worcester, E. M., & Evan, A. P. (2015). Micro-CT imaging of Randall's plaques. *Urolithiasis, 43 Suppl 1*, 13-17. doi:10.1007/s00240-014-0702-z

119. Williams, J. C., Jr., Matlaga, B. R., Kim, S. C., Jackson, M. E., Sommer, A. J., McAteer, J. A., . . . Evan, A. P. (2006). Calcium oxalate calculi found attached to the renal papilla: Preliminary evidence for early mechanisms in stone formation. *J Endourol, 20*(11), 885-890. doi:10.1089/end.2006.20.885

120. Williams, J. C., Jr., & McAteer, J. A. (2013). Retention and growth of urinary stones: insights from imaging. *Journal of nephrology, 26*(1), 25-31. doi:10.5301/jn.5000208

121. Williams, J. C., Jr., McAteer, J. A., Evan, A. P., & Lingeman, J. E. (2010). Micro-computed tomography for analysis of urinary calculi. *Urol Res, 38*(6), 477-484. doi:10.1007/s00240-010-0326-x

122. Williams, J. C., Jr., Worcester, E., & Lingeman, J. E. (2017). What can the microstructure of stones tell us? *Urolithiasis, 45*(1), 19-25. doi:10.1007/s00240-016-0944-z

123. Winfree, S., Weiler, C., Bledsoe, S. B., Gardner, T., Sommer, A. J., Evan, A. P., . . . Williams, J. C., Jr. (2021). Multimodal imaging reveals a unique autofluorescence signature of Randall's plaque. *Urolithiasis, 49*(2), 123-135. doi:10.1007/s00240-020-01216-4

124. Witzmann, F. A., Evan, A. P., Coe, F. L., Worcester, E. M., Lingeman, J. E., & Williams, J. C., Jr. (2016). Label-free proteomic methodology for the analysis of human kidney stone matrix composition. *Proteome Sci, 14*, 4. doi:10.1186/s12953-016-0093-x

125. Worcester, E. M., & Coe, F. L. (2010). Clinical practice. Calcium kidney stones. *N Engl J Med, 363*(10), 954-963. doi:10.1056/NEJMcp1001011

126. Yang, Y., Hong, S., Li, C., Zhang, J., Hu, H., Chen, X., . . . Wang, S. (2021). Proteomic analysis reveals some common proteins in the kidney stone matrix. *PeerJ, 9*, e11872. doi:10.7717/peerj.11872

127. Yao, J., Guihard, P. J., Blazquez-Medela, A. M., Guo, Y., Liu, T., Bostrom, K. I., & Yao, Y. (2016). Matrix Gla protein regulates differentiation of endothelial cells derived from mouse embryonic stem cells. *Angiogenesis, 19*(1), 1-7. doi:10.1007/s10456-015-9484-3

128. Yiu, A. J., Callaghan, D., Sultana, R., & Bandyopadhyay, B. C. (2015). Vascular Calcification and Stone Disease: A New Look towards the Mechanism. *J Cardiovasc Dev Dis, 2*(3), 141-164. doi:10.3390/jcdd2030141

129. Zarse, C. A., McAteer, J. A., Sommer, A. J., Kim, S. C., Hatt, E. K., Lingeman, J. E., . . . Williams, J. C., Jr. (2004). Nondestructive analysis of urinary calculi using micro computed tomography. *BMC Urol, 4*(1), 15. doi:10.1186/1471-2490-4-15

130. Zhang, J., Kumar, S., Jayachandran, M., Herrera Hernandez, L. P., Wang, S., Wilson, E. M., & Lieske, J. C. (2021). Excretion of urine extracellular vesicles bearing markers of activated immune cells and calcium/phosphorus physiology differ between calcium kidney stone formers and non-stone formers. *BMC Nephrol, 22*(1), 204. doi:10.1186/s12882-021-02417-8

131. Zhou, D., Tian, Y., Sun, L., Zhou, L., Xiao, L., Tan, R. J., . . . Liu, Y. (2017). Matrix Metalloproteinase-7 Is a Urinary Biomarker and Pathogenic Mediator of Kidney Fibrosis. *J Am Soc Nephrol, 28*(2), 598-611. doi:10.1681/ASN.2016030354

<div align="center">**Curriculum Vitae**</div>

Victor Hugo Canela

Education

Ph.D. in Anatomy and Cell Biology	2022
Indiana University, Indianapolis, IN	
Master of Science, Biology	2014
California State University, Dominguez Hills, Carson, CA	
Bachelor of Science, Biology (Cell & Molecular Biology)	2011
California State University, Carson, CA	

Honors/Awards

American Society of Nephrology (ASN) Kidney STARS Award	2021
ASN Tutored Research and Education for Kidney Scholars (TREKS)	2021
Travel Award from the American Association for Anatomy (AAA)	2020
NIH NIDDK R-13 Conference Grant/Stone Lab Symposium	2019
Indiana University School of Medicine Travel Award (ASN)	2019
ASN Kidney STARS Award	2019

American Urological Association (AUA) Travel Award   2019

Honorable Mention List (Ford Foundation)   2019

Yale Ciencia Academy Fellow   2018

Indiana University School of Medicine Travel Award (AAN)   2017

Indiana University School of Medicine Travel Award   2017

Bridges to the Doctorate Program   2012-2014

1st Place Best Poster Presentation, CSUDH Student Research Day   2012

National Science Foundation Travel Award   2010

Academic Research

Doctoral Research   2017-2021

Indiana University School of Medicine Department of Anatomy, Cell Biology &

Physiology, Indianapolis, IN

Principal Investigator: James C. Williams, Jr., Ph.D.

Research Assistant   2012-2014

Department of Endocrinology and Reproductive Medicine at Los Angeles Biomed

Research Center/UCLA Harbor

Principal Investigators: Ronald Swerdloff, M.D. & Christina Wang, M.D.

- The Potent Humanin Analog (HNG) Protects Germ Cells from Apoptosis and Additively Suppresses Metastatic Lung Melanoma Formation after Cyclophosphamide Treatment in Mice

Master's Research   2012-2014

Indiana University School of Medicine, Department of Microbiology & Immunology, Herman B Wells Center for Pediatric Research

Principal Investigator: Reuben Kapur, Ph.D.

- The Regulation of Stat5 by p21 Activated Kinases in c-KIT Induced Acute Myeloid Leukemia and Systemic Mastocytosis
- Inhibition of FAK as a Potential Therapeutic Option in treating FLT-3 and c-KIT induced Lekemogenesis

Undergraduate Research   2010-2011

California State University Dominguez Hills, Department of Biology

Principle Investigator: Terry McGlynn, Ph.D.

- National Science Foundation - Costa Rica International Research Experience for Students: Tropical Ecology Mentorship Program of Southern California

Professional Memberships

National Science Policy Network	2020-2021
American Association of Anatomy	2019-2021
American Society of Nephrology	2019-2021
American Urological Association	2019-2021
The Endocrine Society	2013-2015

Publications

Original manuscripts

- Chatterjee A, Ghosh J, Ramdas B, et al. Regulation of Stat5 by FAK and PAK1 in Oncogenic FLT3- and KIT-Driven Leukemogenesis. Cell Rep. 2014;9(4):1333-1348. doi:10.1016/j.celrep.2014.10.039

- Lue, Y, Swerdloff, R, Wan, J, et. al. The Potent Humanin Analogue (HNG) Protects Germ Cells and Leucocytes While Enhancing Chemotherapy-Induced Suppression of Cancer Metastases in Male Mice, Endocrinology, Volume 156, Issue 12, 1 December 2015, Pages 4511–4521, https://doi.org/10.1210/en.2015-1542

- Stage, EC, Svaldi, D, Phillips, M, **Canela, VH**, et al. Neurodegenerative changes in early- and late0 onset cognitive impairment with and without brain amyloidosis. Alz Res Therapy 12, 93 (2020). https://doi.org/10.1186/s13195-020-00647-w

- **Canela, VH**, Bledsoe, SB, Lingeman, JE, et al. Demineralization and sectioning of human kidney stones: A molecular investigation revealing the spatial heterogeneity of the stone matrix. Physiol Rep. 2021; 9:e14658. https://doi.org/10.14814/phy2.14658

- **Canela, V.H.**, Dzien, C., Bledsoe, S.B. et al. Human jackstone arms show a protein-rich, X-ray lucent core, suggesting that proteins drive their rapid and linear growth. Urolithiasis (2021). https://doi.org/10.1007/s00240-021-01275-1

- **Canela, V.H.**, Bledsoe, S.B., Lingeman, J.E. et al. Collagen fibrils and cell nuclei are entrapped within Randall's plaques but not in CaOx matrix overgrowth: A microscopic inquiry into Randall's plaque stone pathogenesis.

In Preparation

- **Canela, V.H.**, Bowen, B. et al. Spatial Transcriptomics of the human kidney papilla reveals signaling pathways of leukocyte activation, response to oxidative stress, ossification and extracellular structure organization in nephrolithiasis

Academic Teaching

Indiana University School of Medicine – Jumpstart to Teaching Certificate of Completion 2019

- Awarded for participation in and completion of the IU School of Medicine Jumpstart to Teaching series, after successful completion of sessions related to the nature of teaching and learning, the design and development of a lesson, strategies for teaching in the sciences, assessment of learning, inclusive teaching, two electives, and the delivery of a 15-minute lesson in a practice experience.

Teaching Assistant: Indiana University School of Medicine, Department of Anatomy & Cell Biology 2019-2020

- Basic Histology: ANAT-D502

Assisting Prosector: Indiana University School of Medicine, Department of Anatomy & Cell Biology 2019-2020

- Human Gross Anatomy: ANAT-D528, Anatomy for Health Care Professionals
- Human Gross Anatomy: BIOL-N 461, Cadaveric Human Anatomy

Adjunct Professor (Instructor of Record): Cerritos College, Department of Science, Engineering & Mathematics 2014-2016

- Biology 120: Introduction to Biological Science

Lecturer (Instructor of Record): California State University Dominguez Hills, Department of Biology   2014-2016

- BIO102: General Biology (Lecture)

- BIO103: General Biology (Laboratory)

- BIO121: Principles of Biology I (Laboratory)

- BIO254: Human Biology (Lecture)

- BIO313: Animal Physiology (Laboratory)

Adjunct Professor (Instructor of Record): El Camino College (Compton Center), Department of Natural Sciences   2015-2016

- Biology 10: Introduction to General Biology (Lecture and laboratory section)

Conferences/Presentations

Oral Presentations

Canela, VH. et al. Analysis of Human Jackstone Protrusions Show a Protein-Rich Core, Suggesting That Proteins Drive Their Rapid and Linear Growth. Basic Research Forum for Emerging Kidney Scientists: A Partnership Between American Physiological Society (APS) and American Society of Nephrology (ASN). Kidney Week 2020 Reimagined: Annual Conference of the ASN.

Canela, VH. et al. Laser microdissection of human calcium oxalate monohydrate stones enables structurally specific exploration of the stone proteome. Annual Conference for the American Urological Association 2019 in Chicago, IL.

Canela, VH. et al. Ph.D. Green-book: A survival Guide for Navigating Graduate School A panel discussion presented at the annual biomedical research conference for minority students (ABRCMS) 2018 in Indianapolis, IN.

Poster Presentations

Canela, VH. et al. Analysis of Human Jackstone Protrusions Show a Protein-Rich Core, Suggesting That Proteins Drive Their Rapid and Linear Growth. American Society of Nephrology (ASN) 2020

Canela, VH. et al. Second Harmonic Generation and Fluorescence Imaging Reveal Collagen Fibrils and Cell Nuclei in Mature Randall Plaque. American Society of Nephrology (ASN) 2020

Canela, VH. et al. Laser microdissection of human calcium oxalate monohydrate stones enables structurally specific exploration of the stone proteome. American Urological Association (AUA). StoneLab Scientific Symposium in Linthicum, MD. 2019

Canela, VH. et al. Laser microdissection of human calcium oxalate monohydrate stones enables structurally specific exploration of the stone proteome. American Society of Nephrology (ASN) in Washington, D.C. 2019

Canela, VH. et al. Laser microdissection of human calcium oxalate monohydrate stones enables structurally specific exploration of the stone proteome. American Urological Association (AUA) in Chicago, IL. 2019

Canela, VH. et al. Differences in brain metabolism in Early and Late Onset Alzheimer's Disease and Suspected Non-Alzheimer's Pathophysiology. American Academy of Neurology (ANN) in Boston, MA. 2017

Canela, VH. et. al. Inhibition of FAK as a Potential Therapeutic Option in treating FLT-3 and c-KIT induced Leukemogenesis. CSUDH. Student Research Day. Carson, CA. 2012

Canela, VH. et. al. Inhibition of FAK as a Potential Therapeutic Option in treating FLT-3 and c-KIT induced Leukemogenesis. Center for Learning Summer Research Program

Symposium. Indiana University-Purdue University Indianapolis and Indiana University

Bloomington. 2012